Self-organization of polymers in bulk and at interfaces

Marat Charlaganov

Thesis committee

Thesis supervisors

Prof. dr. ir. F.A.M. Leermakers
Personal chair at the Laboratory of Physical Chemistry and Colloid Science
Wageningen University

Prof. dr. M.A. Cohen Stuart
Professor of Physical Chemistry and Colloid Science
Wageningen University

Thesis co-supervisor

Prof. dr. O.V. Borisov
Professor at Institut Pluridisciplinaire de Recherche sur l'Environnement et les Matériaux
Pau, France

Other members

Prof. dr. G. ten Brinke	University of Groningen
Prof. dr. E. van der Linden	Wageningen University
Dr.ir. P.P.A.M. van der Schoot	Eindhoven University of Technology
Dr. R. Tuinier	DSM Research, Geleen

This research was conducted under the auspices of Graduate School VLAG.

Self-organization of polymers in bulk and at interfaces

Marat Charlaganov

Thesis
submitted in partial fulfilment of the requirements
for the degree of doctor
at Wageningen University
by the authority of the Rector Magnificus
Prof. dr. M.J. Kropff
in the presence of the
Thesis Committee appointed by the Doctorate Board
to be defended in public
on Friday 4 December 2009
at 4 p.m. in de Aula.

ISBN 978-90-8585-502-6

To my parents.

Contents

CHAPTER 1

General Introduction

1.1 Self-organization

Consider an egg after it was laid by a hen. Its organization in the initial stages is rather simple: it mainly consists of a yolk and an egg-white, both containing proteins and smaller molecules (mostly water). What comes out in three weeks is a fluffy chick with a non-trivial skeleton, muscles, skin, beak, eyes, and some brain. While not completely understood, the processes responsible for this transformation can be subdivided into (bio-)chemical and (bio-)physical. The chemical processes act on the molecular level where the synthesis of new molecules occurs. On the inter-molecular level physical interactions drive the organization of molecules into tissues and organs. As a result, the internal organization of the egg becomes more complex without being guided from the outside. We call such processes self-organization.

The egg is only apparently a closed system. In reality the shell is permeable for gazes. More importantly, it allows for heat transfer. Increasing complexity implies decreasing entropy of the system. According to the laws of thermodynamics this requires energy. In the egg the energy for self-organization comes through the shell from the external world. However, the evolution of an out of equilibrium system does not necessarily yield a higher entropy even without supply of external energy.

The energy may also originate from the inside of the system, that is at the cost of internal energy. This special case of self-organization is known as self-assembly. One of the examples of this is the folding of proteins. The energy necessary to compensate for the increased order in a folded protein comes from reducing the number of contacts between hydrophobic regions of a protein with water and the formation of hydrogen bonds. In most cases, the chemical structure of a protein defines its unique spatial organization. It is fair to assume that the information

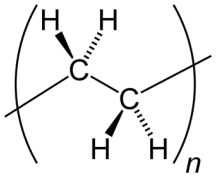

Figure 1.1: *Structural formula of linear polyethylene.*

necessary to fold the protein is coded in the protein sequence.

We distinguish equilibrium and non-equilibrium self-assembly. The result of the equilibrium self-assembly process corresponds to an extremum of an appropriate thermodynamic potential. This means that it depends only on the current values of thermodynamical variables such as temperature, pressure, volume and so on. In contrast the state of an out-of-equilibrium system depends on the history of the process and is not necessarily the most favorable one. Although in isolation all non-equilibrium systems evolve towards an equilibrium state, the equilibration may take longer than any reasonable time of observation. There are many examples of self-assembly, both exploited in biology as well as in man-made systems that exploit the same principles and equilibrate surprisingly fast. In part this has to do with the structure of the molecules that are involved in the assembly process and in part this has to do with the strength of the relevant interactions.

In this thesis we will deal with equilibrium self-assembly of long molecules known as polymers. We search for the relation between the molecular structure and the structural properties of the assemblies that result from it. Indeed it is reasonable to assume that self-assembly is the consequence of the molecular structure, that is the chemical entities enclosed in the primary sequence of the molecules, as well as the interactions that these entities experience in their environment. We will first discuss these elements of our systems separately before we elaborate on what aspects we have studied in detail, and what approach we took to study these.

1.2 Macromolecules

Macromolecules consist of large number of repeating structural units. The simplest subclass of macromolecules, homopolymers, consist of just one unit type connected as a linear chain. Fig 1.1 shows the structural formula of linear polyethylene. The carbon atoms in the main chain form a long backbone. The hydrogen atoms that are attached to this backbone are called side groups. The typical backbone length of polyethylene in an ordinary plastic bag ranges from 10^3 to 10^4 monomers. [1]

The term monomer usually refers to the repeating unit of the polymer corresponding to the low molecular weight compound it was synthesized from. Though

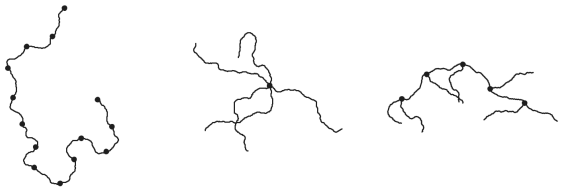

Figure 1.2: *Linear, star, and comb polymer architectures. Beads on the linear chain mark the length of statistical segment.*

the elementary repeating unit in a polyethylene chain is a single carbon with two hydrogens, the word monomer refers to a chain fragment containing two carbons or to an ethylene molecule. The number of monomers in a chain is known as the degree of polymerization. It turns out that many physical properties of polymers strongly depend on the degree of polymerization.

Industrial production of polymers often yields molecules of different length. Depending on the method of synthesis, the number of monomers in different molecules produced in one batch may differ by orders of magnitude. The degree of polymerization then refers to the most probable size of a molecule and the polymer is said to be *polydisperse*. Monodisperse samples have a well-defined size. Polymers produced by living organisms are sometimes remarkably monodisperse despite their impressive size. The longest human DNA, for example, is strictly monodisperse and consists of more than $2 \cdot 10^8$ monomers (nucleotides) and measures more than 7cm when fully stretched. Indeed, "macromolecule" seems to be a proper name for a molecule that long.

In contrast to biological systems many industrial applications are tolerant to polydispersity. The properties of materials in general depend on average molecular characteristics. Although in this thesis we will concentrate on monodisperse systems, the main conclusions and qualitative results are equally valid for their polydisperse counterparts.

Already from the early days of polymer science, we know that not all polymers are just linear objects. Branching of the chains occurs during the synthesis in presence of monomers capable of making more than two bonds. Some polymers may cross-link after the synthesis under influence of light or temperature. Each cross-linking event results in a bigger non-linear macromolecule. Eventually, if the number of cross-links keeps growing, all the chains become connected and the whole sample turns into a single molecule – a gel.

Uncontrolled branching and cross-linking usually yields randomly branched polymers. However, it is possible to design a synthesis that brings highly regular architectures. Although the number of architectures is virtually limitless, in this thesis we will discuss only the simplest regularly branched macromolecules such as polymer stars and combs (Fig 1.2). Stars are formed by identical polymeric chains connected to a central unit. In polymer combs side-chains are grafted

to a backbone at equal intervals. It is clear that terminal monomers and the monomers where branching occurs are chemically different from monomers that form the linear chain fragments.

Macromolecules may consist of more than one type of monomers. The number of different monomers present in the linear fragments is often reflected in a Greek prefix co- ter- quatro- and so on. Copolymers are composed of two types of monomers, for example, monomer types A and B. There are various types of copolymers. When the monomers are randomly distributed, we refer to these as random copolymers. With respect to self-organisation, regularly ordered copolymers are of more interest. In block copolymers the monomers are grouped. For example, in the diblock copolymer $(A)_N - (B)_M$, N monomers of type A are followed in the molecule by a string of M monomers of type B. The number of blocks in a polymer is usually indicated by a latin prefix. So triblock copolymer is a macromolecule consisting of three blocks made of two different types of monomers.

We can summarize the previous as follows. To understand the role of macromolecule in self-assembly we usually start with the description of the units it consists of. Then, the degree of polymerization and the ratios between different monomer types should be put into the equation as we need to know the physical consequences of it. In particular, the way the monomers are connected in the macromolecule is crucial for its function. Such bottom-up description is rarely necessary in the physics of low molecular weight species. Typically one is interested in the properties of a molecule as a whole. The reason for this notable difference is basically that no macromolecule is like another even if they are chemically identical. To understand more of this we need to discuss polymer conformations and understand more about the way the conformations are influenced by the various interactions that these molecules experience.

1.3 Polymer conformations and interactions

Humans have a relatively short experience of studying and manipulating microscopical objects. The history of the microworld exploration starts in the second half of the nineteenth century at the time when the atomistic theory of matter was established. For thousands of years the human thought was mainly concentrated on the objects that can be directly manipulated or observed. The limits of our intuition regarding atoms and molecules forces us to make analogies with the world we are used to – the macro world.

A good model of a macromolecule allows one to predict properties of a real system. The microstate of a macromolecule is rarely accessible in experiments. The observable properties usually depend on the collective behavior of many molecules during a certain interval of time. The requirements to the model change depending on the experiment and the time of observation.

There are various models to describe polymeric chains in solution. One of the

simplest models is the freely jointed chain. In this model the chain is represented by a set of N rigid rods of length l each connected by perfectly flexible hinges. As the directions of the connected links are not correlated there is a strong analogy between the freely jointed chain model and a random walk in three-dimensional space. Hence, the average distance between the chain ends is $R_e = lN^{\frac{1}{2}}$. The end-to-end distance is a valuable measure of the space occupied by the macromolecule and is proportional to the experimentally accessible radius of gyration and hydrodynamic radius.

The freely jointed chain model is far from being microscopically realistic. Real molecules do not consist of absolutely rigid and perfectly flexible fragments. For example, turns of 180 degrees which are allowed by the freely jointed chain model never occur in real molecules just because two segments cannot occupy the same place in space. In reality connected segments always interact with each other and their conformations are correlated. However, the correlations decay exponentially with the distance along the backbone and it is possible to divide the chain into segments of sufficient length such that the correlations between them become negligibly small. Hence long enough chains with interactions only along the backbone have the same dependence of the coil size on the chain length as ideal chains described by the freely jointed chain model. In this case the coefficient of proportionality in $R_e = lN^{\frac{1}{2}}$ gives the average distance in the three-dimensional space between uncorrelated fragments. On the length scale of l the direction of the chain is likely to become inverted. Thus, the length of a statistical segment l is small for flexible chains and large for rigid ones. The freely jointed chain model yields meaningful results only when the length of the chain exceeds the length of the statistical segment. Rigid molecules that are not long enough are typically described with other models.

While it is possible to account for interactions between neighboring segments by using the freely jointed chain model, segments that are far apart in the chain but close in space need special consideration. Intermolecular forces between uncharged molecules are usually characterized by a strongly repulsive short-range potential and a weak attraction at longer distances. The same forces act on units of a macromolecule. It is convenient to attribute interactions to monomers, as in many cases isotropic potentials fit reasonably well.

Surroundings of a monomer in solution include monomers belonging to the same chain, monomers of other chains, and solvent molecules. The solvent molecules interact with monomers of the polymer and with each other. In many cases it is possible to renormalize the monomer-monomer potential such that it includes interactions with the solvent. Although interactions between similar monomers is typically attractive, favorable interactions with the solvent can make the effective monomer-monomer potential repulsive. Moreover, even in absence of interactions between the polymer and the solvent, so called good solvent conditions, the effective monomer-monomer potential becomes repulsive due to entropic reasons. This makes the polymer coil swell with respect to the size of the ideal chain.

Flory was the first to point out that polymers in good solvent are not ideal.[2]

In a good solvent, the polymer optimizes its contacts with the solvent. This happens, for example, when we dissolve polyethylene in hexane (a short alkane). There are important consequences of the fact that a polymer chain cannot cross itself. To avoid intersections, the coil size must expand with respect to the random walk. Flory balanced the entropy loss due to the expansion with an estimate for the number of contacts that occur in a chain to arrive at the prediction that $R_e = lN^{\alpha}$ with $\alpha = \frac{3}{5}$.

In a poor solvent the coil collapses and pushes all the solvent away. This would happen, e.g. when we try to dissolve polyethylene in water. In such case the polymer forms a compact globule with a homogeneous density. From very simple geometrical arguments it follows that $R \propto N^{\frac{1}{3}}$. Only at the borderline between a good and a poor solvent we may expect that the random walk result ($\alpha = \frac{1}{2}$) is found. Such a solvent is known as a theta-solvent. For polymers in theta-conditions the interactions between segments in the coil are balanced with interaction between the segments and the solvent.

Conformations of a polymer chain in a good solvent depend on the overall concentration of the polymer. In the dilute regime the collisions of polymer coils are rare, so the result for a single chain still holds – the size of the coil scales with power $\alpha = \frac{3}{5}$.

The concentrated regime, also known as the polymer melt, may look at first glance extremely complex. However, as pointed out by Flory, at high polymer concentration the polymers become entangled and strongly interpenetrate. As a result the coils will assume the Gaussian dimensions. One way to understand this result is to realise that when two segments meet, it becomes impossible to say whether the segments are coming from different chains or not and therefore there is no guideline either to swell or to shrink.

In between the concentrated and the dilute regimes there is a semi-dilute regime which was advocated extensively by De Gennes.[3] In this regime a concentration dependent length scale ξ is found which corresponds to the range over which excluded volume correlations are felt. Pictorially, the chain now splits up in a string of $n = N/g$ blobs of size ξ, each consisting of g segments. Now the coil size is given by $R \propto \xi n^{\frac{1}{2}}$ where it is understood that the Flory relation applies for $\xi(g)$, namely $\xi = g^{\frac{3}{5}}$. By equating the density in a single blob to the polymer density c one obtains that $\xi = c^{-\frac{3}{4}}$.

The analysis of conformations shows that many important properties of macromolecules are described by simple power law dependencies. The regimes where the respective laws are applicable typically depend on the strength of interactions and the polymer concentration. In heterogeneous systems such as polymer solutions near interfaces, spacial coordinates become an important parameter. Nevertheless, the notion of dilute, semi-dilute, and concentrated regimes is very useful.

1.4 Macromolecules at interfaces

Macromolecules order in intricate ways at boundaries. Because of the large number of monomers in a single polymer chain the behavior of macromolecules is highly cooperative. Near solid interfaces this results in two possible scenarios. Repulsive interactions between the polymer and the wall, or even the lack thereof, yield a very low concentration of polymer near the interface which increases with the distance from the wall. This phenomenon is known as depletion. The other case, where there is an attraction between the wall and the polymer, typically results in concentrations of the order unity which then decreases towards the bulk and is known as adsorption.

Not only polymer properties change near boundaries, the properties of the interface itself are greatly affected by the presence of polymers. Adsorbed polymer layers are industrially used to protect surfaces from corrosion and change their mechanical properties. In medicine polymers are employed to enhance biocompatibility of artificial organs and so on.

With their low volume to surface ratios colloidal systems change their properties dramatically in presence of polymers. Depending on the monomer-interface interaction parameter and the architecture of the macromolecule the effective forces between particles may change from attractive to repulsive and the other way around.

Previous research has resulted in a reasonably good understanding of how the simplest polymers (linear homopolymers) organize themselves at solid-liquid interfaces.[4] In the case of adsorption from a dilute solution one should expect formation of a polymer layer with a high polymer concentration near the wall and the bulk concentration far from it. The dependence of the polymer concentration on the distance from the wall has three distinct regimes. The proximal part which is closest to the wall is dominated by the energy of interaction between monomers and the wall. The thickness of this part is of the order of monomer size. In the intermediate part the concentration decays as $z^{-\frac{4}{3}}$ where z is the distance from the wall. This result is obtained by using the arguments as for semi-dilute solutions with the correlation length proportional to the distance from the wall. In the distal regime the density decays exponentially towards the bulk concentration.

Much less is known about the interfacial characteristics of copolymers or architecturally complex molecules. One of the peculiar features of copolymers is that they are able to self-assemble in bulk solutions thus creating objects of colloidal size with their own interfaces.

1.5 Self-assembled polymer structures

In the following we will consider water to be the solvent if not mentioned otherwise. It is a natural choice for biological systems. Also in technological applications the effort to move more processes to aqueous solutions was a major trend in the recent

decade. The main reasons for this choice are, apart from abundance of water in nature, are ecological and health concerns.

Polymers that are soluble in water are known as hydrophilic. In the language of Flory-Huggins theory this means the effective interaction parameter, χ is less than 0.5. The theory predicts that polymers with $\chi > 0.5$ are not soluble. These are known as hydrophobic. Insoluble polymers tend to coalesce and form a separate macroscopic phase of polymer with only minor content of water.

Copolymers consisting of both hydrophilic and hydrophobic blocks are called amphiphiles. These molecules are able to experience self-assembly in aqueous solutions. Self-assembly, one aspect of self-organization, is the term we use to refer to the spontaneous organization of microscopical objects (macromolecules) without any external help in the absence of an energy supply. Self-assembly is driven by local non-covalent interactions and results in aggregates or structures that are significantly larger in size than single components and the ranges of the driving forces.

An example of self-assembly that is employed e.g. in cleaning, paint formulations, is the formation of copolymer micelles. The assembly in this case is driven by hydrophobic blocks which tend to minimize unfavorable contacts with water. However, the formation of a macroscopically big polymer phase is impossible as hydrophilic blocks prefer to remain solvated. This dilemma is solved by formation of micelles – aggregates containing a finite number of molecules. Micelles have two distinct parts – a core formed by the hydrophobic blocks and a corona containing the hydrophilic part of the copolymers. The properties of the aggregates ultimately depend on the structure of the macromolecules.

The balance between the hydrophobic and hydrophilic blocks in the copolymer defines the size and the shape of the micelle. The number of molecules that form a micelle is generally limited by the bulkiness of the hydrophilic corona block. Longer corona blocks yield spherical micelles with a well defined aggregation number of the order of tens of molecules. Shorter corona blocks result in elongated worm-like micelles. Solutions of worm-like micelles are typically characterized by a broader distribution of sizes. Finally, copolymers with a dominating hydrophobic block are able to form vesicles and lamellar aggregates.

The hydrophobic core of a micelle is able to accommodate molecules and particles that are not soluble in water. In living organisms micelles and vesicles often incorporate biological compounds that would be destroyed without shielding. Also in medicine self-assembled structures are used as carriers for toxic or poorly soluble drugs.

The feature that makes copolymer micelles particularly interesting for applications is their ability to adopt the size and the geometry to external conditions. Factors that can trigger the assembly or a transition from one geometry to an other include temperature, pH, and salinity of the solution. Understanding the mechanisms of these transitions opens opportunities for targeted drug delivery and designing stimuli-responsive smart materials with a well defined microstructure.

1.6 Scheutjens-Fleer self-consistent field theory

Ideally one would like to cast the above mentioned characteristics of polymer molecules in a theoretical framework and use this to predict the self-organization of polymers near interfaces and in solution. Realistic theoretical descriptions are important to rationally design experiments and to analyze the outcome of such experiments, two important steps in the research cycle.

There are several relevant approaches that should be mentioned here which are being used to unravel the complex behavior of macromolecular self-assembly at interfaces or in bulk solutions. Arguably, the most exact route is the one using computer simulations that have the possibility to take all relevant degrees of freedom into account. Rigorous simulations are computationally limited to small system sizes (nm) and short time scale (ns) phenomena. On the other end of the spectrum there is the so-called scaling approach which focused on large scale phenomena. Using rather sophisticated arguments (some of these were used above), one focuses on predicting relations between polymeric input parameters and measurable dependencies. Although chemical details are ignored, scaling approaches are very important because they provide a framework for understanding the system from a very coarse perspective.

The work that is presented in this thesis makes use of the self-consistent field method. Without going into details, it is positioned in between the simulation- and the scaling approaches. The method is not as rigorous as simulations. One reason is that some molecular details are ignored and some of the excluded volume interactions are accounted for in an average sense. The method is more informative than scaling approaches as it is (in contrast to scaling relations) is also capable to capture prefactors.

There are many kinds of self-consistent field models which may help to understand the self-organization of polymeric systems. In this work we have built upon the framework of Scheutjens and Fleer (SF-SCF). These authors introduced a lattice to evaluate the characteristics of these systems. The lattice serves as a mesh onto which the polymer segments as well as the solvent molecules are distributed. The polymer chains are described using the freely-jointed chain model and excluded volume interactions are treated on the Bragg-Williams mean field level using the Flory-Huggins chi-parameter to quantify the strength of interactions.

The SF-SCF model was first used to consider how linear polymer chains stick onto a solid interface while administered from a dilute solution. Later the model was elaborated to deal with self-assembly of surfactants into association colloids such as micelles and membranes. Many researchers have contributed to the development of this model, e.g., accounting for electrostatic interactions, or by putting constraints on the polymer chains leading to so-called polymer brushes. As a result the SF-SCF model has developed into a versatile tool to study polymers in inhomogeneous systems. The method has been compared to simulations and confronted to scaling predictions.

Although qualitatively the results are rigorous, important problems with the

SF-SCF model have been identified. The most essential problem of the SF-SCF model is the neglect of intra-molecular excluded volume interactions for polymers. In this thesis we have formulated a beginning of an improved SCF model that accounts for excluded volume interactions both near the inhomogeneities in the system as well as in the bulk and reference states.

1.7 Outline of this thesis

The field of self-organization of polymers in bulk and at interfaces is huge and it will be clear that in a thesis only few aspects can be covered. Instead of focusing on one specific system we have decided to work on several different problems each with its own character. More specifically, this thesis is organized as follows.

In Chapter 2 we discuss how constraints imposed on the ends of a single homopolymer chain affects its conformations in a poor solvent. Different regimes are identified by a series of intramolecular morphological transitions and by changes in elastic response upon changing the distance between the fixed segments. An analytical model is suggested and compared to the results of SCF modeling.

In Chapter 3 we consider the self-assembly of double-hydrophilic symmetrical triblock terpolymers with a hydrophobic central block. These triblocks form spherical micelles with two types of segments in the corona. Upon certain circumstances the corona blocks segregate and form a two-faced Janus corona. We consider the thermodynamic stability, the size, and the size fluctuations of these micelles. Special attention is paid to the transition from a mixed- to a Janus-type corona and the structure of the interface between the faces of the Janus corona.

In Chapter 4 we revisit the classical problem of homopolymer adsorption at the solid-liquid interface. We show, that the self-organization of comb polymers near a solid wall has non-trivial implications for the colloidal stability. In particular, the side chains of the polymer are able to suppress the bridging effect, even for very long main chains. Contrary to linear polymers comb polymers have a stabilizing effect on colloidal systems.

In Chapter 5 we propose an efficient two-stage modeling approach for inhomogeneous polymer solutions. A coarse-grained Monte Carlo simulation on a set of soft particles representing polymer chains is used to obtain relevant sets of coordinates, which are subsequently used as constraints in complementary molecularly realistic 3d self-consistent field (SCF) calculations. The method is illustrated by polymer depletion near a flat wall for semi-dilute solutions in good solvent. The depletion profile and layer thickness is consistent with full scale computer simulations and scaling considerations.

Finally, in Chapter 6 we summarize the results of our work and give an outlook on future research.

CHAPTER 2

Mechanical unfolding of a homopolymer globule [1]

[1] Published with minor changes by Alexey A. Polotsky, Marat I. Charlaganov, Frans A.M. Leermakers, Mohamed Daoud, Oleg V. Borisov, Tatiana M. Birshtein in Macromolecules 42 (2009) p 5360.

We present results of numerical self-consistent field calculations for the equilibrium mechanical unfolding of a globule formed by a single flexible polymer chain collapsed in a poor solvent. In accordance with earlier scaling theory and stochastic dynamics simulations findings we have identified three regimes of extensional deformation: (i) a linear response regime characterized by a weakly elongated shape of the globule at small deformations; (ii) a tadpole structure with a globular "head" co-existing with a stretched "tail" at intermediate ranges of deformations and (iii) an uniformly stretched chain at strong extensions. The conformational transition from the tadpole to the stretched chain is accompanied by an abrupt unfolding of the depleted globular head and a corresponding jump-wise drop in the intra-chain tension. The unfolding-refolding cycle demonstrates a hysteresis loop in the vicinity of the transition point. These three regimes of deformation, as well as the first-order like transition between the tadpole and the stretched chain conformations, can be experimentally observable provided that the number of monomer units in the chain is large and/or the solvent quality is sufficiently poor. For short chains at moderately poor solvent strength conditions the unfolding transition is continuous. Upon an increase in the imposed end-to-end distance the extended globule retains a longitudinally uniform shape at any degree of deformation. In all cases the system exhibits a negative extensional modulus in the intermediate range of deformations. We anticipate that predictions of patterns in force-deformation curves for polymer molecules in poor solvent can be observed in single molecule atomic spectroscopy experiments.

2.1 Introduction

The particular interest in the globular state of individual macromolecules and in the conformational collapse-to-swelling or unfolding transitions in individual polymer chains is motivated by the existing physical analogy between globules of synthetic polymers stabilized by solvophobic interactions between the monomer units in poor solvents and the compact structures found for biopolymers, e.g., for globular proteins.[5]

Despite this profound analogy and the fact that these objects share the same name, homopolymer globules differ markedly from protein ones. A globular protein, which is a copolymer with a large number of different amino acid residues, typically has a unique intra-molecular structure being a "aperiodic crystal".[6] In contrast, a globule of a flexible homopolymer can be compared to a liquid droplet. In this case, the coil-globule transition is similar to the usual gas-liquid transition upon a decrease in the temperature. The connectivity of the interacting monomers inside a chain changes the characteristics of this transition to some extent; the transition keeps its phase nature but becomes a continuous second order phase transition. The conformational and thermodynamic characteristics of a globule stabilized by monomer-monomer attractions are functions of the strength of this attraction, or in other words, are determined by the solvent quality. The density of the globule grows monotonously upon worsening of the solvent quality from a very low value in the Gaussian coil to a value of order unity in a densely packed globule. The remainder of the volume of a globule is occupied by solvent molecules. The density of a protein globule is always close to unity.

Recent developments in AFM force spectroscopy and optical tweezers techniques have made it possible to manipulate individual molecules and to subject them to mechanical force, for example, to stretch the chain by extending the distance between its two ends.[7–11]

In essence, there are two possible scenarios for such extension. In the first case the governing parameter is the distance between two points in a macromolecule (for example between the two end segments) which is fixed to a specified value or changed with a given velocity. The observable in this case is the restoring force. In the second case the applied force is fixed and plays the role of the control parameter. The observable in this case is the average end-to-end distance. A force-extension relation is obtained in both scenarios. Note that in experiments with individual macromolecules the relevant distances are in the nanometer (nm) domain, whereas the force is in the piconewton (pN) range. Recently it was demonstrated that the constant extension ensemble (the first scenario) which is mostly used in experiments, leads to a remarkably rich deformation behavior.[12]

There exists a large number of experimental works devoted to the extension of globular proteins. The objectives of such studies are to find, e.g., "weak spots" in a globule structure, or to discover a possible folding pathway. It has been shown in experiments on unfolding of proteins that the force versus deformation curves may exhibit quite complex patterns and are essentially non-monotonic.[13]

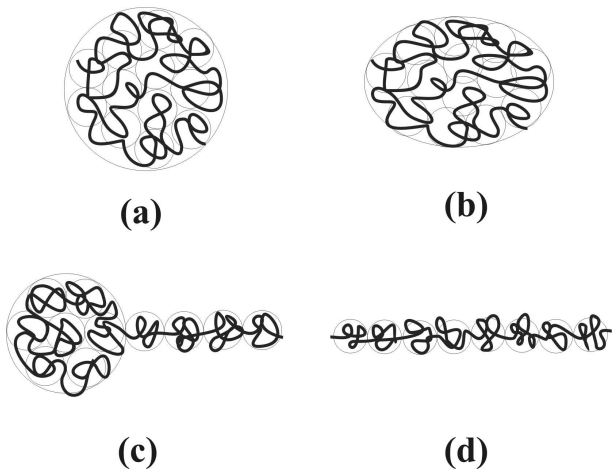

Figure 2.1: *Unperturbed spherical (a) and ellipsoidal (b) globules, tadpole (c), and uniformly stretched (d) conformations.*

The pioneering theory of unfolding homopolymer globules subjected to an extensional deformation, was proposed by Halperin and Zhulina.[14] This theory envisions that a weak extensional deformation of a spherical globule, Fig. 2.1 (a), produces a prolate ellipsoid of increasing asymmetry, Fig. 2.1 (b). The reaction (restoring) force was predicted to grow linearly at this stage. Under a moderate extensional deformation, a coexistence between a collapsed globular core and an extended "tail" takes place within a single macromolecule, Fig. 2.1 (c). The deformation in this "tadpole" regime is accompanied by a progressive unfolding of the globular core which occurs at an almost constant reaction force. This stage ends when a stretched string of thermal blobs is obtained, i.e. when the size of the tadpole's globular head becomes of the order of the thermal blob size, Fig. 2.1 (d). From this point onward the reaction force grows again with the following extension of the unfolded chain.

Later on, Cooke and Williams demonstrated the existence of a first-order conformational transition in the stretching of a collapsed (dry) polymer: at a certain extension the chain suddenly unravels from the tadpole conformation, Fig. 2.1 (c), to the open chain conformation, Fig. 2.1 (d).[15] In the force-extension curve this transition appears as a discontinuous drop in the force. The collapsed "head" in the transition point contains $\sim N^{3/4}$ monomer units. The discontinuous drop in the force disappears, however, in the thermodynamic limit of infinitely long chain, $N \to \infty$. Similar unraveling transition was found by Craig and Terentiev who studied unfolding of a globule formed by a semi-flexible polymer.[16]

The analogy between a homopolymer globule and a liquid droplet has been mentioned already. This analogy is also important for understanding the globule

unfolding. The chain stretching, that is, the progressive increase in the end-to-end distance of the chain, is similar to increasing the available volume in the liquid-gas transition. The role of the gas phase is played in this case by the extended tail drawn out of the globule. Gas-liquid phase coexistence in a certain range of volumes (in our case - in the certain range of the given end-to-end distances) or at a constant pressure (in our case - at a constant reaction force) is well-known.[17] In the case of the polymer globule two phases coexist in a single macromolecule. This behavior is closely related to the Rayleigh instability in a liquid droplet.[18] In the case of a polymer in poor solvent an additional connectivity constraint of the solvophobic monomers in the chain comes into play.[19] Similar force-deformation patterns have been predicted for the unfolding transition in globular structures of amphiphilic associating copolymers.[20] The topological complexity, that is, the grafting of polymer chains onto a surface (a brush), introduces even more interesting features in the scenario of the unfolding transition.[21,22]

The aim of the present study is to develop a general theory of the polymer globule deformation as a function of the degree of polymerization N (number of monomer units in the chain) and the solvent quality. These two parameters determine the properties of the free unperturbed globule. Our work includes several stages. In the first part of this paper, we use the Scheutjens-Fleer self-consistent field (SF-SCF) lattice approach in its two-gradient version to study the evolution of the conformational and thermodynamic properties of a polymer globule upon a uniaxial extension (i.e. with an increase in the distance between the chain ends). We consider a wide range of N and polymer-solvent interaction parameter values. In the second part, an analytical Flory-type theory for the unfolding of a globule is advanced. The analytical theory uses, as input parameters, the properties of an unperturbed globule found with the aid of SF-SCF approach. This theory allows us to go beyond the limits of the SF-SCF modeling (first of all, to consider the limit of very long chains) and to calculate phase diagrams of the deformed globule as well as the properties of the globule in the transition point. The issues related to the phase diagrams, however, will be presented elsewhere.

The remainder of the paper is organized as follows. In the section “Model and method” we introduce the SF-SCF approach. The results of the calculations are summarized in the section “Results”. In the section “Blob picture of globule deformation” we discuss the obtained results in terms of the classical scaling theory by Halperin and Zhulina for the extension of a flexible linear polymer chain collapsed in a poor solvent, and this is followed by the Conclusions.

2.2 Model and method

Theoretical background of the self-consistent field (SCF) approach

At the basis of the SCF approach is a mean-field free energy which is expressed as a functional of the volume fraction profiles (normalized concentrations) and the self-consistent field potentials. The minimization of this free energy leads for polymer chains to the Edwards diffusion differential equation,[3] which for an arbitrary coordinate system may be expressed as

$$\frac{\partial G(\mathbf{r}', \mathbf{r}; n)}{\partial n} = \frac{a^2}{6}\nabla^2 G(\mathbf{r}', \mathbf{r}; n) - \frac{u(\mathbf{r})}{k_B T} G(\mathbf{r}', \mathbf{r}; n) \tag{2.1}$$

(k_B is the Boltzmann constant, T is the absolute temperature).

The Green's function $G((\mathbf{r}', \mathbf{r}, n)$ used in Eq. (2.1) is the statistical weight of a probe chain with the length n having its ends fixed in the points $\mathbf{r}'$ and $\mathbf{r}$. The self-consistent potential $u(\mathbf{r})$ represents the surrounding of the chain and serves as an external field used in the Boltzmann equation to find the statistical weight for each chain conformation. Consequently, the Green's functions $G(\mathbf{r}', \mathbf{r}; n)$ that obey Eq. (2.1) is related to the volume fraction profile of the polymer by a composition law:

$$\varphi(\mathbf{r}) = \frac{\sum_{\mathbf{r}'} \sum_{\mathbf{r}''} \sum_n G(\mathbf{r}', \mathbf{r}; n) G(\mathbf{r}, \mathbf{r}''; N - n)}{\sum_{\mathbf{r}'} \sum_{\mathbf{r}''} G(\mathbf{r}'', \mathbf{r}'; N)}. \tag{2.2}$$

In our case the ends of the chain are "pinned" at the points $\mathbf{r}'$ and $\mathbf{r}''$, so, the usual summation over the end points position should be omitted:

$$\varphi(\mathbf{r}) \equiv \varphi(\mathbf{r}; \mathbf{r}', \mathbf{r}'') = \frac{\sum_n G(\mathbf{r}', \mathbf{r}; n) G(\mathbf{r}, \mathbf{r}''; N - n)}{G(\mathbf{r}'', \mathbf{r}'; N)}. \tag{2.3}$$

The boundary conditions and incompressibility condition: $\varphi(\mathbf{r}) + \varphi_S(\mathbf{r}) = 1$, where $\varphi_S(\mathbf{r})$ is the volume fraction of the monomeric solvent, provide constraints on the spatial solutions. The potential $u(\mathbf{r})$ is local (i.e. there are no long-range forces) and depends on the local volume fraction $\varphi(\mathbf{r})$

$$u(\mathbf{r}) = u[\varphi(\mathbf{r})], \tag{2.4}$$

The explicit concentration dependence will be specified below (see Eq. (2.7)). Equations (2.1), (2.3), and (2.4) make up the system of self-consistent field equations which is solved iteratively: one assumes an initial volume fraction profile $\varphi(\mathbf{r})$, then computes the potential $u(\mathbf{r})$ using Eq. (2.4), the set of the Green's functions, Eq. (2.1), and derives a new volume fraction profile $\varphi'(\mathbf{r})$, Eq. (2.3). The procedure is then repeated until the sequence of approximations $\varphi(\mathbf{r}) \to \varphi'(\mathbf{r}) \to \ldots$ converges to a stable solution $\varphi^*(\mathbf{r}) = \varphi(\mathbf{r})$.

To solve the self-consistent field equations rigorously, it is necessary to introduce a numerical algorithm. Such numerical scheme involves space discretization

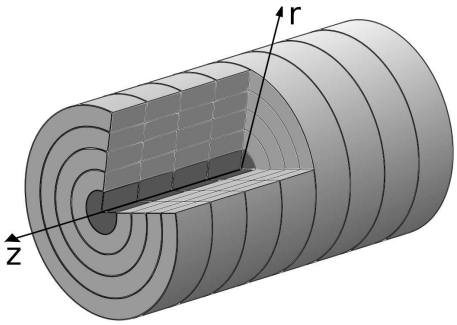

Figure 2.2: *Cylindrical lattice used in two-gradient SCF calculations.*

(i.e., the use of a lattice). Here we follow the method of Scheutjens and Fleer (SF-SCF), who used the segment size a as the lattice cell size.[4] The lattice sites are organized in *layers*, each of these layers is referred to with a single coordinate $\mathbf{r}$. Within a layer, a mean-field approximation is applied, i.e., the volume fractions of the monomeric components and the self-consistent potential within the layer are constant. The way the sites are organized in layers depends on the symmetry in the system and must be preassumed. The approach allows for volume fraction and self-consistent field gradients between these layers.

In order to consider the stretching of a single polymer chain (globule), it is necessary to use a two-gradient version of the SCF algorithm, taking into account the symmetry of the problem.[23] The natural geometry for this is a cylindrical coordinate system for which $\mathbf{r} = (r, z)$, Fig. 2.2. In this case, all volume fraction profiles as well as other thermodynamic values depend explicitly on the radial coordinate r and the axial coordinate z. The system is rotationally invariant with respect to the z-axis and the mean-field approximation is applied along the angular coordinate. Therefore a lattice layer $\mathbf{r} = (r, z)$ represents a piece of a tube (a ring) of thickness and height both equal to the lattice unit length a.

A polymer chain is represented on the lattice as a freely-jointed chain walk. The law of such walk on the cylindrical lattice is specified by setting the *a priori* transition probabilities, which are the statistical weights of the steps from the layer with the coordinate (r, z) to a neighboring one $(r + i \cdot a, z + j \cdot a)$, where $i, j \in \{-1, 0, 1\}$, denoted by λ_{ij}. These statistical weights account for possibilities of going to the nearest neighbor (if $i = 0$ but $j \neq 0$, or $i \neq 0$ but $j = 0$), next to nearest neighbor (if $i \neq 0$ and $j \neq 0$) or staying in the same layer (if $i = j = 0$). Since the number of sites in the layer depends on r, λ_{ij} is r-dependent but has no z dependence. The transition probabilities $\lambda_{ij}(r)$ obey the internal balance equation $L(r)\lambda_{1,j}(r) = L(r + a)\lambda_{-1,j}(r + a)$ where $L(r) = \pi(2r - a)/a$ is the number of sites in the layer with the radial coordinate r. The probability to go from the layer with radial coordinate r to that with $r + 1$ should be proportional

to the contact area between these layers $\lambda_{1,j}(r) \sim A(r)$, the latter is given by $A(r) = 2\pi ra$. Similarly, $\lambda_{-1,j}(r) \sim A(r-a)$. Using this area we may write

$$\begin{aligned} \lambda_{1,0}(r) &= \lambda_1 \frac{A(r)}{a^2 L(r)}, \quad \lambda_{-1,0}(r) = \lambda_1 \frac{A(r-a)}{a^2 L(r)}, \\ \lambda_{1,\pm 1}(r) &= \lambda_2 \frac{A(r)}{a^2 L(r)}, \quad \lambda_{-1,\pm 1}(r) = \lambda_2 \frac{A(r-a)}{a^2 L(r)} \end{aligned} \tag{2.5}$$

For the transition probabilities in z direction $\lambda_{0,\pm 1}(r) = \lambda_1$, the probability to stay in the same ring $\lambda_{0,0}(r) = \lambda_0$. The probabilities $\lambda_{ij}(r)$ should obey the normalization condition

$$\sum_{i=-1,0,1} \sum_{j=-1,0,1} \lambda_{ij}(r) = 1. \tag{2.6}$$

In particular, this gives for the "limiting" transition probabilities $\lambda_0 + 4\lambda_1 + 4\lambda_2 = 1$ (at zero curvature). The set of λ_0, λ_1, and λ_2 determines the character of the walk on the lattice,i.e., the chain entropy and rigidity. For instance, setting $\lambda_2 = 0$ eliminates next-to nearest neighbor steps.

In the lattice approach, the iterative procedure of solving the system of the SCF equations is implemented as follows. Once the initial guess for the volume fraction profile, $\varphi(\mathbf{r})$, is set, the self-consistent segment potential $u(\mathbf{r})$ is calculated as follows

$$\frac{u(\mathbf{r})}{k_B T} = \ln(1 - \varphi(\mathbf{r})) - 2\chi \left\langle \varphi(\mathbf{r}) \right\rangle . \tag{2.7}$$

where χ is the Flory-Huggins parameter describing the polymer-solvent interaction. The angular brackets in (2.7) denote a local *layer average* over the nearest and next-to-nearest lattice layers

$$\langle X(\mathbf{r}) \rangle = \langle X(r,z) \rangle = \sum_{i=-1,0,1} \sum_{j=-1,0,1} \lambda_{ij}(r) X(r + i \cdot a, z + j \cdot a). \tag{2.8}$$

Here the set of transition probabilities $\{\lambda_{i,j}(r)\}$ introduced above for specifying the lattice walk is also used as the set of weight coefficients for averaging.

The Green's functions $G(\mathbf{r}', \mathbf{r}; n)$ can be computed from the recurrence relation expressing the fact that a chain of n monomers can be obtained by adding a monomer to a chain of $n-1$ monomers:

$$G(\mathbf{r}', \mathbf{r}; n) = \langle G(\mathbf{r}', \mathbf{r}; n-1) \rangle \, G(\mathbf{r}; 1), \tag{2.9}$$

where $G(\mathbf{r}; 1)$ is the partition function of a monomer which is simply given by the Boltzman law: $G(\mathbf{r}; 1) = \exp[-u(\mathbf{r})/k_B T]$. The angular brackets denote here the weighted sum over the neighbors of the layer $\mathbf{r} = (r, z)$ which is calculated alike the nearest and next to nearest neighbor average, Eq. (2.8).

Note that the set of $\{\lambda_{i,j}(r)\}$ may be in principle different for density average and the Green's function calculation. Indeed, one might want to exclude the

"diagonal" or next-to-nearest neighbor steps and set λ_2 to zero for the *walk* (i.e. in the calculation of $G(\mathbf{r}', \mathbf{r}; n)$), but take into account next-to-nearest neighbor for *interactions* and set the corresponding λ_2 nonzero.

Implementation of the SCF approach

Numerical calculations using the SF-SCF approach described above were implemented using `sfbox` software developed in Wageningen University.[24] It allows to perform efficient high-speed calculations, even on a personal computer. `sfbox` uses the same set of $\{\lambda_0, \lambda_1, \lambda_2\}$ both for modelling the chain walk, Eq. (2.9), and performing the neighbor average, Eq. (2.8). For our calculations $\lambda_0 = \lambda_1 = \lambda_2 = 1/9$ were chosen. This means that both nearest neighbor and next-to-nearest neighbor layers are taking into account in performing site average, Eq. (2.8) as well as in modeling the chain trajectory (calculating Green's function), Eq. (2.9).

In the calculations we use a cylindrical lattice. The size of the simulation box, i.e. the range for r and z: $r \in [a, r_{max}]$ and $z \in [a, z_{max}]$ should be properly set. The simulation box should not be too large to make the calculations low time- and memory consuming. However, it should not be too small in order to avoid the edge-effects. In all cases we used r_{max} larger then the radius of the unperturbed globule R_0. The system size in the z-direction depends on the value of the extension.

The macromolecule is placed symmetrically in the box so that its ends are pinned at the z-axis, $\mathbf{r}_1 = (a, z_1)$, $\mathbf{r}_N = (a, z_N)$, equidistant from the corresponding boundaries: $z_1 - a = z_{max} - z_N > 2R_0$. The distance between the chain ends is $D = z_N - z_1$.

We followed a specific protocol to study the unfolding of the globule. The first calculation (the first run of `sfbox`) is made for the minimum distance between the ends of the chain $D/a = 1$. Then both z_N/a and, correspondingly, the size of the box z_{max}/a direction are successively increased by unity and the following run is made, etc. The solution obtained at i-th step is used as initial guess for $(i+1)$-th step. This procedure is repeated up to strong stretching, $D/a \sim N$ (in practice - up to $D/a \approx N/2$).

Then a second series of runs is made. This series corresponding to the *refolding* of the globule. It starts from $D/a \sim N$. Subsequently both z_N/a and z_{max}/a are successively decreased by unity down to $D/a = 1$. Again, the solution obtained at the previous step is used as initial guess in the following run. For each run we obtain the free energy and detailed profiles of the volume fractions.

As a result, two free energy dependencies on the chain extension and two sets of the force-deformation profiles, i.e. for the forward (unfolding) and backward (refolding) runs, respectively, are obtained for each given pair $\{N, \chi\}$. Note that in the described scheme of SF-SCF modeling only one chain end corresponding to the N-th monomer is moved, while the first monomer remains pinned in the same point (z_1 remains unchanged).

The parameters of our model are as follows. The number of monomers units is equal to N. Unoccupied lattice sites are taken by a monomeric solvent (incompressible system) and the corresponding Flory-Huggins parameters for the polymer-solvent interactions is χ.

2.3 Results

We have performed SCF calculations for several chain length N ranging from 200 to 1000 and a series of χ values ranging from $\chi = 0.8$ to 2.0. In the SCF calculations, the results of two types are obtained: (1) large-scale thermodynamic properties, first and foremost the free energy, and (2) polymer and solvent volume fraction distribution profiles (i.e. local properties).

First we consider how the free energy of the globule behaves with a consecutive increase or decrease in the distance D between the ends of the chain (i.e. upon the mechanical unfolding or refolding, respectively, of the globule) and obtain the force-extension curves - force vs. deformation dependencies - for different N and χ values. Then, by considering the evolution of the density profiles, we analyze what conformational changes occur in the globule upon deformation and correlate these with the features of the force-extension curve.

Free energy curves

Figure 2.3 shows an example of the free energy F as a function of the extension D calculated for $N = 200$ and a series of χ-values. Both unfolding and refolding branches are plotted in this figure and, as one can see, two branches coincide both at small and high stretching values D, whereas at moderate extensions they differ within some range of D-values provided the Flory parameter χ is high enough. This means that at moderate deformations, there exist two local minima of the free energy. The position and the width of the region where these two minima coexist depends on the χ-value. The free energy is a functional of the density distribution $F = F[\varphi(r, z)]$ and the two minima correspond to different states of the deformed globule, and there are two different volume fraction profiles $\varphi_1(r, z)$ and $\varphi_2(r, z)$. The state that has a lower free energy corresponds to the global minimum and is stable, the other state is metastable. At the point where the unfolding and the refolding branches intersect the system experiences a first-order-like phase transition.

However, the two minima are separated by a free energy barrier. For finite chain length this barrier has a finite height and in reality the transition is smooth; the system can fluctuate between local minima. However in SCF calculations, where thermal fluctuations are suppressed, the system stays in the metastable state until it reaches the *spinodal point*, where the metastable minimum disappears, and then jumps to the global minimum. Hence, the mechanical unfolding-refolding cycle exhibits a hysteresis loop in a SCF calculation.

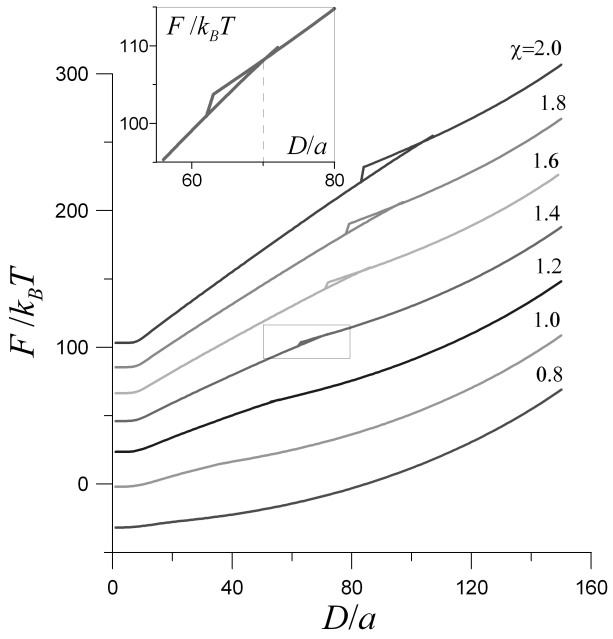

Figure 2.3: *Free energy as function of chain extension for $N = 200$ and various values of χ. Inset: free energy for $\chi = 1.4$ in the vicinity of the transition point.*

At lower values of χ ($\chi = 0.8$ and 1.0) the dependence of the free energy on deformation is different: unfolding and refolding branches of the free energy superimpose completely.

Force-extension curves

Once the dependence of the free energy vs. extension is known, the reaction, or restoring, force can be found by differentiating the free energy F with respect to end-to-end distance D. The value of the reaction force is $f = \partial F/\partial D$ and it acts against the extension. Fig. 2.4 shows force-extension curves obtained from the free energy dependencies on deformation, Fig. 2.3, by numerical differentiation of the *equilibrium* free energy. The true transition point (in thermodynamic sense) D_{tr} is obtained from the condition $F_1(D_{tr}) = F_2(D_{tr})$ whereas the metastable states are excluded from these consideration. The kink in the free energy curves at the transition point gives rise to a jump in the reaction force.

If the metastable states are taken into account, i.e. unfolding and refolding free energy branches are different, one obtains the hysteresis loop on the force-extension curve. As an example one of such curves is shown for $\chi = 1.4$ in the inset of Fig. 2.4.

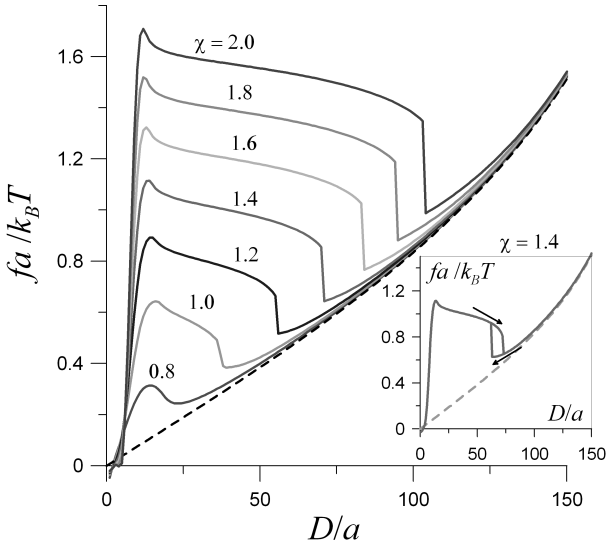

Figure 2.4: *Equlibrium reaction force vs. extension curves for the globule with* $N = 200$ *at various values of* χ*. Inset: Reaction force calculated for forward (unfolding) and backward (refolding) runs for* $\chi = 1.4$*.*

Inspection of the force-extension curves clearly reveals three different deformation regimes. (1) At small deformations the reaction force strongly increases with extension. Note that at very small extension, $D/a \simeq 1$, the force is negative: Fixing the chain ends to very small distances imposes high local concentration of the monomer units that is larger than the average equilibrium concentration in the globule; this is penalized by an increase in the free energy and this causes a repulsion between the end-monomers. (2) After reaching a peak value the reaction force slightly decreases (quasi-plateau) in a wide range of D/a and then drops down at the transition point $D = D_{tr}$, where the equilibrium free energy dependence has a kink, Fig. 2.3. Neither the extensive plateau nor the jump in the force are observed in the case of $\chi = 0.8$. This is consistent with observation that the unfolding and refolding branches are equivalent and that there was no kink / transition point in this case. Interestingly, at $\chi = 1.0$ the unfolding and refolding free energy branches coincide too, but the corresponding force-extension curve shows a pronounced jump. This can be attributed to the narrow width of the region where the two free energy minima coexist; this region cannot be resolved within our lattice approach since the latter has the resolution $\Delta D/a \geq 1$. (3) After the jump, at strong deformations, the reaction force starts to grow again. The force-extension dependence in this regime is universal and is independent of the solvent quality χ. This free energy and hence the reaction force have a purely

entropic origin. As is discussed in Appendix, for a lattice chain, an analytical expression for the force dependence on deformation exists for this branch (in the whole range of chain extensions). This analytical result is shown in Fig. 2.4 by the dashed line.

At this stage we mention that the transition between regimes (1) and (2) occurs continuously. In summary, an increase in χ leads to (i) an increase of the reaction force at fixed end-to-end distance; (ii) the broadening of the quasi-plateau (regime (2)), and (iii) an increase in the value of the jump of the force at the transition point.

Density profiles

To correlate the observed deformation regimes with (possible) conformational changes in the globule, profiles of polymer volume fraction distribution in the deformed globule should be analyzed. As it was mentioned above, the SF-SCF approach gives access to these polymer density distribution profiles $\varphi(r, z)$. The volume fraction is a function of two variables that can best be presented in two-dimensional contour plot, Fig. 2.5.

Another interesting and illustrative quantity that characterizes the conformations of the deformed globule is the "integral" profile - the axial distribution of monomer units

$$n(z) = \sum_{r \geq a} L(r)\varphi(r, z). \tag{2.10}$$

A set of $n(z)$ profiles for different extensions can be conveniently represented as a 3-dimensional plot, Fig. 2.6.

Fig. 2.5 and Fig. 2.6 show the evolution of $\varphi(r, z)$ and $n(z)$ upon the imposed deformation for $\chi = 1.4$ and $N = 200$. This choice of χ and N represents the typical case where three regimes of globule deformation, Fig. 2.4, are well distinguished. One can see that at small extensions (regime (1)) the globule changes its shape from spherically symmetric (at $D/a = 1$), to an asymmetric one similar to that of a prolate ellipsoid (at $D/a = 10$). When the extension grows, the prolate globule conformation becomes unstable and the globule splits into a dense "head" and a stretched "tail" coexisting in one macromolecule (at $D/a = 20$), thus acquiring a tadpole conformation. This corresponds to regime (2) on the force-extension curve. When the distance between the ends of the chain increases, a redistribution of monomers between two phases occurs: the tail length grows and the head size decreases, this corresponds to the range of extensions from approximately $D/a = 20$ to $D/a = 70$. In spite of the decrease in the size of the globular head, the density of the globular core (i.e., except of the density in the diffuse interfacial layer) remains virtually constant. Close inspection reveals that the number of monomer units per unit length in the tail weakly increases. This is in accordance with a very weak decay of the reaction force f in the plateau regime, Fig. 2.4, because the number of monomers per unit length is the inverse of chain extension: $f \sim dz/dn = 1/n(z)$.

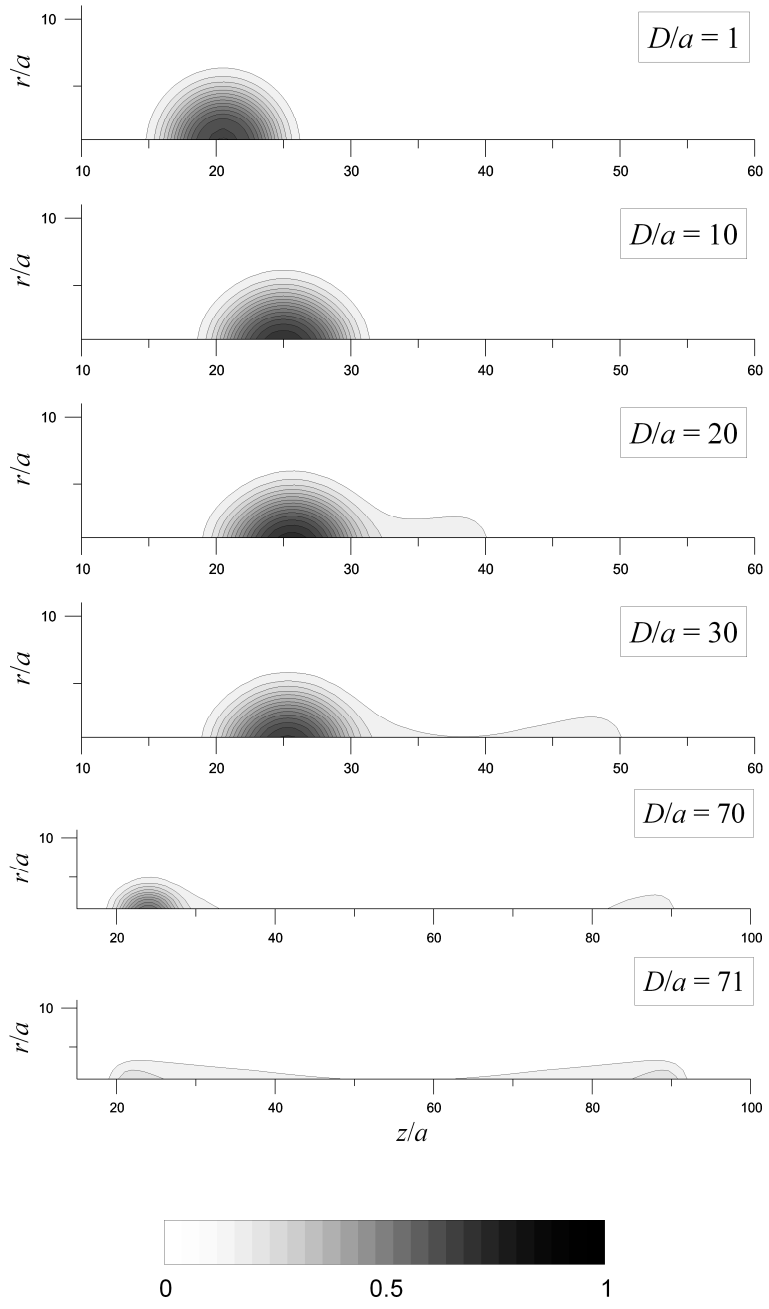

Figure 2.5: *Polymer density profiles $\varphi(r, z)$ for the globule with $N = 200$ and $\chi = 1.4$ at various chain extensions.*

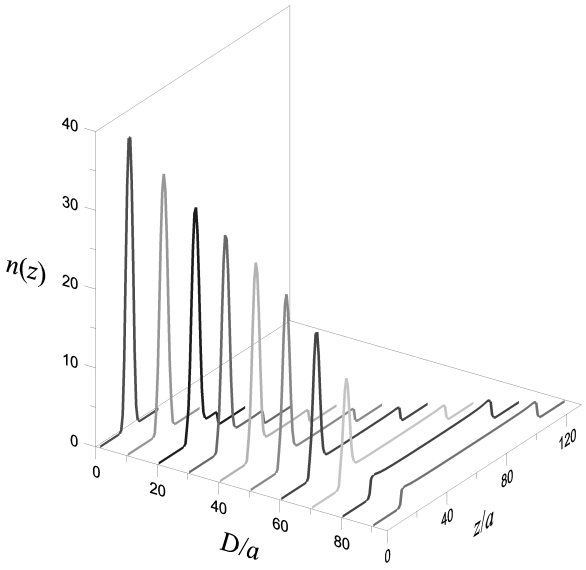

Figure 2.6: *Number of monomer units per z axis unit length, $n(z)$, for the globule with $N = 200$ and $\chi = 1.4$ at various chain extensions.*

At a certain extension (at $D/a \approx 71 = D_{tr}/a$, at the transition point) the globular head disappears. The chain gets completely unfolded and enters the regime (3) Fig. 2.5 at $D/a = 71$. The disappearance of the globular head in the transition point leads to (i) a gain in the surface energy (since the interface disappears), (ii) a gain in the conformational entropy (since the chain tension decreases) and (iii) a penalty in the volume interaction free energy (since the monomer units that constituted the globular head get exposed to the solvent). The mutual cancelation of these three contribution determines the transition point. At larger extensions the tadpole conformation is metastable and the globule completely unfolds. The size of the disappearing globule in the transition point is still quite large (at $D/a = 71$ the numbers of monomer units in the tail and in the head can be estimated from Fig. 2.5 and Fig. 2.6 as $n_{tail} \approx 120$, $n_{head} \approx 80$).

The density profile in the strong stretching regime has the shape of a homogeneous sphero-cylinder with local maxima in the points where the chain end are fixed.

Special case: $\chi = 0.8$, $N = 200$

The case $\chi = 0.8$, $N = 200$ calls for special attention. The force extension curve, Fig. 2.4, has an untypical shape compared to those for larger χ values: there is no quasi-plateau regime at intermediate extensions and the force jump is missing. In

this case the unfolding and refolding branches of the free energy vs. deformation coincide, see Fig. 2.3.

The analysis of the density profiles and the axial monomer distributions, Fig. 2.7 and Fig. 2.8, respectively, demonstrates that in the considered case we encounter an essentially different unfolding mechanism: upon stretching the globule becomes more asymmetric and the density of its core decreases. What is also important, this transformation occurs *continuously*.

The reason of such a behavior can be explained as follows. The globule has an interfacial layer with a finite thickness which increases as χ decreases (as the solvent becomes better for the polymer). In the case of a short chain, the width of the interface becomes comparable to the size of the globule (radius). It appears that it is thermodynamically more preferable to reduce the density in the globular core rather than to form an extended tail keeping the (high) core density. Therefore, instead of a redistribution of the monomer units between a collapsed (globular) and a stretched phase, these are transferred from the core to the interfacial layer, as D increases.

Effect of the polymerization degree on the globule deformation

Let us consider in more detail the influence of the degree of polymerization N and polymer-solvent interaction parameter χ on the force-extension curves. Fig. 2.9 presents the force extension curves calculated for different values of N and χ. In order to compare the data for different N the forces were plotted vs the reduced extension $D/(Na)$. Fig. 2.9 shows that for all considered cases, except of $\chi = 0.8$, $N = 200$, three deformation regimes are observed: (i) a linear force growth with an increase in $D/(Na)$ at small extensions and (ii) a quasi-plateau in a wide range of $D/(Na)$ values ending by a sharp decrease in f followed by (iii) a universal force-extension dependence of the ideal chain (see Appendix 2.6, Eq. (2.32)). The position of boundaries between the regimes and the dependencies of the restoring force on the deformation in regimes (i) and (ii) are determined by N and χ, the force-extension relation in regime (iii) depends only on N. The χ-dependence was already discussed for $N = 200$, Fig. 2.4. Analysis of Fig. 2.9 shows that an increase in either N or χ has a similar qualitative effect on the shape of the force-extension curve. With an increase in χ or N the quasi-plateau region broadens mostly due to a noticeable shift of its right-hand boundary to larger $D/(Na)$ values and the weak displacement of its left-hand boundary to smaller $D/(Na)$. Therefore, it can be concluded that an increase in the chain length favors micro-segregation within the deformed globule. In particular we see that, in contrast to the case of $N = 200$ considered above, at $\chi = 0.8$ the globule formed by a longer chain unfolds via the formation of a micro-segregated (tadpole) structure with a subsequent drop in the reaction force. The height and the decaying slope of quasi-plateau also changes: with an increase in N and/or χ it shifts up and flattens. Upon a progressive increase in N the plateau level approaches some

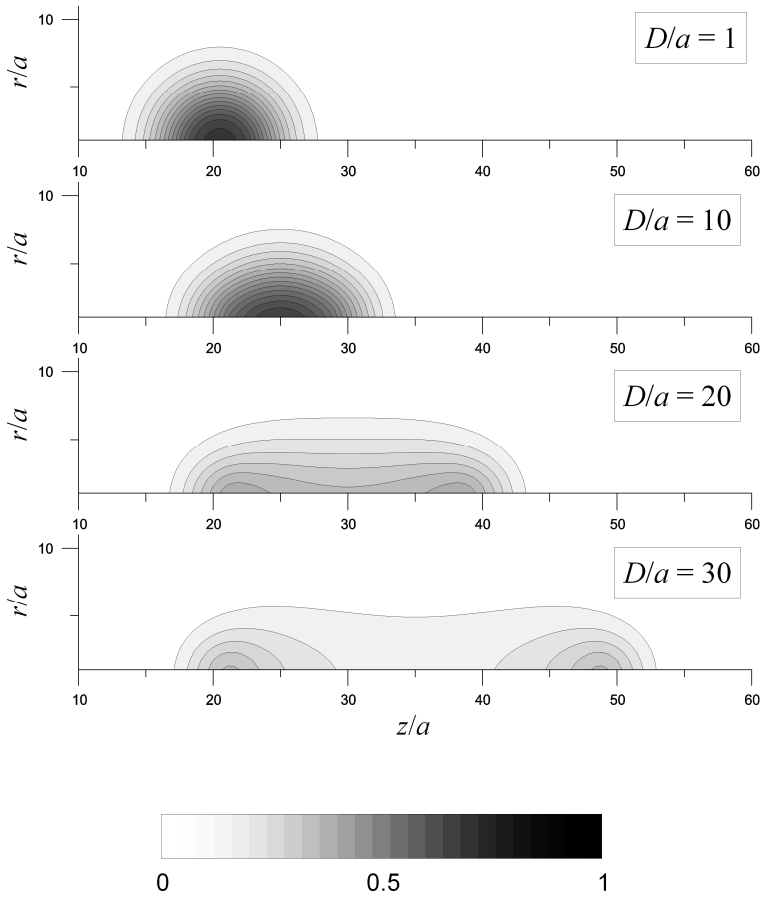

Figure 2.7: *Polymer density profiles $\varphi(r, z)$ for the globule with $N = 200$ and $\chi = 0.8$ at various chain extensions.*

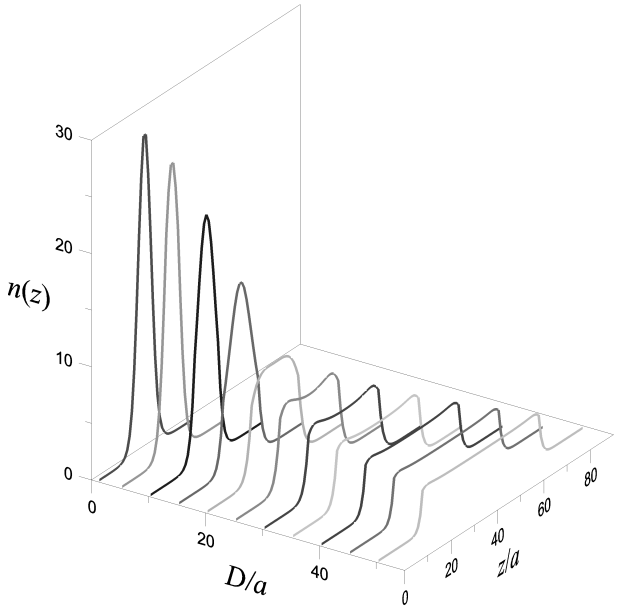

Figure 2.8: *Number of monomer units per z axis unit length, $n(z)$, for the globule with $N = 200$ and $\chi = 0.8$ at various chain extensions.*

asymptotic height controlled by the value of χ, whereas for given value of N it monotonously increases as a function of χ.

Taking into account the analysis of the conformations for $N = 200$ as discussed above, we can presume that the picture of the unfolding of the globule as predicted by the SF-SCF method retains the main general features such as (i) the three stages of unfolding (three deformation regimes), i.e., (cf Fig. 2.1) the growth of the force at small and strong deformations and its weakly decaying "quasi-plateau" behavior in the intermediate micro-segregated regime; (ii) a continuous microphase segregation (ellipsoid-tadpole) transition and the drop of the force in the second transition point where the micro-segregated structure becomes unstable and the globule completely unfolds. When the microphase segregation takes place, the head of the tadpole has a clear prolate ellipsoidal and not a spherical shape. On the other hand our SCF results clearly indicate that at moderately poor solvent quality the small globule unfolds without intra-molecular microphase segregated state.

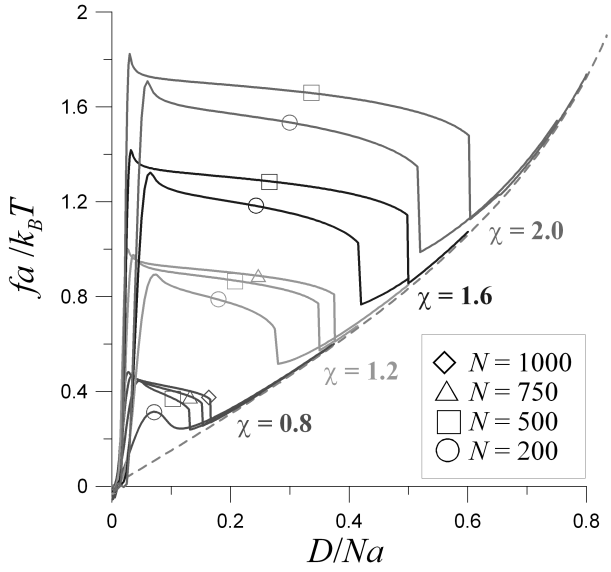

Figure 2.9: *Force extension curves at various values of N and χ.*

2.4 Blob picture of globule deformation

In this section we discuss the above described results obtained using SF-SCF approach in terms of the blob picture of globule deformation.

A blob picture of polymer globule

Let us consider again a single polymer chain with a degree of polymerization N immersed into a poor monomeric solvent. The chain is assumed to be intrinsically flexible, that is, the statistical segment length is of the order of a monomer unit length a, the latter coincides with the chain thickness. The binary attractive short-range (van der Waals) interactions between the monomer units are described in terms of Flory-Huggins interaction parameter $\chi > 0.5$. It is well known that in a poor solvent the polymer chain collapses into a spherical globule with a density φ which is a function of χ. Under moderately poor solvent strength conditions, that is when $(\chi - 0.5) \ll 1$, the monomer unit volume fraction in the globule scales as $\tau \sim (\chi - 0.5)$. The globule can be envisioned as an array of closely packed Gaussian thermal blobs, Fig. 2.1 a. The blob size, $\xi_t \simeq \tau^{-1}a$ is determined by the correlation length of the density fluctuations inside the globule. The size of an unperturbed globule scales as

$$R_0 \simeq (N/g_t)^{1/3}\xi_t \simeq (N/\tau)^{1/3}a \tag{2.11}$$

The chain fragments within a thermal blob retains Gaussian statistics, the number of monomer units per thermal blob scales as $g_t \simeq (\xi_t/a)^2$. The free energy of attractive monomer-monomer interaction per blob is of the order of thermal energy k_BT. Therefore the free energy of the globule scales (in the main term or in so called "volume approximation") as $F_{globule,v}/k_BT \simeq -N/g_t \simeq -Na^2/\xi_t^2 \simeq -N\tau^2$. A lower order correction in N arises due to the excess free energy of the interface between the collapsed globule and the (poor) solvent: the monomer units that are localized close to the interface exhibit in average more unfavorable contacts with the solvent than monomer units in the interior of the globule. In the scaling approximation an excess free energy of the order of $\simeq k_BT$ is attributed to each thermal blob localized at the globule interface. Hence, the excess free energy of the interface scales as $F_{globule,s}/k_BT \simeq (R_0/\xi_t)^2 = (N\tau^2)^{2/3}$. This excess interfacial free energy stabilizes the spherical shape of a free (non-deformed) globule.

Thus, thermodynamic properties of the globule are determined by the number of blobs (i.e. by the total number of blobs and by the number of surface blobs), while the globule size is controlled by both the number and the size of the blobs which are the functions of χ.

Globule deformation

Following the scaling approach of Halperin and Zhulina we now consider a deformed polymer globule as these occur when the end-to-end distance D is imposed.[14] The extensional deformation $D > 2R_0$ of the globule leads (under the constraint of the conservation of its volume) to an increase in the area of the interface, thus giving rise to an additional free energy penalty. The excess surface area of a weakly deformed globule, Fig. 2.1 b, grows as $\Delta S \simeq (D - 2R_0)^2$ as long as $(D - 2R_0) \lesssim R_0$ and here subscript "0" refers to the unperturbed globule. Hence, at weak deformations the restoring force that develops upon the extension of the globule, grows linearly with deformation,

$$f/k_BT = \partial(F_{globule,s}/k_BT)/\partial D \simeq (D - 2R_0)/\xi_t^2 \tag{2.12}$$

In the opposite limit of strong extensions, Fig. 2.1 d, $D \geq (N/g_t)\xi_t$, the intramolecular interactions do not affect the elastic response. Such chain obeys Gaussian entropic elasticity,

$$f/k_BT \simeq D/Na^2 \tag{2.13}$$

and can be presented as a string of Gaussian elastic blobs

$$D \simeq (N/g)\xi \tag{2.14}$$

of the size $\xi \leq \xi_t$.[25] We remark that here we do not consider the non-linear elasticity effects that may occur due to the finite chain extensibility of the chains. The latter becomes important at limiting extensions, $D \simeq Na$, see Appendix 2.6.

As has been noted by Halperin and Zhulina, in the intermediate range of extensions, $2R_0 \ll D \ll (N/g_t)\xi_t$, the surface area and the excess interfacial free energy of a homogeneously elongated (cylindrical or prolate ellipsoidal) globule scales as $F_{globule,s} \sim D^{1/2}$. This leads to a *decrease* of the restoring force as a function of the extension. The non-monotonic behavior may be identified as a van der Waals loop, suggesting an intra-molecular co-existence of an extended chain fragment ("tail") with a depleted spherical globular core, Fig. 2.1 c. According to Halperin and Zhulina the unfolding of the globule in the intermediate range of extensions occurs at fairly constant force,

$$f/k_BT \simeq 1/\xi_t \tag{2.15}$$

that corresponds to a tail consisting of a string of elastic blobs with a size equal to that of thermal blobs, ξ_t. If finite size corrections are considered, the coexistence plateau $f/k_BT \simeq 1/\xi_t \sim D^0$ is replaced by a region where the force f is a weakly decreasing function of the extension D. Indeed, consider the globule in the tadpole conformation, Fig. 2.1 c. Let us assume that the head of the tadpole has a spherical shape (that is, in the scaling analysis we can neglect the asphericity of the head) and is composed of n monomers. Then, the radius of the head scales as $R_{globule} \simeq (n/g_t)^{1/3}\xi_t \simeq (na^2\xi_t)^{1/3}$. The free energy of the tadpole accounts both for the contributions of the globule and the tail: $F_{tadpole} = F_{globule} + F_{tail}$. The free energy of the globule contains volume and surface terms

$$\frac{F_{globule}}{k_BT} \simeq -\frac{n}{g_t} + \frac{S_{globule}}{\xi_t^2} \simeq -\frac{na^2}{\xi_t^2} + \left(\frac{na^2}{\xi_t^2}\right)^{2/3}. \tag{2.16}$$

The tail consists of $N - n$ monomers and can be represented as a stretched string of thermal blobs. The tail length is $D - 2R_{globule}$. The number of blobs in the tail scales as $(N - n)/g_t \simeq (N - n)(a/\xi_t)^2$. Therefore the tail length can also be expressed as $D - 2R_{globule} \simeq (N - n)a^2/\xi_t$. The free energy of the tail comprises an elastic contribution which is proportional to the number of thermal blobs in the tail

$$\frac{F_{tail}}{k_BT} \simeq \frac{(D - R_{globule})^2}{(N - n)a^2} \simeq \frac{(N - n)a^2}{\xi_t^2}. \tag{2.17}$$

As a result, the free energy of the tadpole is

$$\frac{F_{tadpole}}{k_BT} \simeq \left(\frac{na^2}{\xi_t^2}\right)^{2/3} + \frac{(N - 2n)a^2}{\xi_t^2}. \tag{2.18}$$

The restoring force is calculated as

$$\frac{f_{tadpole}}{k_BT} = \frac{1}{k_BT} \cdot \frac{dF_{tadpole}/dn}{dD/dn} \simeq \frac{1}{\xi_t}\left[1 - \left(\frac{\xi_t}{a}\right)^{2/3}\frac{1}{n^{1/3}}\right] \simeq \frac{1}{\xi_t}\left[1 - \left(\frac{g_t}{n}\right)^{1/3}\right] \tag{2.19}$$

and we notice that as D increases, then both n and thus f decrease.

Ellipsoid-to-tadpole transition

The location of the ellipsoid to tadpole transition can be estimated using simple arguments. A weak deformation of the globule, Fig. 2.1 a, into the ellipsoid, Fig. 2.1 b, produces a restoring force (2.12). The phase segregation inside the weakly deformed globule starts when this force becomes equal or comparable to the plateau force, Eq. (2.15) . This gives the threshold extension

$$D \simeq 2(\xi_t + R_0) \simeq 2[\xi_t + (Na^2\xi_t)^{1/3}] \simeq 2(Na^2\xi_t)^{1/3} \tag{2.20}$$

which size is of the same order as that of the unperturbed globule.

Tadpole-to-open chain transition

The next step is to consider the transition from a microphase segregated tadpole, Fig. 2.1 c, to the open conformation, Fig. 2.1 d. In the transition point the free energies of the tadpole and open conformation should be equal: $F_{tadpole} = F_{chain}$. The free energy of the tadpole is given by Eq. (2.18). The free energy of the extended (open) chain is calculated similarly to F_{tail}, Eq. (2.17).

$$\frac{F_{chain}}{k_BT} \simeq \frac{D^2}{Na^2} \simeq \frac{(N-n)^2a^2}{\xi_t^2 N}. \tag{2.21}$$

where we have use the approximation that in the vicinity of the transition point the tail length is much larger than the globule size and, therefore, the tail size can be considered as being approximately equal to the overall chain extension

$$D \simeq \frac{N-n}{g_t}\,\xi_t \simeq \frac{(N-n)a^2}{\xi_t} \tag{2.22}$$

Equating the free energies of the tadpole and the open chain, we obtain that the number of monomers in the head of the tadpole (globule) in the transition point scales as

$$n \simeq N^{3/4}\left(\frac{\xi_t}{a}\right)^{1/2} \tag{2.23}$$

or

$$\frac{n}{g_t} \simeq \left(\frac{N}{g_t}\right)^{3/4} \tag{2.24}$$

that is, the number of blobs in the "minimal globule" is determined by the number of blobs in the whole chain. Scaling dependence of n vs. N in the transition point with the chain length N was obtained by Cooke and Williams, who considered the limiting case of a "dry" globule.[15]

As a result, the size of the head at the transition point $R_{globule} \simeq (na^2\xi_t)^{1/3} \simeq N^{1/4}(\xi_t a)^{1/2}$ depends on N and is much larger than the thermal blob size ξ_t. The

jump in the reaction force is

$$\frac{\Delta f}{k_B T} = \frac{f_{chain} - f_{tadpole}}{k_B T} \simeq \frac{D}{(N-n)a^2} - \frac{D}{Na^2} \simeq \frac{1}{a} \cdot N^{-1/4} \left(\frac{\xi_t}{a}\right)^{-1/2}. \quad (2.25)$$

We see that the jump in the force at the transition point should increase with an increase in χ and decrease with an increase in N thus vanishing in the thermodynamic limit $N \to \infty$.

Arbitrary d case

The above scaling analysis can be generalized in a way that takes into account an arbitrary dimensionality of the system d. In addition to the spherical globule case, which is the main subject of the present paper, corresponding to $d = 3$, we consider a polymer "bridging brush" immersed into a poor solvent and pulled by an external force, which is effectively a one-dimensional system, $d = 1$.[22] Similarly, as a two-dimensional case, $d = 2$, we can propose a cylindrical brush (bottle-brush) whose arms are simultaneously and equally pulled out in the radial direction (out of main chain or the grafting line).

If the globular head contains n monomers, the size of the globule scales as $R_{globule} \sim \xi_t \left(na^2/\xi_t^2\right)^{1/d}$. Hence, the surface area per globule (per chain) is $S_{globule} \sim \left(R_{globule}/\xi_t\right)^{d-1} \xi_t^2 \sim \left(na^2/\xi_t^2\right)^{(d-1)/d} \xi_t^2$. This will generalize the surface contribution to the free energy of the tadpole, the second term in Eq. (2.18), the other contributions to $F_{tadpole}$ as well as to F_{chain} remain unchanged. The relation between the tail length and n is $D - 2R_{globule} \simeq (N-n)a^2/\xi_t$.

Taking this into account, the generalized expressions for the reaction force in the tadpole regime (2.19) reads

$$\frac{f_{tadpole}}{k_B T} \simeq \frac{1}{\xi_t}\left[1 - \frac{d-1}{d}\left(\frac{na^2}{\xi_t^2}\right)^{-1/d}\right] \simeq \frac{1}{\xi_t}\left[1 - \frac{d-1}{d}\left(\frac{n}{g_t}\right)^{-1/d}\right] \quad (2.26)$$

Since with an increase in D, n obviously decreases. Eq. (2.26) shows that $f_{tadpole}$ is a (weakly) decreasing function of the extension D for $d = 2$ and 3, whereas for $d = 1$ it is constant giving a true plateau on the force-extension curve.

For the location of the transition of the tadpole to the open chain the expression (2.23) for the number of monomers in the tadpole's head is modified as

$$n \simeq N^{\frac{d}{d+1}} \left(\frac{\xi_t}{a}\right)^{\frac{2}{d+1}} \simeq N^{\frac{d}{d+1}} g_t^{\frac{1}{d+1}} \quad (2.27)$$

and for the force jump, Eq. (2.25), we have

$$\frac{\Delta f}{k_B T} \simeq \frac{1}{\xi_t} \cdot \left(\frac{\xi_t^2}{Na^2}\right)^{\frac{1}{d+1}} \simeq \frac{1}{\xi_t} \cdot \left(\frac{g_t}{N}\right)^{\frac{1}{d+1}}. \quad (2.28)$$

Remark that in the case $d = 1$ corresponding to the planar polymer brush we recover the scaling $n \sim N^{1/2}$ obtained earlier for the size of the microphase emerging in the brush capable to undergo a first order phase transition.[26–29]

Comparison of SCF results and scaling dependencies

The numerical results of the SCF modeling are in good qualitative agreement with the scaling laws obtained in the framework of the blob picture. In more detail, the result of the SCF theory have confirmed the existence of three regimes of extension of the globule as predicted by the blob model, namely (i) the deformation (extension) of the globule as a whole, (ii) the coexistence of a globular and unfolded (extended) phases, (iii) the disappearance of the globule and the further extension of the unfolded chain. The SCF results have further pointed to the possible departure from this scheme in the case of short chains and moderate values of the solvent quality χ.

A qualitative agreement of results of the SCF calculations and the blob model is also found for the dependences of the shape of the force-extension curve on the solvent quality and chain length. The parameters of the blob model are: (i) the blob size which decreases with χ and (ii) the total number of blobs in the chain, the latter grows as a function of N and χ. According to the blob model, the formation of an extended tail starts when the extension slightly exceeds the unperturbed globule size $D \sim (Na^2\xi_t)^{1/3}$. Correspondingly, the value of the ratio $D/(Na)$ at this transition point should decrease upon an increase in χ and N, exactly as is observed in the SCF modeling. According to the blob model, the height of the quasi-plateau on the force-extension curve should increase as a function of χ (due to the decrease in ξ_t) and N, that is, upon the increase in the total number of blobs. The latter determines the magnitude of the correction term in Eq. (2.19). A decrease in the number of blobs in the globular phase, n/g_t, leads to a decreasing reaction force. Also, the jump-like decomposition of the globule at large $D/(Na)$, as predicted by the scaling analysis is in agreement with the SCF analysis.

At this stage it is necessary to realize that the blob model is not strictly applicable for the values of χ and N used in our SF-SCF simulations. The notion of a Gaussian thermal blob itself only has a meaning when the number of the monomer units in the blob, g_t, is large enough. This is only the case at relatively small deviation from the Θ-point, $\tau = (\Theta - T)/T \ll 1$. The range of χ-values considered in the present work obviously does not satisfy this demand. Furthermore, the total number of thermal blobs in the chain is $\sim N\tau^2$ and this number should be large to use scaling arguments. Hence, the scaling parameter of the blob model is $N^{1/2}\tau$, that requires at small values of τ much larger chain lengths N as compared to those used in the numerical analysis. In the SCF modeling the value of N used in the calculations was restricted from above by computational reasons.

Admittedly, the blob model includes some simplifying assumptions as well. In

particular, it is assumed that in the tadpole conformation, the globular head has a spherical shape. However, as one can see from the density profiles, Fig. 2.5, the head has a prolate (ellipsoidal) shape rather than a spherical one. As a consequence, in the prolate globule, there appears a reaction force tending to restore its unperturbed spherical shape. In the tadpole this force is balanced by the elastic force from the tail. The analytical model that takes into account the non-spherical shape of the tadpole head and properly accounts for the force equilibrium will be considered in a follow up publication. We note, however, that the "spherical head assumption" does not affect the scaling dependencies obtained in this section.

2.5 Conclusions

We have performed detailed SCF calculations of the equilibrium unfolding of a globule formed by a flexible homopolymer chain collapsed in a poor solvent and subjected to an extensional deformation. More specifically, we consider the conformational characteristics adopted by a chain with imposed end-to-end distances in a wide range of (poor) solvent qualities (expressed in terms of Flory-Huggins solubility parameter χ) and polymerization degrees N. The fluctuating restoring force (i.e., the elastic force) is calculated as a function of the end-to-end distance. These results are collected in force-deformation curves.

In accordance to predictions of the scaling theory by Halperin and Zhulina, we have observed a sequence of intra-molecular conformational transitions that occur upon an increase of the deformation. We have found that there is a linear response regime (found at small deformations). This is followed by an intra-molecular micro-phase segregation regime (found at intermediate extension): here a uniformly stretched segment of the chain (a "tail") co-exists with a collapsed globular domain (a "core"). A progressive increase in the end-to-end distance of the chain is accompanied by a systematic depletion of the globular core and a re-partitioning of the monomer units into the stretched tail. We have found that the unfolding of the globular core occurs at a weakly decreasing (fairly constant) reaction force, whereas the entropic elasticity is predicted to be recovered at strong extensions.

The general shape of the force-extension curves obtained using the SF-SCF approach appears to be unconventional, showing a more or less extended region with an anomalous dependence with $df/dD < 0$, i.e. with a negative extensional modulus. In fact, $f(D)$ curves exhibit the van der Waals loop, which is usually an indicator of the instability of a system. However, if the role of the governing parameter is played by the end-to-end distance, the system cannot avoid these states and passes through them step by step thus undergoing a sequence of intra-molecular conformational transitions.

We have found that the intra-molecular co-existence occurs only for sufficiently long polymers and at large values of the χ parameter. In other cases,

that is, for relatively short chains (number of segments of the order of 10^2) and mild solvent conditions $\chi \sim 1$, a uniformly stretched conformation is retained and no microphase segregation is predicted to occur in the whole range of extensional deformations. Nevertheless the force-extension curve exhibits a region with $df/dD < 0$. Hence, we predict that the phase diagram of the system in N, D or χ, D coordinates contains an one-phase and two-phase regions and thus exhibits a critical point.

Furthermore, we have analyzed two conformational transitions: (i) the first one is from the weakly elongated (ellipsoidal) globule to the tadpole, which consists of a ellipsoidal globular core coexisting with a stretched tail and (ii) the second one is from the tadpole conformation to that of a uniformly stretched chain – the unraveling transition discovered by Cooke and Williams.[15] The first transition, that is the formation of a stretched intra-molecular micro-phase occurs continuously, whereas the second transition occurs as the first order phase transition and the reaction force drops abruptly down at certain elongation threshold.

We anticipate that the patterns predicted by our theory should manifest in force-deformation spectra that can be obtained, e.g., by means of single-molecule AFM spectroscopy on end-grafted polymers collapsed upon a decrease in the solvent strength. The latter can be achieved by variation in temperature or in pH for thermo- or pH sensitive polymers, respectively. The most straightforward way for a synthetic implementation of this system is to graft polymer chains to a solid surface, for example by means of radical polymerization initiated at the surface. Typical degrees of polymerization obtained in controlled radical polymerization approach values as high as $10^2 - 10^3$.

It is interesting to point to other polymeric systems that behave similarly to the stretched globule in a sense that these relieve the stress caused by an external field by "throwing out" a part of the chain as a new phase, thus forming a microphase segregated state. This is for example the case for a Gaussian chain compressed between two pistons. This chain undergoes an abrupt transition from a confined coil state to an inhomogeneous flower-like conformation partially escaped from the gap.[30,31] In the transition (microphase coexistence) region this system exhibits a negative compressibility, i.e. the reaction force decreases with an increase in deformation (corresponding to a decrease in a distance between the pistons, or chain squeezing) whereas at small and large deformation it grows.

In the presented paper all results concern the deformation of a globule in the constant extension ensemble. In the conjugate constant force ensemble, one should expect that the tadpole conformation will be unstable and the globule will unfold jumpwise, as a transition going from the ellipsoid globule directly to the open chain. This is confirmed by the results of molecular dynamics[32] and Monte Carlo[33] simulations. However, in the case of lattice models or when the formation of helical conformation is possible a multistep transition can be observed.[34,35]

2.6 Appendix. Conformational free energy of strongly stretched chains on a cylindrical lattice

The aim of this Appendix is to derive the conformational free energy of a chain in a cylindrical lattice as a function of the end-to-end distance D. It can be easily calculated if we consider an ideal chain extended by an external force (external field), i.e. we temporarily "switch" from the fixed stretching ensemble studied in this paper to the fixed force ensemble, that is the common Ansatz in statistical physics, and then switch back to the fixed deformation ensemble studied in this work.

Suppose that the chain walking on the cylindrical lattice is subjected to a force f directed along the z-axis. For the sake of comparison with numerical results, we set the transition probabilities for the random walk according to SF-SCF model. Namely, the probability to make a step either in r or in z direction is given by λ_1, the probability of a step in "rz"-direction, i.e. simultaneously changing both r and z coordinates by ± 1 is λ_2 whereas the rest, $\lambda_0 = 1 - 4\lambda_1 - 4\lambda_2$ is the probability to change the angular coordinate φ. Then the statistical weight of a monomer (of a link) is given by

$$\begin{aligned} w &= (\lambda_0 + 2\lambda_1)e^0 + (\lambda_1 + 2\lambda_2)e^{fa/k_BT} + (\lambda_1 + 2\lambda_2)e^{-fa/k_BT} \\ &= 1 - 2\lambda_1 - 4\lambda_2 + 2(\lambda_1 + 2\lambda_2)\cosh\left(\frac{fa}{k_BT}\right) \end{aligned} \tag{2.29}$$

Then the partition function of the chain is

$$Z = \left[1 - 2\lambda_1 - 4\lambda_2 + 2(\lambda_1 + 2\lambda_2)\cosh\left(\frac{fa}{k_BT}\right)\right]^N \tag{2.30}$$

The logarithm of the partition function gives us *the Gibbs free energy*,

$$G_f = -k_BT\log Z = -Nk_BT\cdot\log\left[1 - 2\lambda_1 - 4\lambda_2 + 2(\lambda_1 + 2\lambda_2)\cosh\left(\frac{fa}{k_BT}\right)\right] \tag{2.31}$$

Once the partition function (the Gibbs free energy) is known, the extension D corresponding to the force f can be found straightforwardly:

$$D = -k_BT\cdot\frac{\partial G_f}{\partial f} = Na\cdot\frac{2(\lambda_1 + 2\lambda_2)\sinh\left(\frac{fa}{k_BT}\right)}{1 + 2(\lambda_1 + 2\lambda_2)\left[\cosh\left(\frac{fa}{k_BT}\right) - 1\right]} \tag{2.32}$$

and we see that the force is a universal function of the *reduced* extension $D/(Na)$.

In order to return to the fixed extension ensemble, one can use the standard relation between the free energies in f- and D- ensembles (Gibbs and *Helmholz* free energies, respectively)

$$F_D = G_f + D\cdot f \tag{2.33}$$

this gives the conformational free energy of the chain having its ends fixed at the distance D:

$$F_{chain} = F_D = -Nk_BT \cdot \log\left[1 - 2\lambda_1 - 4\lambda_2 + 2(\lambda_1 + 2\lambda_2)\cosh\left(\frac{fa}{k_BT}\right)\right] + Naf \cdot \frac{2(\lambda_1 + 2\lambda_2)\sinh\left(\frac{fa}{k_BT}\right)}{1 + 2(\lambda_1 + 2\lambda_2)\left[\cosh\left(\frac{fa}{k_BT}\right) - 1\right]} \tag{2.34}$$

In Eq. (2.34) F is expressed as a function of f but together with Eq. (2.32) it parametrically defines F as a function of D.

In the weak deformation limit we obtain

$$\frac{F_{chain}}{k_BT} = \frac{1}{4(\lambda_1 + 2\lambda_2)} \cdot \frac{D^2}{Na^2}. \tag{2.35}$$

So, we see that the elastic free energy has the Gaussian form

$$\frac{F_{chain}}{k_BT} = k \cdot \frac{D^2}{Na^2} \tag{2.36}$$

with $k = 1/4(\lambda_1 + 2\lambda_2)$. The corresponding reaction force is

$$\frac{f_{chain}}{k_BT} = 2k \cdot \frac{D}{Na^2}. \tag{2.37}$$

In the strong deformation limit $\sinh(fa/k_BT) \simeq \cosh(fa/k_BT) \simeq \frac{1}{2}\exp(fa/k_BT)$ and Eq. (2.32) gives

$$\frac{f_{chain}}{k_BT} = \log\left[\frac{2(2k-1) \cdot D/(Na)}{1 - D/(Na)}\right]. \tag{2.38}$$

The reaction force asymptotically tends to infinity as D approaches Na.

Comparing analytical force-extension curve (2.32) with SF-SCF numerical results (Figures 2.4 and 2.9; analytical curves are shown by dotted lines), we see a perfect correspondence in the uniformly stretched chain regime.

Acknowledgement

This work has been performed as a part of the collaborative research project SONS-AMPHI within the European Science Foundation EUROCORES Program, and has been partially supported by funds from the EC Sixth Framework Program through the Marie Curie Research and Training Network POLYAMPHI. Support by the Dutch National Science Foundation (NWO) and the Russian Foundation for Basic Research (RFBR) through Joint Project 047.017.026/06.04.89402 and Project 08-03-00336a is gratefully acknowledged.

CHAPTER 3

Modeling of triblock terpolymer micelles with a segregated corona [1]

[1] Published with minor changes by Marat Charlaganov, Oleg V. Borisov, Frans A.M. Leermakers in Macromolecules 41 (2008) p.3668.

We report on self-consistent field predictions for the formation of spherical micelles by $A_N B_M C_N$ triblock terpolymers in a selective solvent, i.e., a good solvent for the A_N and C_N blocks and a poor solvent for the middle B_M block. Above some threshold value for the repulsion between the A and C monomers, we find micelles with a laterally segregated corona, i.e., Janus micelles. We consider the thermodynamic stability, the size, and the size fluctuations of these micelles. The transition between the homogeneous and the segregated states is smooth not only because of the finite size of the system, but also due to the compositional symmetry within the triblock terpolymer. It is found that the aggregation number decreases with increasing repulsion between A and C below-, and increases above the transition point. The formation of the interface is triggered by the high polymer density near the core. The interface between the A and C rich regions occupies a constant angle in spherical coordinates. This means that it widens in the radial direction. In these micelles the lateral segregation gives a new fluctuation mode to the micelles, as the lateral segregation is strongly coupled to the aggregation number, we anticipate a rich behavior in experimental systems.

3.1 Introduction

The field of molecular self-assembly enjoys continuous interest already over several decades.[36,37] The best known example is the micellization of short chain surfactants. The number of applications is many. They are used as detergents, in formulation science and as wetting agents to name a few.[38] High molecular weight counterparts become increasingly studied because well-defined specimen are nowadays readily available. Much of what is known for surfactants is being applied to polymeric analogues.

Amphiphilic diblock copolymers are the simplest polymers able to form micelles. Similar to low molecular weight surfactants they feature a solvophobic block which escapes from the solvent and forms a dense core and a solvophilic block which accumulates on the outside and forms the corona. Simple geometric considerations indicate that when the aggregation number, i.e. the number of molecules in the micelle, increases the surface area per molecule decreases. As a result the corona-forming block becomes stretched and this gives the main stopping mechanism for the assembly. The critical polymer concentration at which micelles start to form spontaneously (cmc) is typically very low.

There are several advantages of using polymeric micelles over surfactant ones.[39] From an application point of view it is important that polymeric micelles are usually substantially larger than their low molecular weight analogues. Then, for macromolecules there exists a large degree of flexibility to choose the chemical composition of the blocks, resulting in weak to strong segregation of the solvophobic block with the solvent. Moreover, one can introduce chemical groups with tunable interaction and employ the cooperative nature of macromolecules to obtain responsive systems.

Recently, the self-assembly of ABC triblock terpolymers attracted substantial attention. In comparison with diblock copolymers, terpolymers offer additional flexibility for controlling the self-assembly process. They are known to demonstrate rich bulk phase behavior resulting in various microsegregated structures.[40] In solution block terpolymers are able to form aggregates with complex morphology.[41–43] For example, the corona of a micelle formed by a double solvophylic terpolymer unavoidably contains two chemically different blocks. From polymer solution theory we know that two chemically different polymers have the tendency to demix above some critical concentration. Thus, we may expect microphase segregation in the micellar corona.

Segregation in micellar coronas was observed experimentally in micelles with a cross-linked core[44,45] and complex coacervate core micelles.[46,47] The micelles reported in ref.[44–46] feature a laterally segregated two-compartment corona. Micelles of this type are usually referred to as Janus micelles. The micelles with a cross-linked core were shown to act as super-surfactants and experience higher levels of self-assembly.[44,45]

Below we will use a self-consistent field (SCF) approach to study the structural as well as thermodynamical properties of micelles formed by $A_N B_M C_N$

triblock terpolymers. We consider highly symmetrical terpolymers with an insoluble middle block B and two equally soluble side blocks A and C. The length of the corona blocks N is chosen to be long enough to be in the spherical micellar regime.[48] In the SCF method the interactions between the monomers are accounted for using Flory-Huggins dimensionless exchange interaction parameters.[2] The value of this parameter is negative for attraction and positive for repulsion. The triblock terpolymer $A_N B_M C_N$ is equivalent to the copolymer $A_N B_M A_N$ if the monomers A and C have a zero interaction parameter with each other ($\chi_{AC} = 0$) and equal interaction parameters with the other monomers ($\chi_{AS} = \chi_{CS}$, $\chi_{AB} = \chi_{BC}$). Therefore in the limit of low χ_{AC} the thermodynamic and structural properties of terpolymer micelles are similar to those of copolymer ones. However, above some critical value of χ_{AC} we expect a transition to Janus-type micelles with various novel characteristics.

The theory indicates that in the corona of spherical micelles one can distinguish at least three distinct regions.[49,50] The inner region, that is closest to the core, is characterized by a power law density decay (depending on the solvent quality) which is forbidden for the free chain ends (best seen when the micelle resembles a star, i.e., for a small core). Then, further away from the core the curvature of the micelle is less pronounced, i.e. the local curvature is quasi-planar and as a consequence the density profile is parabolic-like. Finally, at the periphery the profile decays exponentially towards the bulk. The same regions must exist in micelles with a segregated corona.

Also relevant for Janus micelles, we know that macrophase segregation of polymers in bulk solutions depends on interaction parameters, polymer concentrations, chain lengths, etc.[2] One of the issues is which known results of the bulk phase behavior are transferable to the present problem. For example, the critical condition for segregation of two polymers A and C of equal length N, and total volume fraction φ_p in a non-selective good solvent, is given by $N\varphi_p\chi_{AC} = 2$.[2,3] Due to the dependence of the polymer volume fraction in the corona on the distance from the core, it is not *a priori* known how and when segregation will occur. Also, from macroscopic phase studies we know that the interface between two phases diverges upon the approach of the critical point.[51] For Janus micelles, however, we expect a non-trivial structure of the interface between A and C and it is clear that the width of the interface can not exceed the size of the micelle. Indeed, the characterization of the interface in the corona is one of the main issues of this paper. At this stage we may anticipate various other consequences of having an interface between A and C. One of these is that the spherical topology of the micelle not necessarily is found even when the length of the A and C blocks are sufficiently large.

In the most naive model the micellization is a first-order phase transition. In this picture the micelle size is constant. Upon an increase in overall polymer concentration above the cmc only the number of micelles increases. This occurs in the naive model at a fixed polymer chemical potential. However, as the size of the micelles remains finite, it must be the case that the micellization transition

is smooth, i.e., it can not be first order. The fundamental issue here is that each micelle has translational degrees of freedom and the mixing entropy on the micellar level depends on the micelle concentration. In the surfactant science community this fact is well-recognized.[52] It is well-known that upon increasing the overall surfactant concentration the micelle concentration increases sharply (in line with the naive model). The free surfactant (unimer) concentration, however, does not remain constant, but increases slightly. This increase of the unimer concentration has corresponding effects on the micelle size. Indeed, with increasing micelle concentration the micelle size increases necessarily. In many cases, this increase in aggregation number is, above some threshold concentration, accompanied by a change in micellar geometry.[53] This point is often referred to as the second cmc, and also occurs as a cooperative, but smooth transition.[54,55]

For simple diblock copolymer micelles there exist scaling predictions for many of its properties such as the aggregation number, the size of the core and corona, etc., as a function of the block lengths.[48] For these predictions, typically the translational degrees of freedom of the micelles is ignored, i.e., these are made in the naive phase transition picture. The arguments that are used to motivate this naive picture is that with increasing size of the micelles, that is, with increasing aggregation number, the micellization transition gradually becomes closer to a true first-order transition. Below we will keep the micellar translational entropy in our considerations.

The remainder of this paper is the following. Before we can examine the structure of micelles in the SCF model, it is necessary to verify that the micelles that have been generated are thermodynamically stable. We therefore will start our theoretical section with a short review of the thermodynamics of small systems that is used for this. This is followed by a brief review of the SCF model. In the result section we will focus on the symmetrical case only, i.e. $N_A = N_C$, for which the solvent is good and non-selective for the corona chains, and poor for the core block. The conclusions are formulated at the end as usual.

3.2 Theory

Small system thermodynamics

Self-consistent field theory for self-assembly rests on the notion of thermodynamics of small systems. The approach developed by Hill,[56] assumes that the real system is divided into $\aleph$ subsystems, which each have the same composition as the overall system. The Gibbs energy is then optimized with respect to the number of small systems. In the case of micellar solution each subsystem will contain one micelle and thus $\aleph$ is identified as the number of micelles.[52] Combination of first and second law of thermodynamics gives for the differential of the Gibbs energy of the macroscopic system

$$\mathrm{d}F = -S\mathrm{d}T + V\mathrm{d}P + \sum_i \mu_i \mathrm{d}n_i + \epsilon \mathrm{d}\aleph \tag{3.1}$$

where the value conjugated to the number of small systems is the subdivision work. All other quantities have their usual meaning. The subdivision work is also the work necessary to create one more micelle in the system with fixed number of molecules n_i of each type i, therefore it can be alternatively identified as the aggregation work. For an incompressible system with fixed number of molecules and temperature T the minimum of the Gibbs energy is defined by

$$\left.\frac{\partial F}{\partial \aleph}\right|_{T,P,n_i} = \epsilon = 0 \tag{3.2}$$

$$\left.\frac{\partial \epsilon}{\partial \aleph}\right|_{T,P,n_i} > 0 \tag{3.3}$$

Note that the aggregation work ϵ is related to the overall grand potential in the system, i.e. $\epsilon\aleph = F - \sum_i n_i\mu_i$. Indeed, for homogeneous bulk systems this quantity is necessarily zero.

Even though we have introduced just one number, $\aleph$, of the total number of micelles in the system, this does not imply that it is assumed that all micelles are identical. In fact the result thus far is completely general and allows for any micelle size distribution, as well as for the case that micelles strongly interact. As usual however, classical thermodynamics can not provide us with much more molecular insight. For this we must turn to a molecular model. Within such model we have to make approximations. Even though in real-life micelles are not uniform, our model will consider the so-called most-probable micelle. This is reasonable because the size distribution (of spherical micelles) is usually sharp. Of course there will always be a distribution in sizes and, sometimes, shapes. Fluctuations in micelle size and shape can be estimated from the theoretical model, but this usually involves approximations as well.

Realising that ϵ is the conjugate variable coupled to the number of micelles $\aleph$, we can also identify ϵ as an excess chemical potential of the micelle. From this perspective it is natural to write for dilute micellar solutions

$$\epsilon = \ln \varphi_m + \epsilon_m \tag{3.4}$$

Here, as well as in the remainder of this paper, we have omitted the thermal energy k_BT factors. This means that all energy units are expressed in units of k_BT. In Eq. 3.4 φ_m is the volume fraction of micelles, and thus the first term on the right hand side gives the entropic contribution that accounts for the translational degree of freedom of the micelle. Then, ϵ_m may be identified as the (dimensionless) translationally restricted grand potential of the micelle. As we will see, the latter quantity is the primary thermodynamic quantity in the SCF analysis.

Self-consistent field modeling

In the previous paragraph we have presented generally applicable thermodynamic considerations for self-assembling systems. In a molecular model there are always details and approximations such that the application of these general considerations is delicate. We will therefore first go into details about the thermodynamic aspects from the perspective of the SCF modeling. Only after that we will outline the machinery of the SCF method. From here on, all lengths are made dimensionless with the segment length l.

Thermodynamics of self-assembly for the SCF approach

The first issue is that we need to solve the SCF equations (to be specified below) numerically. To do this we need to introduce a discretization scheme. We will use the method of Scheutjens and Fleer for this[4,61]. According to this method there is a system of lattice coordinates in which layers are identified over which the mean-field approximation (to be specified below) is implemented. Effectively this implies that one can find only those micellar geometries that are consistent with the chosen geometry. In addition it appears that the micelles that are predicted in this method have no collective degree of freedom. Usually one considers just a single micelle in the (small) system and effectively one thus focuses on so-called most-likely micelles. One advantage of a lattice model is that the volume of the molecules is quite naturally accounted for as each monomer or each segment of the chain occupies a single lattice site. This is usually combined with an incompressibility condition which effectively says that the volume is fully occupied by molecular species. In such an approach there is no volume work in the thermodynamic description and therefore we can write for the Gibbs energy (which in the incompressible limit equals the Helmholtz energy) of a small system F as it appears in the SCF model

$$F = \sum_i n_i \mu_i + \epsilon_m \tag{3.5}$$

Introducing excess quantities by subtracting all bulk quantities, i.e. $F = F^\sigma + V f^b$ where V is the volume of the small system and f^b if the free energy density in the bulk, we obtain

$$F^\sigma = \sum_j n_j^\sigma \mu_i + \epsilon_m \tag{3.6}$$

Below we will show that from optimizing the canonical partition function the F is available and Eq. 3.5 is then used to compute ϵ_m. The differential of the translationally-restricted grand potential is given by

$$\mathrm{d}\epsilon_\mathrm{m} = -\mathrm{sdT} - \sum_\mathrm{j} \mathrm{n}_\mathrm{j}^\sigma \mathrm{d}\mu_\mathrm{j} \tag{3.7}$$

where the summation over j is over all non-solvent components. Below we will have only one polymeric component (p) and use for the aggregation number $g \equiv n_p^\sigma$. The Gibbs-Duhem equation for this case is, for fixed temperature, given by:

$$\frac{\partial \epsilon_m}{\partial \mu_p} = -g \tag{3.8}$$

From the modeling we obtain information on the aggregation number dependence of the translationally-restricted grand potential $\epsilon_m(g)$, as well as that for the chemical potential $\mu_p(g)$. From Eq. 3.8 we can find

$$-\frac{\partial g}{\partial \epsilon_m} = \frac{1}{g}\frac{\partial g}{\partial \mu_p} = \frac{\sigma_g^2}{g} \tag{3.9}$$

Where $\sigma_g^2 = \langle g^2 \rangle - \langle g \rangle^2$ is a measure for the fluctuation in aggregation number of the micelles. As this number is necessarily positive, we conclude that for stability $\epsilon_m(g)$ is a decreasing function with g or equivalently $\mu_p(g)$ is an increasing function of g. At this point it is illustrative to make a link to the classical thermodynamics. It is quite natural to expect that the average aggregation number is a decreasing function of the number of micelles in the system and thus that $\partial \aleph / \partial g < 0$. The stability in the small system $\partial \epsilon_m / \partial g < 0$ is thus closely related to that in the overall system $\partial \epsilon / \partial \aleph > 0$.

At this point it is necessary to understand that in the SCF calculation the total volume available for a micelle is not influencing the calculations (as long as this volume is sufficiently large such the micelle does not interact with its neighbors). The simple reason for this is that the micelle is effectively fixed with its center of mass to a point in the coordinate system. For example in a spherical coordinate system the micelle is fixed in the center. We may use Eq. 3.4 to estimate the actual volume available for a given micelle with known aggregation number g. This equation implies $\varphi_m = e^{-\epsilon_m(g)}$ (recall that the ϵ_m is made dimensionless by the thermal energy $k_B T$). Assuming that a micelle is composed of a dense packing of chains, the volume fraction of micelles may be approximated by $\varphi_m \approx vgN/V_{ss}$, where v is a unit volume occupied by a segment. Using this we can compute the overall volume fraction of polymer chains

$$\varphi_p^t = \varphi_p^b + \varphi_m = \varphi_p^b + e^{-\epsilon_m} \tag{3.10}$$

Using this we can distinguish two regimes. Below the cmc we will have $\varphi_m << \varphi_p^b$ and $\varphi_p^t \approx \varphi_p^b$, whereas above the cmc $\varphi_m > \varphi^b$ and $\varphi_p^t \approx \varphi_m$. From this it is easy to see that φ_m is limited to unity, or equivalently $\epsilon_m > 0$. Indeed for small values of ϵ_m one should account for the interaction between micelles. This condition requires special attention. We will consider dilute micellar systems only.

The machinery of SCF modeling

At the basis of the SCF theory is the free energy which is a functional of the volume fraction profiles $\varphi(\mathbf{r})$ and so-called self-consistent potential profiles $u(\mathbf{r})$. As told above this free energy is optimized numerically. We follow Scheutjens and Fleer[4] who suggest to use one characteristic length l, both to discretize the space and to segmentise the chains. The discretization of space leads to lattices in which layers of sites are identified. We will refer to each layer by a coordinate $\mathbf{r}$. Typically we can consider several lattice geometries. Spherical micelles can be modeled using a spherical geometry. In this case $\mathbf{r} \equiv r = 1, \cdots, M_r$ are lattice layers with an increasing number of lattice sites $L(r) \propto r^2$. Long cylindrical micelles can also be modeled using a single coordinate, that is when end-effects are ignored. In this case the number of lattice sites per unit length of the cylinder obeys $L(r) \propto r$. Bilayers are flat association colloids and for this system we use $\mathbf{r} \equiv z = 0, \cdots, M_z$. Again, using one single coordinate implies that boundary effects are ignored. Now the number of lattice sites in layer z is constant, i.e. per unit area it is $L(z) = 1$ for all z. In these three coordinate systems we have just a single coordinate and we will refer to these systems as the one-gradient version of the SCF model. Typically we have reflecting boundary conditions at the system boundaries.

Below we will also use a two-gradient version in which the coordinate $\mathbf{r} = (r, z)$, where $r = 1, \cdots, M_r$ are concentric rings of lattice sites in which the number of lattice sites $L(r) \propto r$ and $z = 1, \cdots, M_z$ are flat lattice layers along the long axis of the cylinder.[57–59] We have reflecting (mirror-like) boundary conditions at all lattice boundaries.

For the general case we can write the (dimensionless) free energy of the systems in terms of two conjugated quantities, namely the segment volume fractions $\varphi(\mathbf{r})$ and the segment self-consistent potentials $u(\mathbf{r})$

$$F = -\ln Q[u] - \sum_{\mathbf{r}} L(\mathbf{r}) \sum_{x} u_x(\mathbf{r})\varphi_x(\mathbf{r}) + F^{int}[\varphi] + \sum_{\mathbf{r}} u'(\mathbf{r})L(\mathbf{r}) \left(\sum_{x} \varphi_x(\mathbf{r}) - 1 \right) \tag{3.11}$$

with

$$F^{int} = \frac{1}{2} \sum_{\mathbf{r}} L(\mathbf{r}) \sum_{x,y} \varphi_x(\mathbf{r})\chi_{xy} \left\langle \varphi_y(\mathbf{r}) - \varphi_y^b \right\rangle \tag{3.12}$$

In Eqs. 3.11 and 3.12, the indices x and y run over all segment types (i.e. A, B, C, S), the χ expresses, as in the Flory-Huggins theory, the strength of the nearest-neighbor interactions. The φ^b refers to the volume fraction in bulk defined as the region of space far from the micelle. The site average, indicated by the angular brackets, account for local and nonlocal contributions to the interaction energy and computed by $\langle X(\mathbf{r}) \rangle = \sum_{\mathbf{r}'}' \lambda_{\mathbf{r}'-\mathbf{r}}(\mathbf{r}) X(\mathbf{r}') \approx X(\mathbf{r}) + \lambda \nabla^2 X(\mathbf{r})$, where the prime on the sum-sign indicates that the sum is over all neighboring sites of $\mathbf{r}$. The *a priori* step probabilities λ are geometry dependent and obey the detailed balance

$L(\mathbf{r}')\lambda_{\mathbf{r}-\mathbf{r}'}(\mathbf{r}') = L(\mathbf{r})\lambda_{\mathbf{r}'-\mathbf{r}}((\mathbf{r})$. Moreover, they are normalized $\sum_{\mathbf{r}'}^{'} \lambda_{\mathbf{r}'-\mathbf{r}}(\mathbf{r}) = 1$. The fourth term in Eq. 3.11 decouples the volume fractions of the components, where the Lagrange parameter $u'(r)$ is linked to the incompressibility constraint (sum over all volume fractions equals unity). The first term of Eq. 3.11 features the partition function for the (u, V, T) ensemble $Q = \Pi_i \frac{(q_i([u_i]))^{n_i}}{n_i!}$, where i runs of the type of molecule, i.e. the solvent, polymer etc. Finally, the second term in Eq. 3.11 is a Legendre transformation such that the first two terms essentially give the dimensionless entropy.

The optimization of the free energy leads to the equations

$$\frac{\partial F}{\partial \varphi_x(\mathbf{r})} = -u_x(\mathbf{r}) + u'(\mathbf{r}) + \sum_y \chi_{xy} \left\langle \varphi_y(\mathbf{r}) - \varphi_y^b \right\rangle = 0 \tag{3.13}$$

$$\frac{\partial F}{\partial u_x(\mathbf{r})} = -\frac{\partial \ln Q}{\partial u_x(\mathbf{r})} - L(\mathbf{r})\varphi_x(\mathbf{r}) = 0 \tag{3.14}$$

$$\frac{\partial F}{\partial u'(\mathbf{r})} = L(\mathbf{r}) \left(\sum_x \varphi_x(\mathbf{r}) - 1 \right) = 0 \tag{3.15}$$

These equations form the basis of the SCF machinery. Eq. 3.13 specifies how the segment potentials follow from the volume fractions. Eq. 3.14 gives a method to compute the volume fraction from the potentials. Below we present a more practical alternative (but equivalent) route. Equation 3.15 gives the compressibility constraint.

An efficient route to compute the partition function starts with the Boltzmann weights $G_x(\mathbf{r}) = \exp -u_x(\mathbf{r})$, which are generalized to a segment ranking number dependent quantity $G_i(\mathbf{r}, s) = \sum_x G_x(\mathbf{r})\delta_{i,s}^x$, where $\delta_{i,s}^x = 1$ when segment s of molecule i is of segment type x and zero otherwise. These Boltzmann weights are used in the propagator equations, which are the discrete versions of the Edwards equation:[60]

$$G_i(\mathbf{r}, s|1) = G_i(\mathbf{r}, s) \left\langle G_i(\mathbf{r}, s-1|1) \right\rangle \tag{3.16}$$

$$G_i(\mathbf{r}, s|N) = G_i(\mathbf{r}, s) \left\langle G_i(\mathbf{r}, s+1|N) \right\rangle \tag{3.17}$$

for $s = 1, \cdots N_i$ (in our case the block copolymer has $N = N_A + N_B + N_C$ segments), where the angular brackets again indicate a geometry-dependent site averaging. The propagators are started with $G_i(\mathbf{r}, 1|1) = G_i(\mathbf{r}, 1)$ and $G_i(\mathbf{r}, N|N) = G_i(\mathbf{r}, N)$, $\forall \mathbf{r}$ and produces $q_i = \sum_{\mathbf{r}} L(\mathbf{r}) G_i(\mathbf{r}, N|1)$. Now Eq. 3.14 may be used to evaluate the volume fraction profiles. An efficient implementation of this is by the use of the so-called composition law which combines two sub-partition functions:

$$\varphi_i(\mathbf{r}) = \frac{n_i}{q_i} \sum_{s=1}^{N_i} \frac{G_i(\mathbf{r}, s|1) G_i(\mathbf{r}, s|N)}{G_i(\mathbf{r}, s)} \tag{3.18}$$

The volume fraction of the solvent in the bulk as an input parameter and Eq. 3.18 applied for the solvent gives $\varphi_S(\mathbf{r}) = \varphi_S^b G_S(\mathbf{r})$. Note that in a two-component system $\varphi_S^b = 1 - \varphi_p^b$ where $\varphi_p^b = n_p N_p / q_p$.

The equations are solved numerically up to high precision.[61] For the self-consistent solution it is possible to evaluate the grand potential $\epsilon_m = \sum_{\mathbf{r}} L(\mathbf{r})\omega(\mathbf{r})$, where the dimensionless grand potential density is $\omega(\mathbf{r})$ is

$$\omega(\mathbf{r}) = -\sum_x \varphi_x(\mathbf{r}) u_x(\mathbf{r}) - \sum_i \frac{\varphi_i(\mathbf{r}) - \varphi_i^b}{N_i} + \frac{1}{2}\sum_{x,y} \chi_{xy} \left\{ \varphi_x(\mathbf{r}) \left(\langle \varphi_y(\mathbf{r}) \rangle - \varphi_y^b \right) - \varphi_x^b \left(\varphi_y(\mathbf{r}) - \varphi_y^b \right) \right\} \tag{3.19}$$

The chemical potential of the components can be expressed in terms of the bulk volume fractions as the bulk is in full equilibrium with the micellar objects:

$$\mu_i - \mu_i^{\#} = \ln \varphi_i^b + 1 - N_i \sum_j \frac{\varphi_j^b}{N_j} - \frac{N_i}{2} \sum_{x,y} \left(\varphi_x^b - \varphi_{Ai}^* \right) \chi_{AB} \left(\varphi_B^b - \varphi_{Bi}^* \right) \tag{3.20}$$

where $\varphi_{Ai}^* = \sum_{s=1}^{N_i} \delta_{i,s}^A / N_i$ is the fraction of A segments in molecule i and $\mu_i^{\#}$ is the chemical potential of molecule i in the reference phase (which is a phase composed of purely molecules of type i).

3.3 Results

ABA micelles

In this sections we employ the 1-gradient version of the SCF method on a spherical lattice to collect properties of $A_N B_M A_N$ polymer micelles. In this geometry all properties of the system depend only on the distance r from the center of the coordinate system. All values within concentric spherical layers are averaged implementing the mean-field approximation along the angular coordinates. Hence spherical symmetry is imposed on the system. We use local volume fractions of components to characterize the structural properties of the micelle.

To reduce the number of variables involved, we fix the parameters related to the micellar core and vary only those related to the corona. The Flory-Huggins interaction parameter between B and the solvent S, χ_{BS} is 2 and the length of the solvophobic block (M) is 70 segments. The interaction parameter between the different segments in the copolymer χ_{AB} is also set to 2. This parameter is very important for the ordering in polymer melts, where it drives the self-organization. In our case it mainly defines the sharpness of the interface between the core and corona segments in the micelle. In the dilute polymer system the micellization is governed by the polymer-solvent interactions. The insolubility of

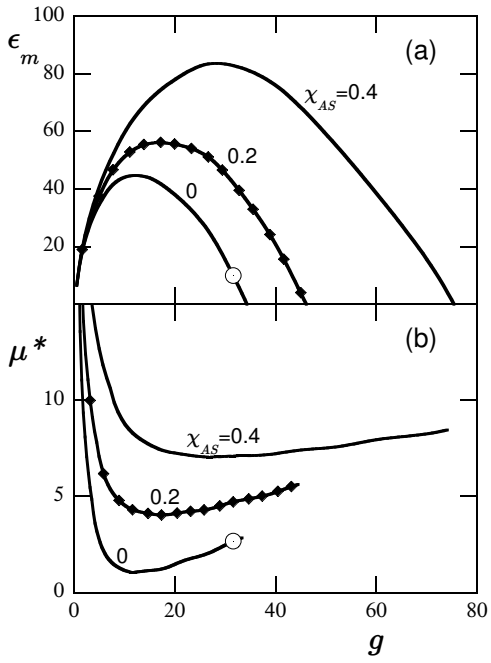

Figure 3.1: *Translationally restricted grand potential ϵ_m of $A_{100}B_{70}A_{100}$ micelle (a) and copolymer chemical potential, where $\mu^* = \mu_p - \Delta\mu$ (b) versus aggregation number g for $\chi_{AS} = 0$, 0.2 and 0.4. With diamonds we show ϵ_m and μ_p for $A_{100}B_{70}C_{100}$ terpolymer micelle with $\chi_{AS} = \chi_{CS} = 0.4$ and $\chi_{AC} = 0.8$. Note, that due to repulsion in the two-component corona the diamonds go on top of the curves for copolymeric micelle with $\chi_{AS} = 0.2$. For presentation purposes the chemical potential values are shifted by constant values $\Delta\mu_{\chi_{AS}}$ with $\Delta\mu_0 = 278$, $\Delta\mu_{0.2} = 244$, $\Delta\mu_{0.4} = 211$, and $\Delta\mu = 234$ for the $A_{100}B_{70}C_{100}$ micelle. The point corresponding to the profile on the Fig. 3.2 is indicated with an open circle.*

the middle block drives the aggregation, whereas crowding and repulsion of the chains in the solvated micellar corona provides the stopping force. The efficiency of the stopping mechanism is strongly affected by the length N of corona blocks and the interaction parameter χ_{AS}. Unless specified otherwise, the corona block consists of $N_A = 100$ segments and $\chi_{AS} = 0$. We summarize the set of "default" parameters in the Table 3.1.

Before we turn to the structural properties of spherical $A_{100}B_{70}A_{100}$ micelles, let us first discuss their stability from the view point of thermodynamics of small systems. In Fig. 3.1 we plot the translationally-restricted grand potentials (Fig. 3.1(a)) of the micelles and the chemical potential of the terpolymers (Fig. 3.1(b)) as a function of aggregation number g, for selected set of χ_{AS} values. The criterion for thermodynamic stability is defined by Eqs. (3.2) and (3.3). At low

Table 3.1: *List of all default Flory-Huggins interaction parameters. The default block copolymer is A_{100}-B_{70}-A_{100}. The monomeric solvent is S and in some of the calculations one A block is replaced by a block of C segments with equal length of the A block.*

χ	S	A	B	C
S	0	0	2	0
A	0	0	2	0
B	2	2	0	2
C	0	0	2	0

aggregation numbers the translationally-restricted grand potential first grows. This means that micelles with aggregation number less than a certain threshold value are unstable. The smallest thermodynamically stable micelle appears at the maximum of the $\epsilon_m(g)$ curve, which coincides with the minimum of the chemical potential (cf Fig. 3.1(b)). For example, in the case of our "default" system with athermal corona blocks ($\chi_{AS} = 0$), only micelles with $g > 12$ are stable. Using Eq. 3.10 one can estimate both the cmc and the overall polymer volume fraction corresponding to the smallest stable micelle. The cmc for micelles with athermal corona chains turns out to be as low as $\varphi = 10^{-18}$, which is well below experimental resolution. The cmc's for less soluble corona chains are even lower. In other words we expect the chosen triblocks to form micelles at all practical polymer concentrations.

One of the approximations implied in our model is that micelles do not interact with each other. This assumption does not hold at high polymer concentrations. Thus the results of the present SCF modeling are inaccurate when the micelles start to overlap. Below, we will select typical conditions, defined as those systems for which the translationally-restricted grand potential $\epsilon_m = 10$. The range of deviations from the chosen typical conditions that are still experimentally relevant is quite narrow due to the exponential dependence of the polymer volume fraction φ_p on the grand potential ϵ_m (cf Eq. 3.10). A rough evaluation shows that our estimate for the entropy of the micelles becomes inaccurate for micelles with $\epsilon_m = 5$, meaning that for these micelles the micellar interactions should be accounted for. On the other hand, micelles with a translationally-restricted grand potential $\epsilon_m = 25$ are the most probable ones at overall volume fraction of polymer $\varphi_m \approx 10^{-11}$. Concentrations as low as this are irrelevant for any experimental technique. Thus the relevant aggregation numbers are in the range $g \in [28, 33]$.

For our "default" system (shown with an open circle in the Fig. 3.1(a)) $\epsilon_m = 10$ translates to an overall polymer volume fraction $\varphi_t \approx 4.5 \times 10^{-5}$ and a typical distance between two micelles of $\approx 570l$. The aggregation number of the most probable micelle at this polymer concentration is $g \approx 32$. In Fig. 3.2 we show the radial volume fraction profile of both the core A and the corona B monomers in

this most likely micelle. The micelle consist of a dense core and a solvated corona. The polymer fraction in the core φ_B is constant. Assuming that it depends only on the solubility and the length of the middle block B we should expect the same volume fraction as that of a corresponding collapsed homopolymer in a poor solvent. Indeed, the polymer fraction estimation based on the mean-field type free energy density

$$F = (1-\varphi_B)\ln(1-\varphi_B) + \chi_{BS}\varphi_B(1-\varphi_B) \tag{3.21}$$

and vanishing osmotic pressure:

$$\pi = F - \varphi_B \frac{\partial F}{\partial \varphi_B} = \varphi_B + \ln(1-\varphi_B) + \chi_{BS}\varphi_B^2 = 0 \tag{3.22}$$

yields in $\varphi_B = 0.93$ which fits the SCF results for the polymer fraction in the core very well. In the expression for the free energy Eq. 3.21 we neglected the entropy of the collapsed polymer and used the incompressibility condition Eq. 3.15.

The micellar corona is formed by the A segments immersed in a good solvent. The polymer volume fraction in the corona monotonously decreases from the core surface to the exterior of the micelle. Because of the crowding near the core the chains in micellar corona are stretched as compared to free polymers. The model by Daoud and Cotton[62] predicts that the polymer density φ_A is proportional to $r^{-\frac{4}{3}}$. In Fig. 3.2 we present the density profile of the corona in log-log coordinates. In line with the Daoud Cotton result the region $12 < r < 25$ is approximately a straight line, with a slope close to $-4/3$.

Although the SCF modeling is targeted to a single micelle, the thermodynamic properties of the small system apply to the whole system. We demonstrated this by estimating the volume fraction of micelles using ϵ_m. Next, according to Eq. 3.9, the steepness of the $\epsilon_m(g)$ curve of Fig. 3.1(a) is inversely proportional to the relative fluctuation of the aggregation number. Thus, one can estimate the micellar size distribution at a given chemical potential. Note, that in the SCF model the fluctuations diverge as in a first-order phase transition at the point were the first thermodynamically stable micelles appear. The first appearance of micelles occurs as a jump from a zero micelles concentration to a finite albeit very small value. In this respect the SCF model is wrong: we know, that the micellization transition is smooth. We note however that the error is not severe as the concentration of micelles is exponentially small. Nevertheless, we should be aware of this when micellar properties are considered near this maximum.

One potentially unsafe assumption we made thus far is the choice of a spherical lattice. It is well known, that block copolymers are potentially able to form cylindrical or lamellar structures. While for short surfactants the preference for one geometry over the other depends on the overall surfactant concentration, for polymeric micelles it is mostly defined by the molecular composition. We now explicitly justify our choice of the spherical geometry for the present triblocks. In Fig. 3.3 we present the diagrams of states in the region of the sphere-to-rod

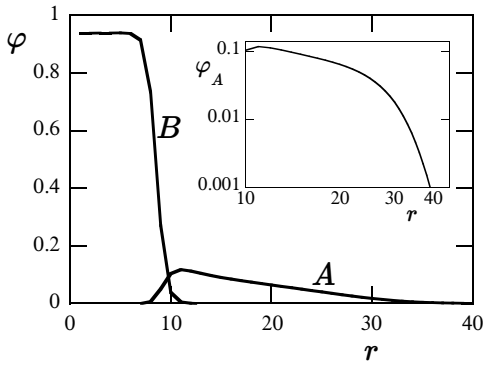

Figure 3.2: *Radial volume fraction profiles of the A and B components in a spherical micelle composed of $A_{100}B_{70}A_{100}$ copolymers. Inset: corona profile, log-log scale.*

transition as a function of the length N of the soluble block for $\chi_{AS} = 0$, 0.2 and 0.4. We obtained this diagram of states by comparing the chemical potentials of unimers in equilibrium with micelles with a spherical or a cylindrical geometry. In a narrow compositional range, where both cylindrical and spherical micelles are thermodynamically stable, i.e. Eqs. (3.2) and (3.3) are satisfied, the structure corresponding to the lowest chemical potential dominates. Exactly at the transition point the chemical potentials of unimers in equilibrium with spherical and cylindrical micelles are equal. In the coexistence region the balance between the two may be shifted by changing the overall polymer concentration. One can note that for micelles with an athermal corona the sphere-to-rod transition occurs around $N \approx 13$. The transition from cylindrical micelles to lamellas (not shown) occurs for triblocks with even shorter soluble blocks. Our default $N = 100$ is much larger and thus our analysis of spherical micelles is sufficient.

The 2-gradient version of the SCF method on a cylindrical lattice, that we use in the next section imposes only the axial symmetry on the system. Therefore, among others, it allows for the formation of spherical, rod-like and lamellar structures. In this way there is no need for an explicit check of the preferred geometry, as the most probable shape of the aggregate will be chosen automatically by the SCF machinery. Nevertheless, the preliminary analysis we made above is still useful, because the energy barriers between different micelle geometries may sometimes prevent SCF from finding the best solution[59]. Hence it is important to know that $A_{100}B_{70}A_{100}$ polymer micelles are spherical.

ABC micelles

In this section we present results of SCF modeling of $A_{100}B_{70}C_{100}$ micelles. The only difference between this and our "default" system from the previous section is, that here we introduce a repulsion between the two soluble blocks A and C. The

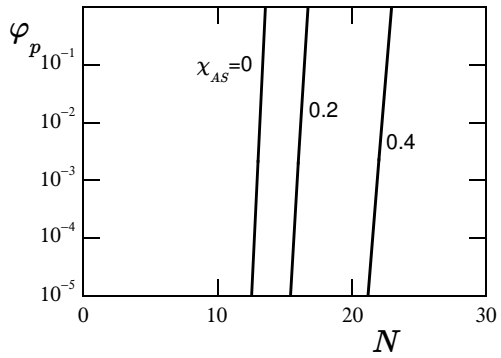

Figure 3.3: *Sphere-to-rod transition for $A_N B_{70} A_N$ copolymer micelles as a function of the corona block length and bulk polymer fraction for $\chi_{AS} = 0$, 0.2 and 0.4. Copolymer compositions to the right from the indicated lines correspond to spherical micelles.*

repulsion between the components has the potential to drive the A and C segments to separate regions in the corona. Micelles with a laterally segregated corona do not have a spherical symmetry, therefore we need to use a 2-gradient version of SCF method on a cylindrical lattice. In this geometry all profiles depend only on the axial coordinate z and the distance from the axis of cylindrical coordinate system r. All properties are averaged along the angular coordinate.

In Fig. 3.4 we present the grand potential ϵ_m of micelles with different segregation factors between blocks A and C. This plot provides the basis for the analysis of the thermodynamic stability of the micelles. In fact, the way to analyze it is the same as above in Fig. 3.1a. As a reference we plot ϵ_m for triblocks with no repulsion between the soluble blocks ($\chi_{AC} = 0$). The same curve is plotted in Fig.3.1a for $\chi_{AS} = 0$. The effect of the repulsion between the corona components has only a minor influence on the $\epsilon_m(g)$ dependence. Hence the aggregation numbers, the cmc's, and the stability regions are close to those of ABA micelles. At the overall polymer fraction $\varphi_t \approx 4.5 \times 10^{-5}$ which, as before, translates to $\epsilon_m = 10$, the aggregation numbers range from 26 to 32 depending on the value of χ_{AC}.

Below a critical value of the segregation factor χ_{AC}^{crit} the corona of the micelle remains mixed. In the special symmetrical case we consider, this means that at any spot in the corona equal fractions of A and B are found. The high symmetry of the triblocks makes it possible to include the segregation factor as a correction to the solvent quality for corona blocks. As shown in the Appendix, in the mean-field approximation the segregation factor enters all analytical expressions for the corona as a part of an effective solvent quality parameter $\chi_S^{eff} = \chi_S - \frac{1}{4}\chi_{AC}$. This substitution suggests that the overall polymer density profile and the aggregation numbers of $A_N B_M C_N$ micelles will be the same as these properties of a $A_N^* B_M A_N^*$ micelle where A^* is identical to A except for the solvent quality which is given

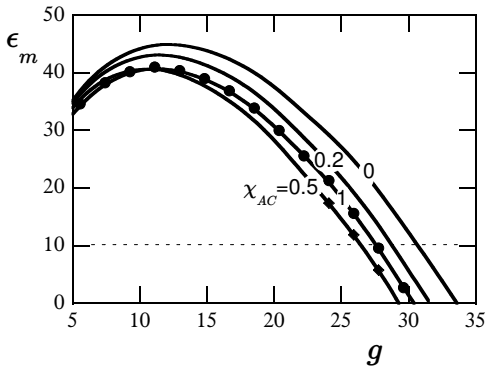

Figure 3.4: *Translationally-restricted grand potential ϵ_m of $A_{100}B_{70}C_{100}$ micelles with $\chi_{AC} = 1,\ 0.5,\ 0.2,$ and 0. Parts of the curves corresponding to micelles with segregated corona are marked with circles. The horizontal dashed line at $\epsilon_m = 10$ points to the 'typical micelle' condition.*

by χ_S^{eff}. In Fig. 3.1 we plot the grand potential of a $A_{100}B_{70}C_{100}$ micelle as a function of aggregation number. Although $\chi_{AS} = \chi_{CS} = 0.4$, $\epsilon_m(g)$ goes on top of a curve corresponding to a $A_{100}B_{70}A_{100}$ micelle with $\chi_{AS} = 0.2$. This is due to the repulsion between the corona components ($\chi_{AC} = 0.8$) which is equivalent to the decrease of the Flory-Huggins parameter for a single component corona from $\chi_{AS} = 0.4$ to $\chi_{AS} = 0.2$. This result was obtained using a spherical lattice hence the segregation was hindered by geometrical constraints.

In the 2-gradient version of the SCF calculations, increasing the χ_{AC} above the critical value results in the segregation of the corona chains into two domains, one rich in A and the other reach in C. The segregation restricts unfavorable contacts between the components to an interface between the domains. In the general case when the A and C blocks have a different affinity with the solvent or with the core or have different lengths, the domains are not necessarily equal and even core-shell corona structures may appear. For the highly symmetrical copolymer considered here, the lateral segregation into two equal hemispheres is the most favorable option. We show in Fig. 3.5 an example of the structure of a micelle with an inhomogeneous corona. In this graph we present both the equal volume fraction contour plots for the core, and the two corona blocks, but also the corresponding two-gradient volume fraction profiles. The center of mass is (by definition) at the $R = 0$ axis (volume fractions for positive R are identical to those at negative R). The numbering of the layers in the z-direction is arbitrary. Clearly visible is the dense core and the more swollen corona. The interface in the corona splits the micelle exactly into two structurally identical halves. This is true because of the symmetrical choice of the parameters used. Micelles with a lateral segregated domain structure are usually referred to as Janus-type in contrast to core-shell-corona (onion) type.

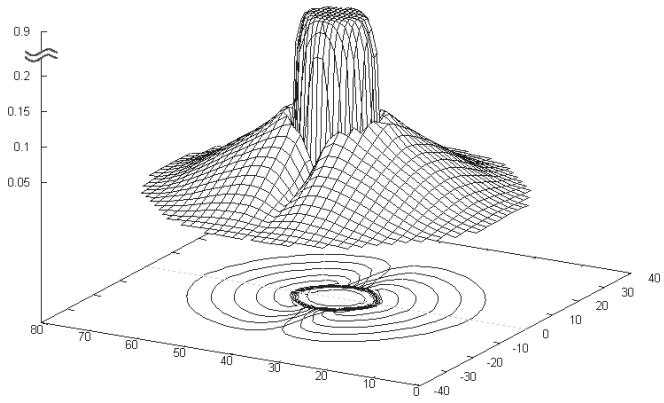

Figure 3.5: *Volume fraction profile of a Janus micelle in a cylindrical coordinate system. The cross section through the center of the micelle is given.* $\chi_{AC} = 1$.

With diamonds in Fig. 3.4 we show the regions corresponding to micelles with a segregated corona. The transition depends on the micellar aggregation number and consequently can be induced by a change in overall polymer concentration. For $\chi_{AC} = 1$ we find micelles with a segregated corona for all aggregation numbers. The contour plots in Fig. 3.6 show the overall polymer volume fraction profiles (a) and the volume fraction profiles of the A and C components (b) at typical conditions ($\epsilon_m = 10$). The interface between the domains is sharp and the fraction of minor components inside the domains is negligible. Due to the presence of an extra interface, the overall shape of the corona deviates from sphericity towards the prolate ellipsoidal shape. The $\chi_{AC} = 0.5$ micelles with a relatively low aggregation number, have a mixed corona. At typical conditions ($\epsilon_m = 10$) the micelle transforms into the Janus type and the contour plots are shown in Fig. 3.6(c,d). As this system is close to its transition point, the interface between the domains is wide, and the contents of the minor component in the 'wrong' phase is high. For example, the volume fraction of monomer A in the C-rich phase near the core of the micelle, depicted in Fig. 3.6(c,d), is approximately $\varphi \approx 0.03$, which is a third of the overall polymer volume fraction at this spot, which is $\varphi \approx 0.1$. The overall polymer volume fraction profile indicates that this micelle is nearly spherical.

Interestingly, the lowest curve in Fig. 3.4 corresponds to $\chi_{AC} = 0.5$. This means that at a fixed grand potential (i.e., a fixed overall polymer (micelle) concentration) the micelle with $\chi_{AC} = 0.5$ is the smallest. From Fig. 3.7 it is clear that the aggregation number as a function of the repulsion between the

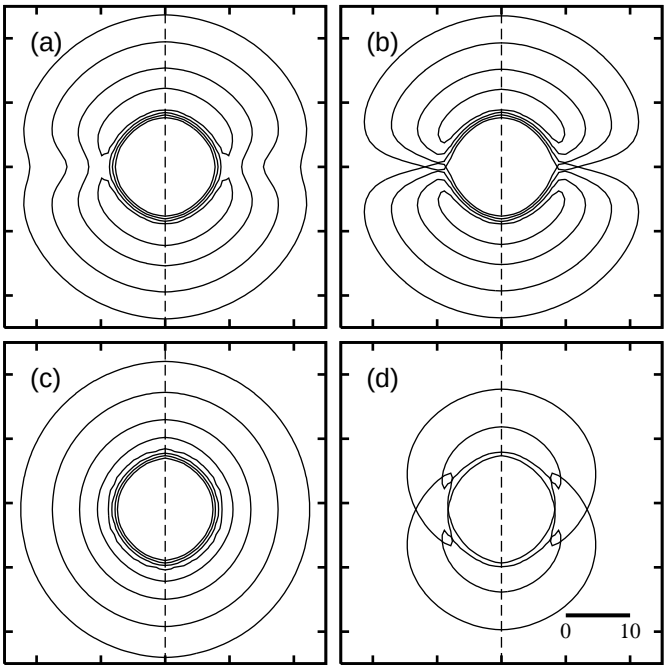

Figure 3.6: *Polymer volume fraction profiles for Janus micelles with a segregated corona. The cross section through the symmetry axis is indicated. The overall volume fraction are shown in view graphs (a, c) and that of the A (solid line) and C (dashed line) components are presented in graphs (b, d).*

corona components $g(\chi_{AC})$ reverses its trend when the transition to the Janus type occurs. An imaginary experiment, in which one would be able to control the repulsion between the corona components without affecting other parameters, would show a non-monotonous dependence of the aggregation number with this χ_{AC} interaction parameter (cf Fig. 3.7). The minimum of the $g(\chi_{AC})$ plot corresponds to the demixing transition point.

Let us next turn our attention to the properties of the interface in the corona. Compared to the classical interface between segregated polymers in bulk solutions, in the Janus corona there are several complications. As anticipated and shown in Fig. 3.6 the polymer volume fraction is not constant along the A-C interface and the stretching of the chains depend on the distance from the core of the micelle. In Fig. 3.8 we plot volume fraction profiles of the corona components near the core ($r = 12$) and in the periphery of the micelle ($r = 30$) in spherical coordinates, that is $\theta = 0, \cdots 180°$. In this spherical coordinate system, connected with the center of the micelle, it is easy to see that the angle occupied by the interface only slightly depends on the distance from the core. This means that the interface widens

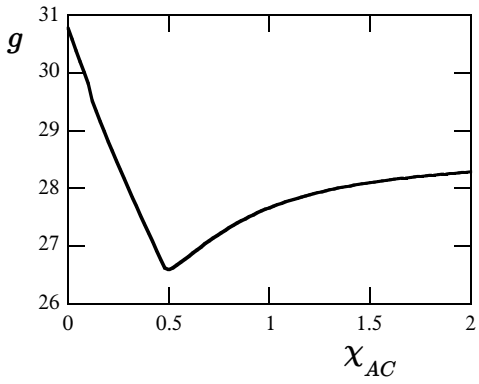

Figure 3.7: *Aggregation number of $A_{100}B_{70}C_{100}$ micelle versus segregation factor χ_{AC}. The minimum corresponds to demixing transition.*

towards the exterior of the micelle and that this dependence is close to linear. Unfavorable interactions between phase separated polymers typically make the interface depleted by polymer and enriched by solvent as compared to the bulk phases.[63] This also holds for the intra-micellar interface, but only up to a certain distance from the core (not shown). This indicates that the contacts between the components A and B are rare in the outer part of the corona. The local volume fraction of the polymer is much lower than that necessary for macrophase segregation of the corresponding homopolymers in solution. Nevertheless the interface persist due to the segregation in the inner part of the corona and the radial stretching of the chains. We will return to this in the discussion.

3.3.1 Discussion

As long as there is no lateral segregation in the corona, the micellization of $A_{100}B_{70}C_{100}$ triblock terpolymers in similar to that of $A_{100}B_{70}A_{100}$ micelles. Any unfavorable interactions between unlike corona segments just result in a renormalization of the solvent quality of the corona segments. However, when the A and C segments repel each other sufficiently, the spherical symmetry is broken and Janus micelles form. As explained in the introduction the critical interaction parameter for the bulk system of two equally long polymers (A_N, C_N) in a common solvent S is given by $\chi_{AC}^{cr} N\varphi_p = 2$. This means that the onset of phase separation occurs at $\varphi_p^{cr} = 2/(N\chi_{AC})$. Translating this result to our problem indicates that as long as the volume fraction of polymer in the corona remains below φ_p^{cr} the corona must remain laterally homogeneous. Inspection of our results shows that this is indeed the case. We only find laterally inhomogeneous coronas when locally the polymer volume fraction exceeds this value.

As discussed above, the highest concentration of corona segments is found just outside the core. We have checked for a number of cases that the onset of

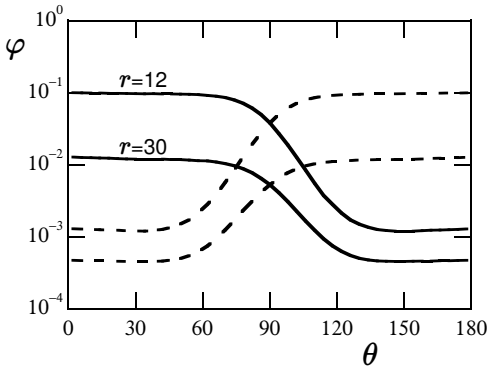

Figure 3.8: *Angular distribution of volume fractions of monomers A (solid lines) and C (dashed lines) at distances* $r = 12$ *and* $r = 30$ *from the center of* $A_{100}B_{70}C_{100}$ *micelle.* $\chi_{AC} = 1$

Janus micelle formation takes place when this highest volume fraction of corona segments just exceeds the critical value. The fact that at the regions further away from the core the volume fraction of polymer is below the critical value does not prevent the transition to occur. Stating it differently, even though only part of the corona chains are subjected to demixing conditions, the full chain has to obey to the formation of the demixed state. The full analysis of this transition will be published elsewhere.

It is of interest to discuss the order of the transition as well. The demixing of polymers in segregated phases usually occurs as a first order transition. However when the binodal is crossed at the critical point the transition is second order. In our system the critical volume fraction is at $\varphi_A^{cr} = \varphi_B^{cr} = 1/(N\chi_{AC})$. Due to the symmetry in our terpolymer, it is true that in the mixed corona $\varphi_A = \varphi_B$ at all coordinates. This means that (in this special case) the demixing can only be initiated by entering the two-phase region through the critical point. As a consequence the transition can not be first order. This observation is consistent with the data presented in figure 3.7, where the aggregation number shows a kink at the transition. This means that the second derivative of the free energy with respect to the chemical potential of the polymer is discontinuous, implying that the transition is second order.

When we would have considered asymmetric terpolymers, we would have obtained even more complicated system. Within the mean field approximation, we might anticipate a first-order transition. However, due to the finite size of the micelle the height of the free energy barrier in the demixing transition will remain finite and the Janus-micelle formation is at best first-order-like, i.e., it can only approach this in the limit of infinitely long chains. This means that an ensemble of micelles will consist of micelles that continuously fluctuate from mixed to demixed coronas. System-wise this means that the transition is always smooth.

From macroscopic two-phase systems, we know that the width of the interface W diverges upon the approach of the critical point. In our system the width of the interface can not exceed the size of the micelle, and this fact probably will influence the onset of Janus-micelle formation slightly. Currently we can not estimate the importance of this effect.

The radial growth of the interfacial as shown in Fig. 3.8 is of special interest as well. It was shown that the interface persists all the way to the dilute part of the corona volume fraction profile. In this region the chains do not feel each other. It is noteworthy though that the local polymer concentration at places where visually there is a clear interface, indeed can drop below the (bulk) critical value φ_P^{cr}. Only near the core the polymer concentration exceeds the critical value and we believe that these higher polymer concentrations drive the formation of the interface. The high stretching of the chains in the radial direction (especially in the dead zone) help to maintain the presence of the interface.

From macroscopic interfaces between polymer solutions, it is known that the interfacial tension γ is an increasing function of the segregation parameter χ_{AC}.[51,64] We therefor should expect that the excess free energy of the interface in the corona will be an increasing function of the interaction parameter. We found that this is the case (result not shown). However, from the above it is obvious that the total amount of free energy present in the interface can not be very high. From the grand potential density profiles $\omega(\mathbf{r})$, it is possible to estimate the excess free energy of the interface. Typically we find values of order several k_BT per micelle. There are a number of important consequences of this. As there is so little free energy needed to create an interface, it must be possible to change the interface, i.e., the shape and position. In other words, the interface should strongly fluctuate. In our SCF model we can not account for interface fluctuations, but they most likely will be large (especially near the critical conditions). We mention however, that the present calculations were performed for relatively short chains and low aggregation numbers. In experimental cases one may go to larger chains and higher aggregation numbers and then expect two-phase Janus micelles as the ground state micelle.

To directly proof, in experimental situations, the existence of the Janus state of micelles is a major challenge.[65] In most cases it will require labeling of the corona chains. This always has the potential effect of perturbing the structure. From Fig. 3.6a we see that there is a deviation from sphericity of both the core and the corona. Because of the high surface tension of the core-solvent interface, the core is almost spherical. Close inspection however shows that the core is an oblate ellipsoid. For micelles with a lower core-solvent interfacial tension, such as for complex coacervate core micelles,[46] the deformation of the core may be much more easily observable. The overall volume fraction profiles of the corona, however, indicate that the overall shape of the Janus micelle is a prolate ellipsoid. Such deviations from sphericity are the direct consequence of the interface in the corona and are the signature for Janus micelles. Finally, we have argued that in some cases the transition from mixed to demixed coronas can be triggered by

increasing the aggregation number. For a given system this may occur as a result of the increase in polymer (or micelle) concentration. Of course for this to be operational one needs to be sure that the aggregation is reversible, i.e., that the core is not frozen in a glassy state. Again, complex coacervate core micelles may be the system of choice to observe this prediction.

3.4 Conclusions

Using a numerical self-consistent field approach we studied the micellization of A_N-B_M-C_N triblock terpolymers in a selective solvent. The B-block forms a dense core and the two A and C block form a highly swollen corona. Using a cylindrical two-gradient coordinate system we were able to study the transition in the corona from a lateral homogeneous (for low values of χ_{AC}) to a phase segregated corona (above a threshold value of χ_{AC}). The transition was shown to be rather abrupt, but not jump-like. For given micellar concentration (fixed translationally-restricted grand potential), we found that below the transition the aggregation number decreases with increasing repulsion between A and C, whereas above the transition there is an increase in aggregation number. The kink in the curve of $g(\chi_{AC})$ shows that the second derivative of the free energy to the chemical potential is discontinuous pointing to the second order phase transition. The interface between A and C rich phases has several peculiarities. The interface widens with increasing distance from the core. Near the core a true interface exists with a finite (local) interfacial tension and a small accumulation of solvent between the two phases. In the periphery of the corona the A and C chains are only separated because they are forced to be separated near the core. Another peculiarity is that the orientation of the molecules in the A and C rich phases are parallel to the interface. In the regime of strong segregation we find that neither the core, nor the overall micelle remains perfectly spherical. This is noteworthy because the lengths of the corona blocks were chosen sufficiently large to prevent non-spherical topology for micelles with a homogeneous corona to form. One of the interesting findings was that the transition from a mixed to segregated corona can be induced by increasing the aggregation number. As the micelle size is a weakly increasing function of the overall micelle concentration, we anticipate that the occurrence of Janus micelles may depend (in some cases) on the polymer concentration in the system. Near the transition point, the first appearance of Janus micelles is accompanied by a weak segregation between the two polymer segments, and diffuse interfaces with an ultra-low interfacial tension. In this regime we expect that thermal fluctuations can disrupt the two-phase structure and induce a multiple domain structure of the corona. For strong segregation, however, the two-face Janus structure should be the ground state.

Acknowledgments

The authors acknowledge financial support from Dutch National Science Foundation (NWO) and Russian Foundation for Basic Research (RFBR) through the joint project 047.017.026 "Polymers in nanomedicine: design, synthesis and study of inter-polymer and polymer-virus complexes in search of novel pharmaceutical strategies", Financial support from the EU POLYAMPHI/Marie Curie program (RT6-2002, proposal 505027) and SONS Eurocores program (Project JA016-SONS-AMPHI) is also acknowledged.

3.5 Appendix

In this appendix we show that the free energy Eq.3.11 of the system consisting of triblock terpolymer $A_N B_M C_N$ and a solvent S is equivalent to the free energy of triblock copolymer $A_N^* B_M A_N^*$ in a solvent. The non-zero interactions between the blocks A and C ($\chi_{AC} > 0$) can be accounted for using renormalized interaction parameters of the monomer A^* with the block B and the solvent. The derivation relies on the *a priori* assumption that the volume fractions of the monomers $\varphi_A(\mathbf{r})$ and $\varphi_B(\mathbf{r})$ are equal to each other at all $\mathbf{r}$ (this is not true for micelles with a segregated corona). As a consequence, structural and thermodynamic properties of the mixed terpolymeric micelles are the same as those of micelles formed by $A_N^* B_M A_N^*$ copolymers with modified interaction parameters.

The density of the free energy of interactions Eq.3.12 may be written as a sum of contributions from each pair of monomers

$$f^{int}(\mathbf{r}) = f_{AS}(\mathbf{r}) + f_{BS}(\mathbf{r}) + f_{CS}(\mathbf{r}) + f_{AB}(\mathbf{r}) + f_{BC}(\mathbf{r}) + f_{AC}(\mathbf{r}) \tag{3.23}$$

For brevity below we will drop the spatial coordinates. Each item in the sum has the form

$$f_{xy} = \frac{1}{2}\chi_{xy}(\varphi_x \left\langle \varphi_y - \varphi_y^b \right\rangle + \varphi_y \left\langle \varphi_x - \varphi_x^b \right\rangle) \tag{3.24}$$

and due to the symmetry of the triblock and the equal fractions of A and C, $\varphi_A = \varphi_C$, Eq.3.23 reduces to

$$f^{int} = 2f_{AS} + f_{BS} + 2f_{AB} + f_{AC} \tag{3.25}$$

Using the incompressibility condition $\varphi_A + \varphi_B + \varphi_C + \varphi_S = 1$ we eliminate the dependence of f_{AC} on φ_C

$$f_{AC} = -\frac{1}{4}\chi_{AC}(\varphi_A \left\langle \varphi_S - \varphi_S^b \right\rangle + \varphi_S \left\langle \varphi_A - \varphi_A^b \right\rangle) - \frac{1}{4}\chi_{AC}(\varphi_A \left\langle \varphi_B - \varphi_B^b \right\rangle + \varphi_B \left\langle \varphi_A - \varphi_A^b \right\rangle) + \frac{1}{4}\chi_{AC} \left\langle \varphi_A - \varphi_A^b \right\rangle \tag{3.26}$$

The last term is linear in φ_A and therefore does not influence the optimization procedure. The first term of Eq.3.26 can now be included in f_{AS} of Eq.3.25, and the second term of Eq.3.26 can be included in f_{AB} of Eq.3.25 leading to

$$f^{int} = f_{A^*S} + f_{BS} + f_{A^*B} \tag{3.27}$$

where f_{A^*S} and f_{A^*B} are defined by Eq.3.24 with $\varphi_{A^*} = \varphi_A + \varphi_C = 2\varphi_A$ and $\chi_{A^*S} = \chi_{AS} - \frac{1}{4}\chi_{AC}$, $\chi_{A^*B} = \chi_{AB} - \frac{1}{4}\chi_{AC}$.

The conformational part of the free energy Eq.3.11 is not affected by this substitution.

CHAPTER 4

Adsorption of comb polymers and the effect on colloidal stability [1]

[1] Published with minor changes by Marat Charlaganov, Peter Košovan, Frans A.M. Leermakers in Soft Matter 5 (2009) p.1448.

In this chapter we consider the classical problem of homopolymer adsorption at the solid-liquid interface and discuss its implications for colloidal stability. More specifically, our focus is on comb-like homopolymers in the strong adsorption limit. A self-consistent field analysis shows that for relatively long side chains but still much longer backbones, the adsorbed layer is dominated by the side chains near the surface, whereas at larger distances the layer has features that belong to the backbone. As a rule, homopolymer adsorption promotes flocculation of colloids. This is attributed to the long polymer chains that form bridges between the colloidal particles. However, the free ends of the chains do not participate in the bridging and thus contribute with a small repulsive term to the mainly attractive pair interaction. For comb polymers, the free ends of the side chains amplify the repulsion dramatically. As a result, in contrast to linear adsorbed homopolymers, comb polymers typically prevent flocculation.

4.1 Introduction

Polymers are the objects of choice to affect the colloidal stability because they adsorb strongly with a high cooperativity on many surfaces.[4] Polymers are also the objects of choice for theoretical modeling because of the many universal aspects that can be expected.[2–4,66] For both reasons there exists a considerable literature on how polymers adsorb onto surfaces and books have been written on this.[4,67] The present status in understanding of adsorbed polymer layers is not fully satisfactory because still significant dilemmas exist.

The theory of polymers at interfaces has been used to address the problem of how polymers affect the colloidal stability.[68] Of course block copolymers are the best to ensure stability. The key idea is that one block of the copolymer is used as an anchor and the other block forms a stabilizing layer. Such mechanism is predicted theoretically[69] and is found in practice.[70] For the issues discussed below it is important to note that the repulsion generated when these adsorbed copolymer layers are forced to overlap can be traced to the fact that the non-adsorbing block is, similarly to a polymer brush, strongly stretched in the normal direction.[71] More specifically, the thickness of this brush layer or the height of the brush H is proportional to the chain length, N and increases slower with the grafting density σ, $H \propto N\sigma^{1/3}$. For brush chains it is true that the segments along the chain are further away from the surface the closer one comes towards the end of the chain. This directionality is essential. In the context of a Landau theory to predict the colloidal stability,[17,72] it is understood that the order parameter is asymmetric in this case. Asymmetric order parameters in combination with symmetric boundary conditions (both surfaces are identical), implies repulsion.

The situation is not as simple for the homopolymer case. Focusing on the polymer solution (good up to theta conditions) the theory essentially predicts a destabilizing effect. When the polymers are strongly adsorbed bridging flocculation is predicted for a wide range of polymer concentrations, i.e., from very dilute polymer solutions up to the semi-dilute. In the absence of any affinity for the surface chains avoid the surface and so-called depletion flocculation is expected (especially near the overlap concentration). Around the critical adsorption energy the polymeric contribution to the inter-particle forces become non-monotonic, but extremely small. In a polymer melt the interactions are basically screened and the forces are also oscillatory (as near the critical conditions) and short-ranged.[73]

Depletion flocculation is an active research field in recent years basically because of its universal character.[4,74] It must be stressed, however, that the depletion force is rarely the major player because, unless one has taken the necessary precautions, the attractive Van der Waals forces overwhelm the depletion forces.

Bridging flocculation on the other hand is much stronger. This can be understood from the origin of bridging. One way to characterize an adsorbed polymer layer is to identify structural elements such as trains (sequences of segments that are directly adsorbed on the surface), loops (sequences of polymer chains that are not in direct contact with the surface but are connected by both ends to train

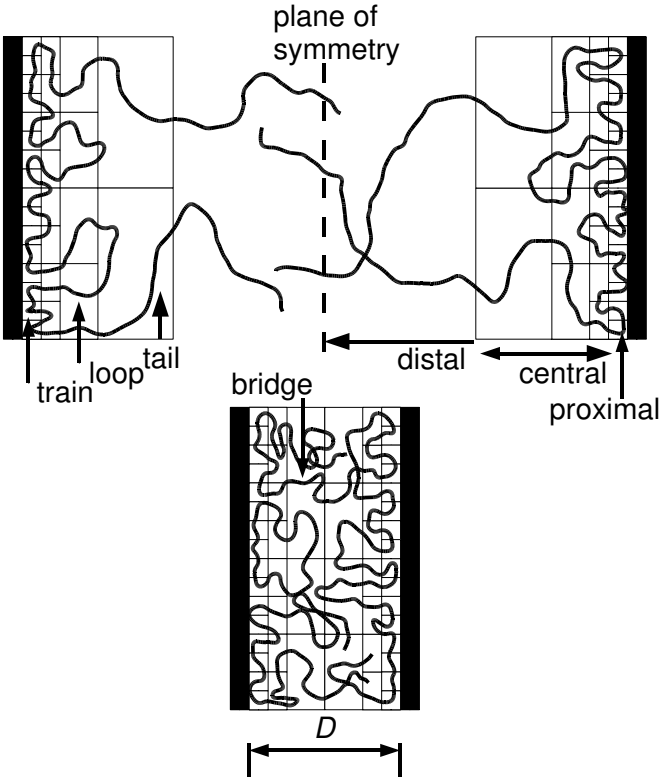

Figure 4.1: *Illustration of (top) two weakly overlapping polymer layers and (bottom) two layers at somewhat stronger confinement. The distance D is indicated. The train, loop and tail configurations are identified in the top graph. In the bottom graph the bridge configuration is shown. Surfaces are indicated in black. Half-way between the surfaces the symmetry plane is pointed (in the drawing the conformations do not obey the symmetry; on the ensemble level they should). The thin lines are drawn to help identify the self-similar character of the adsorption layer (in the central part of the profile where the polymer concentration is in the semi-dilute regime). The distal as well as the proximal parts of the polymer layers are identified.*

segments, and tails (sequences of polymer chains that are not in direct contact with the surface but are connected by one of the ends to a train), cf. figure 4.1. When two surfaces come in close proximity we can identify a symmetry plane halfway between the surfaces (cf fig. 4.1). As soon as the loops reach such symmetry plane, they can transform into bridges (chain fragments that themselves are not adsorbed on the surface but are connected by both ends to trains on different surfaces). This loop-to-bridge transformation can occur without affecting the total number of train segments, thus not affecting the (interaction) energy in the system. Such transformation will increase the entropy (and thus the free energy decreases by $k_B T \ln 2$) per choice given to the system (here k_B is Boltzmann's constant). As the number of loops is large, especially in the plateau of the adsorption isotherm, where the surface is saturated with polymer, a strong attractive interaction is expected (i.e., many bridges form).

In experiments one very often administers adsorbing homopolymers or homopolyelectrolytes to improve the stability of a colloidal system. This is generally known as steric stabilisation.[76] Apparently, in practice one finds that interfacial polymer layers induce a significant repulsion. Focusing on the uncharged polymers, the classical theory to explain this results introduces a kinetic argument.[68] The idea is that there exists a timescale τ_a needed for polymer chains to adsorb or desorb as a response to the confinement. When the collision time τ_c of the particles is much smaller, i.e. $\tau_c << \tau_a$, the particles effectively interact at fixed number of adsorbed chains rather than at fixed chemical potential. This subtle difference is enough to find a repulsion at short separations. Directly coupled to this is the consensus in the literature that bridging flocculation is in practice only possible when the surfaces are partly covered by polymers.[4] The line of reasoning is that for starved polymer layers, the polymers on opposite particles can quickly find empty space to form bridges, whereas in fully covered surfaces the formation of bridges is kinetically prohibited. In starved layers however the polymers are usually laying relatively flat on the surface (not many loops or tails form). As a result the layer thickness remains much smaller than the radius of gyration R_g. Thin adsorption layers may not be able to prevent Van der Waals attraction to dominate the pair interactions. To our mind the kinetic arguments are rather speculative and at best apply for some problems. They would not apply to concentrated particular solutions in the presence of adsorbed polymers.

There is another interesting suggestion in the literature that can potentially explain why adsorbing homopolymers can work as stabilizers against aggregation of colloids. Such property follows directly from the theory of polymer adsorption. The theory which goes beyond the GSA shows that there is a role of tails.[77,78] Tails are known to avoid surfaces and therefore they can not be engaged in the formation of bridges.[79] As the number of tails is conserved (in good approximation there are two tails per adsorbed chain), the confinement of tails gives a repulsive force. We may use the ideal gas Ansatz to estimate the force due to the confinement of tails. The force per unit area, i.e. the pressure, will be estimated by the number of confined tails per unit volume. Comparison with

self-consistent field results show that this estimate is rather close to reality.[75] It directly shows that this repulsion is expected to vanish in the limit of large chains $N \to \infty$. For any finite chain length, however, the overall interaction force is thus non-monotonic. Going from large to small interparticle distances D a repulsion is found when the distance between the surfaces is of the order of the radius of gyration, $D \approx R_g$ of the chains (i.e., the typical size of the tails) which gives way to attraction when the bridges form (i.e., when the distance is a few times less than the coil size, i.e., $D < R_g$).

When discussing the importance of tails, it is essential to discuss the length scale called z^*. For short distances to the surface $z < z^*$, the loops determine the overall adsorption profiles, whereas for larger distances $z > z^*$, the tails are the most important structural feature. For the self-consistent field results a numerical analysis showed[80] that this length is somewhere in the central region, $z^* \propto N^{1/3}$. In a scaling picture there is a slightly larger exponent[77] of $z^* \propto N^{1/2}$. The value of z^* is important to estimate on what distance one should expect the effect of tails to give way to that of loops.

The natural question arises whether the repulsive contribution, i.e. that of the confined tails, is large enough under experimental conditions to explain why homopolymers can stabilize particular solutions. Below we will elaborate on this mechanism. In the context of the Landau theory,[17,72] it thus appears that the homopolymer problem is a two order-parameter problem. One asymmetric order parameter (connected to the properties of the tails) is operational at relatively large separations, whereas a second symmetric order parameter (connected to the loops) dominates at short separations.

There are other, perhaps even more troublesome, observations. Experimentally, it is clear that chemistry matters, implying that there is a role of the chemical structure of the polymers, i.e. on the monomeric level, that manifests on larger scales. This conclusion simply follows from the observation that one polymer behaves differently from the other. The effects of polymers on the colloidal stability is no exception to this rule. Of course there is a role for the persistence length. The way to deal with this, from a theoretical point of view, is to define a new chain with fewer statistical segments (with size of the persistence length).[81] Undoubtedly there is also a role of the solvent quality. However, unless the solvent is very close to the ideal θ-condition, we should, for large enough chains, expect qualitatively similar behavior.[3,4] Finally, there must be a profound effect on the adsorption energy.[4] Here the situation is somewhat complex. Of course the adsorption energy should be above the critical value. If this is the case, one very quickly enters the regime where the adsorption energy has only a small quantitative effect not a qualitative one. However, when the adsorption energy per segment exceeds k_BT significantly, we might anticipate hit-and-stick effects and the adsorption may never reach equilibrium.[82] Such high values indeed can be found in experimental cases.[83]

There are indications in the literature that the molecular weight of the polymers used matters as well. For example in ref.[84] it was found that very long

PEO will form bridges between silica surfaces whereas shorter chains do this less. At present there is no clear theoretical explanation for this.

Here, we will consider yet another scenario where side chains exists that decorate the main chain. For a schematic illustration of these molecules we refer to figure 4.2. Such situation occurs in many macromolecular compounds. One may argue that such side chains induce a large effective persistence length.[85] Indeed such induced increase of the persistence length is expected and the way to treat it is discussed above. However, we believe that there is more to it, which is of particular importance for the issue of colloidal stability, namely that the side groups introduce chain ends. The effect of these end groups is highlighted in this paper.

Below we will first analyze how regular comb polymers adsorb onto solid-liquid interface. There exist few theoretical works on the adsorption of comb polymers on a single surface.[86] The aim here is to search for universal features that can be identified for such adsorbed layers. The volume fraction profile is important to rationalize the way these combs influence the colloidal stability. More specifically we pay attention to the effect of chain ends. The natural quantity to focus on is the free energy of interaction between surfaces. As one can expect from the above, we find that increasing the number of ends per molecule will amplify the repulsion. The goal is to quantify the effects of chain ends and to understand the roles of the overall molecular weight, the length of the teeth t, the length of the spacers, m, and the total number of side chains, n (cf fig. 4.2).

In the final part of this paper the case of short side chains that are densely planted along the backbone is discussed. The idea is that for very long polymer chains (large n), that is for long backbone lengths, one will return to the universal properties for any length of the side group t. The question is how long the backbone must be before this universal behavior is recovered. It is shown that such length can easily be so high that this exceeds the synthetic capabilities.

The remainder of this paper is as follows. First a few key aspects of the self-consistent field theory are discussed. This is followed by a brief outline of using the ground state approximation to obtain first-order information about the volume fraction profiles of the adsorbed polymers. In the results section we will first discuss the adsorption of comb homopolymers on an isolated surface and subsequently analyze the effect of these polymers on the colloidal stability. The search for universal behavior of polymers with small teeth completes the results. In the discussion we will evaluate the status of the SCF modeling the adsorption of comb polymers and put the main predictions of the work in a wider perspective.

4.2 Theory of polymers at interfaces

In principle only the simulation route gives exact information for polymers at interfaces. This route however is quite limited to relatively short chains and small simulation boxes. Our interest is in some universal features for polymer

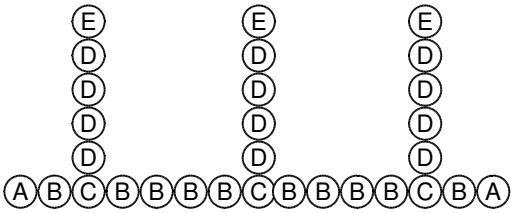

Figure 4.2: *Schematic illustration of the comb homopolymers. The letters A-E are only for ease of reference to the position of the segments in the comb. The total number of segments* $N = N_{bb} + N_T = n(m + t)$*, where* n *is the number of teeth, and* m *equals the number of segments in the spacer, hence the number of backbone segments* $N_{bb} = n \cdot m$*,* t *is the number of segments in one tooth, hence the number of teeth segments* $N_T = n \cdot t$*. The arms are evenly distributed along the backbone. In this example the tooth length* $t = 5$*, the number of repeats* $n = 3$ *and the spacer length* $m = 5$*. Note that we will always take* $N_{bb} >> t$*.*

adsorption which requires, as we will see, long polymers. For such project one must turn to approximate theories. Self-consistent field (SCF) modeling is known to give results that follow experiments at least semi-quantitatively. Moreover this route gives information on thermodynamic parameters which are essential to evaluate how polymers influence the colloidal stability.

The central idea of SCF models for polymer adsorption is to compute single-chain partition functions. Essentially one then solves Edwards diffusion equation, which implements the analogy between the path followed by a diffusing particle and the path followed by a polymer chain. The important difference between these two problems is that the polymer chain has excluded volume effects. This means that the chain should avoid places where it has been already. In the Edwards equation this is done by introducing a self-consistent potential u which is chosen such that it represents the surrounding segments. Scheutjens and Fleer have spent much of their careers to elaborate on the physics of polymers at interfaces using this approach. We will follow their route in detail in the next sub section.

There exists a further analogy between the Edwards equation and the Schrödinger equation used in quantum mechanics (QM). Much of the mathematical machinery can be used to obtain analytical approximations. Below we will briefly discuss, in a dedicated section, the ground state approximation for polymer adsorption which is inspired by the QM analogies and obtain some basic insight in what to expect for the density profiles. For more details however we refer to refs.[3,75].

SCF machinery, Model and Parameters

We use the self-consistent field theory making use of the discretization scheme of Scheutjens and Fleer (SF-SCF).[61,68,87,88] Here we will only give an overview of the method and refrain from too much details. In this method the space is

subdivided into lattice sites with characteristic length b. These sites are organised in flat layers numbered $z = 1, \cdots, D$, where on both sides there exists an impenetrable surface S with property $\varphi_S(0) = \varphi_S(D+1) = 1$ and $\varphi_S(z) = 0$ for the layers in between. The distance between the surfaces is thus $D \cdot b$. Here φ is the volume fraction. We take a cubic lattice for which $\lambda_0 = 4/6$ is the fraction of neighboring sites within a layer and $\lambda_1 = 1/6$ is the fraction of neighboring sites to a previous or next layer.

Polymer molecules are composed of segments with ranking numbers $s = 1, \cdots, N$, where each segment fits one lattice site. The generic structure of the comb homopolymers is depicted in figure 4.2. We distinguish three types of segments based on the position of the segment in the molecule. First there are end-segments $\{s_e\}$ (segments A, E in fig. 4.2). These segments have just one bond. Then there are intermediate segments $\{s_i\}$ between ends and branch points. These segments have two bonds. Finally, there are branch segments $\{s_b\}$ (segments C in fig. 4.2), which have three bonds.

The second molecular component is a monomeric solvent W. We are going to assume that the only non-ideal interaction exists when the segment A is next to a surface, i.e. when such segment is either in layers $z = 1$ or $z = D$. The Silberberg adsorption energy $\chi_s = -\frac{1}{6}(\chi_{AS} - \chi_{WS})$ is positive when the segment is attracted to the surface (that is when $\chi_{AS} < \chi_{WS}$).[89] Calculations are performed in the grand canonical ensemble for which the bulk volume fraction of polymer φ^b, that is, the volume fraction of segments that exists in the bulk in equilibrium with the system that is under investigation is fixed. In all layers (and also in the bulk) there is an incompressibility constraint which implies that for the monomeric solvent $\varphi_W(z) = 1 - \varphi(z)$.

The characteristic function in the grand canonical ensemble is the grand potential per unit area Ω. This quantity can be written as a summation over the grand potential density $\omega(z)$, that is $\Omega(D) = \sum_{z=1}^{D} \omega(z)$ where the grand potential density can explicitly be written in terms of the volume fraction of the polymer $\varphi(z)$.[75]

$$\omega(z) = \left(1 - \frac{1}{N}\right)\left(\varphi(z) - \varphi^b\right) + \ln\left(\frac{1-\varphi(z)}{1-\varphi^b}\right) \tag{4.1}$$

Note that we have made the grand potential density dimensionless by leaving out the thermal energy $k_B T$. The (dimensionless) free energy of interaction (per unit surface area) is given by

$$F^{int}(D) = \Omega(D) - \Omega(\infty) \tag{4.2}$$

where the grand potential at infinite separation $\Omega(\infty)$ ensures that for non-interacting surfaces $F^{int} = 0$.

The only problem remains how to evaluate the optimal volume fraction distribution $\varphi(z)$. The SF-SCF method has an efficient enumeration scheme for this which is the discrete version of the well-known Edwards diffusion equation.[60]

The start of the SF-SCF scheme is to define a dimensionless segment potential for the solvent $u_W(z)$. As solvent is monomeric the volume fractions of the solvent is given by

$$\frac{\varphi_W(z)}{\varphi_W^b} = \exp\left(-u_W(z)\right) = G_W(z) \tag{4.3}$$

Taking the logarithm on both sides leads to

$$u_W(z) = -\ln\frac{\varphi_W(z)}{\varphi_W^b} = \ln\frac{1-\varphi^b}{1-\varphi(z)} \tag{4.4}$$

The segment potential for the polymer segments differs only in the layers next to the surface $u(z) = u_W(z) + \chi_s\delta_{1;D}$, where $\delta_{1;D} = 1$ when $z = 1$ or $z = D$, and zero otherwise. Similar as in Eqn 4.3 we define a (free) segment distribution as $G(z) = \exp\left(-u(z)\right)$. This free segment distribution function is used to generate so-called end-point distribution functions $G(z, s|s_1)$, which is a statistical weight of segment s that accounts only for the part of the molecule connected to segment s_1 next to it. Here and below s_1, s_2, and s_3 refer to ranking numbers of segments which have a bond with segment s. For each bond of segment s we define an end-point distribution function. In this way for each end segment $s \in \{s_e\}$ there is one end-point distribution $G(z, s|s_1)$, for intermediate segments $s \in \{s_i\}$ there are $G(z, s|s_1)$ and $G(z, s|s_2)$, and $G(z, s|s_1)$, $G(z, s|s_2)$, and $G(z, s|s_3)$ for branch segments $s \in \{s_b\}$. Given end-point distribution functions of an intermediate segment $s \in \{s_i\}$, free end distributions of its immediate neighbors s_1 and s_2 may be generated using a pair of propagators, which implement the freely-jointed chain model:

$$G(z, s_2|s) = G(z)\left\langle G(z, s|s_1)\right\rangle \tag{4.5}$$

$$G(z, s_1|s) = G(z)\left\langle G(z, s|s_2)\right\rangle \tag{4.6}$$

where the angular brackets imply a three-layer average, i.e. $\langle X(z)\rangle = \lambda_1 X(z-1) + \lambda_0 X(z) + \lambda_1 X(z+1)$. End-point distribution functions of segments connected to a branch point are defined somewhat differently to account for other branches connected to a branch segment. To propagate from a branch segment $s \in \{s_b\}$ connected to segments s_1 and s_2 to segment s_3 it is necessary to combine $G(z, s_b|s_1)$ and $G(z, s_b|s_2)$:

$$G(z, s_3|s) = G(z)\left\langle \frac{G(z, s|s_1)G(z, s|s_2)}{G(z)}\right\rangle \tag{4.7}$$

Analogous equations for propagation to s_1 and s_2 are obtained from Eq. 4.7 by permutation of s_3 with s_1 or s_2. The propagation starts with an end-segment $s \in \{s_e\}$, which has only one bond with segment s_1. The statistical weight of an end-segment which does not include the bond with s_1 is the free segment distribution, hence,

$$G(z, s_1|s) = G(z)\,\langle G(z)\rangle \tag{4.8}$$

Starting with free ends and propagating through middle segments and branch segments it is possible to calculate all end-point distribution functions of all segments and, finally, calculate polymer volume fraction distribution using the composition law:

$$\varphi(z) = \frac{\varphi^b}{N}\left(\sum_{\forall s\in\{s_e\}} G(z,s|s_1) + \sum_{\forall s\in\{s_i\}} \frac{G(z,s|s_1)G(z,s|s_2)}{G(z)} + \right.$$
$$\left. + \sum_{\forall s\in\{s_b\}} \frac{G(z,s|s_1)G(z,s|s_2)G(z,s|s_3)}{G(z)^2}\right) \tag{4.9}$$

The set of equations is closed and is solved routinely by a numerical algorithm up to at least 7 significant digits. When for the free energy of interaction more precision is needed, the accuracy is increased. If not mentioned otherwise we have for the adsorption energy $\chi_s = 1$ and have a good solvent $\chi_{AW} = 0$.

The ground state approximation

The propagator Eqs. 4.5 - 4.8 are the discrete versions of the Edwards equation,[60] which may be written as

$$\frac{\partial G(z,s)}{\partial s} = \frac{1}{6}\frac{\partial^2 G(z,s)}{\partial z^2} - u(z)G(z,s) \tag{4.10}$$

where we simplified the notation for the end-point distribution $G(z, s)$ by leaving out the starting position. In general it is possible to rewrite this end-point distribution using an eigenfunction expansion and then approximate it with the dominant term:

$$G(z,s) = \sum_k g_k(z)\exp(\epsilon_k s) \approx g(z)\exp(\epsilon s) \tag{4.11}$$

where $\exp(\epsilon)$ is the largest (ground-state) eigenvalue and $g(z)$ the corresponding (ground state) eigenfunction. Within this ground state approximation, e.g., the volume fraction $\varphi(z,s) = \varphi^b G(z,s)G(z,N-s) = g^2\varphi^b\exp(\epsilon N)$ for an interior segment in the chain. Upon substitution of the rhs of Eqn 4.11 into Eqn 4.10 we obtain an ordinary differential equation in g:

$$\frac{\partial^2 g}{\partial z^2} = 6\,(\epsilon + u)\,g \tag{4.12}$$

This equation may be solved when ϵ is known and when u is expressed in terms of g.

Using the Ansatz that for middle segments the computation of the volume fraction becomes simply $\varphi(z) = g^2(z)$ we find that $\epsilon \approx -\frac{1}{N} \ln \varphi^b$. Following de Gennes,[3] we expand the logarithm in Eqn 4.4 and obtain that in good solvents $u(z) \approx \varphi(z) - \varphi^b = g^2(z) - (g^b)^2$.

For dilute solutions we can ignore φ^b in the segment potential and the solution of Eqn 4.12 may be written as

$$g = \frac{1}{\sqrt{3}d} \frac{1}{\sinh \frac{z+p}{d}} \tag{4.13}$$

In this equation two length scales are introduced. The proximal length p is related to the adsorption energy and for strong adsorption it is of the order of the segment size (which is in the lattice language translates to order unity). The distal length is of order the radius of gyration $d = \frac{1}{\sqrt{6\epsilon}} = R_g / \ln \frac{1}{\varphi^b}$. Using $\varphi = g^2$ it is found that the adsorption layer is split into three regions (see also fig. 4.1). For strong adsorption there is (i) the proximal region $z < p$, just next to the surface, where the volume fraction is of order unity, (ii) the central region $p < z < d$ where $\varphi(z) \approx z^{-2}$ and the distal region ($z > d$) where the volume fraction profile relaxes to the bulk exponentially $\varphi(z) \propto \exp \frac{-2z}{d}$, i.e. the decay length is approximately R_g with a logarithmic correction that contains the bulk concentration.

De Gennes first recognized how this result should be generalized for proper excluded-volume effects. The first step is to realize that in the polymer adsorption profile, the semi-dilute polymer concentrations are found in the central region. The mesh size in semi-dilute polymer solutions is known to be $\xi \propto (\varphi^b)^{-3/4}$ in scaling and for mean field $\xi \propto (\varphi^b)^{-1/2}$. For the central part of the profile de Gennes argued that the local mesh size can not exceed the distance to the wall. More specifically he proposed to set the mesh size equal to the distance to the wall $z \propto (\varphi(z))^{-1/2}$ for mean field. Inverting this equation immediately gives the correct self-similar result $\varphi(z) \propto z^{-2}$ and in scaling $\varphi(z) \propto z^{-4/3}$. The argument is quite general and we will see, it can be applied to architecturally complex polymers as well.

It is well known that Eqn 4.13 can also be used to estimate the volume fraction distribution of the ends, because $\varphi_e(z) \propto g(z)$. In the central part the end-point distribution should therefore decay with $\varphi_e(z) \propto z^{-1}$. For branch points on the other hand, three chain fragments come together and therefore we expect for these units an extremely fast decay of the density. More specifically, we expect $\varphi_b(z) \propto g^3$ which translates to $\varphi_b(z) \propto z^{-3}$ for the central region of the density profile. This means that already from a ground-state analysis we expect to find non-trivial differences in the profiles of branch points and teeth ends.

The ground state approximation can also be used to rationalize the free energy of interaction of bringing two surfaces towards each other in the presence of adsorbing polymers.[3] One can start such an analysis by a Landau free energy where the order parameter is expanded up to second order. The Euler-Lagrange equation coincides with Eqn 4.12. This shows that in this case g is the order

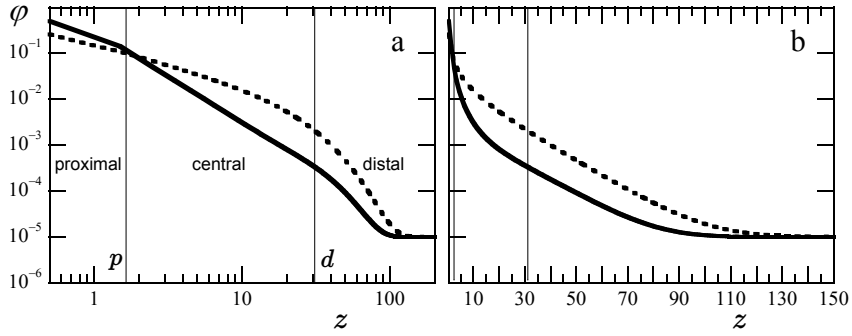

Figure 4.3: *Overall volume fraction profiles of linear polymers (solid lines) and normalized volume fractions of free chain ends E (dotted line) on a) log-log coordinates and b) log-lin coordinates. The thin vertical lines are positioned at the estimated positions of p and d. The proximal, central and distal regimes are indicated. Parameters: Strong adsorption $\chi_s = 1$, good solvent $\chi = 0$, $N = 10^4$, polymer concentration just below overlap, i.e., $\varphi^b = 10^{-5}$.*

parameter. Inserting the known g (cf Eqn 4.13) back into the Landau free energy and subtracting the value for large distances between the surfaces gives the free energy of interaction. From such an approach it is found that the free energy of interaction goes down with decreasing distance. This means that attraction is predicted. Non-attractive contributions to the free energy of interactions must therefore be assigned to the effect of tails.

4.3 Results

Several years ago Van der Linden and coworkers[86] studied the adsorption of comb homopolymers onto an isolated solid-liquid interface. For example Van der Linden showed that branching suppresses the plateau of adsorption isotherms somewhat, but increases the adsorption in the Henry region. The volume fraction distribution was analyzed for a large number of cases and large differences were found with respect to the linear chains. One key result that was reported is that the teeth adsorb less strongly than the backbone and that the teeth have on average some non-isotropic conformation. There was no attempt to analyze the profiles in terms of the de Gennes picture of proximal, central and distal regimes. Below, we will focus therefore more on such analysis. Finally in ref.[86] a systematic investigation was presented on the critical adsorption energy and how this is affected by the teeth length, distance between teeth etc. This will not be repeated here. Instead we exclusively select the strong adsorption case. As in ref.[86] no attention was given to the colloidal stability issues we will pick up this issue below.

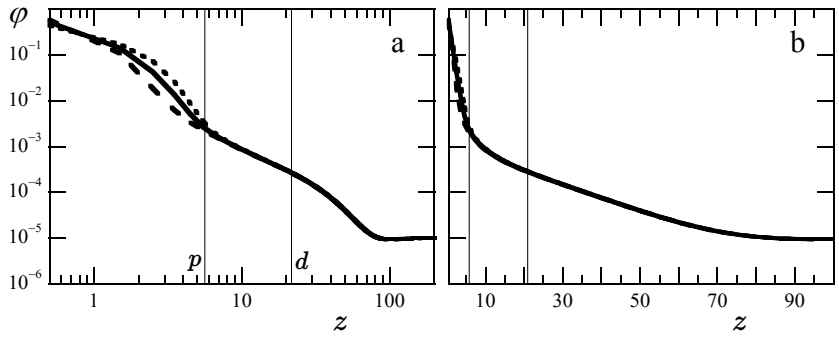

Figure 4.4: *Overall volume fraction profiles of comb polymers (solid lines), normalized volume fractions of free chain ends E (dotted line) and junction points C (dash-dotted line) on a) log-log coordinates and b) log-lin coordinates. Again the vertical lines are placed at estimated valued of p and d. Parameters:* $N = 35000$*, backbone length* $N_{bb} = 10000$*, spacer length* $m = 2$*, tooth length* $t = 5$ *and number of teeth* $n = 5000$*. Other parameters as in fig. 4.3.*

Comb homopolymers at isolated surfaces

For presentation purposes linear chains adsorbed onto a solid-liquid interface from a good solvent are discussed first. Results similar to that of figure 4.3 were reported before in ref.[90]. In a double logarithmic plot, i.e. in fig. 4.3a, one can clearly identify the central regime of the adsorbed layer. The $\varphi(z) \propto z^{-2}$ decay is found in very good approximation, proving that for linear chains the ground state approximation is reasonable. As argued above, the proximal length $p \approx 1$. The cross-over from the central to the distal regime occurs at the length scale $d \propto R_g$. The polymer concentration at this distance $\varphi(d)$ is very close to the overlap concentration which is $\varphi^{ov} \sim N^{-1}$ for the mean field case. The dotted line in fig. 4.3 gives the distribution of the chain ends. The profile is normalized so that in the bulk the profile overlaps with the overall profile, i.e. it is multiplied by $N/2$. Completely in line with the predictions discussed above, we find that the end-point distribution decays in the central part as $\varphi_e(z) = z^{-1}$.

On the log-lin coordinates (cf fig. 4.3b), the distal regime shows up as a straight line, completely in line with the ground state analysis. Again the decay length is of the order R_g as expected. In fig. 4.3 thin vertical lines are drawn at estimates of the positions of the lengths p and d to help identify the proximal (for $z < p$), the central (for $p < z < d$) and the distal ($z > d$) regions in the profile. Clearly the de Gennes picture is obeyed in large detail.

In figure 4.4 we focus on the case of a long comb polymer with many short side chains that are spaced along the back bone close to each other. The idea is that one can view this comb polymer as a long homopolymer with non-trivial structure on the monomer length scale. If this is the case one should be able to identify a similar picture as found in fig. 4.3. Inspection of fig. 4.4 proves that the

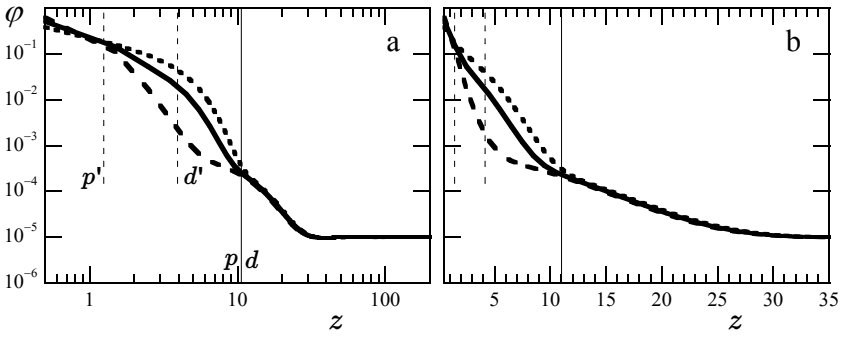

Figure 4.5: *Overall volume fraction profiles of comb polymers (solid lines), normalized volume fractions of free chain ends E (dotted line) and junction points C (dash-dotted line) on a) log-log coordinates and b) log-lin coordinates. Only one vertical line is drawn which carries both labels p and d. In addition we show by two dotted lines the length scales p' and d' associated with the internal structure of the proximal part of the profile. Parameters: Total number of segments $N = 5000$, backbone length $N_{bb} = 1000$, teeth length $t = 20$, spacer $m = 5$ and $n = 200$ Other parameters as in fig. 4.3.*

.

profile is significantly more rich. Starting with fig. 4.4b where the profile is given in log-lin coordinates, one can identify the start of the distal region as before. In this case $d \approx 25$. In figure 4.4a both the normalized profiles for the ends of the teeth as well as the branch points are shown. As expected they differ from each other significantly near the surface. We estimate the position of the proximal length p where the difference between these two profiles vanishes. Clearly at this length the features of the effective monomer vanish. In this case $p \approx 5$ which coincides with the length of the teeth. Indeed, as expected the proximal length increased significantly with respect to the linear homopolymer case. The central regime is still significant as it ranges from $z = 5, \cdots, 25$. The thin vertical lines are drawn once again to help identify the various regimes in the profile. Again the volume fraction $\varphi(d) \sim \varphi^{ov}$; the self-similar concentration profile gives way to an exponential profile as soon as the polymer concentration drops below the overlap concentration.

The most important part of the profile is arguably the proximal region, because the vast majority of the adsorbed chain segments is in fact very close to the surface. We may try to interpret what happens in the proximal part of the profile. From fig. 4.5a it is seen that the teeth end profile deviates much from that of the branching points. Clearly there is some orientation of the teeth. This observation suggests that it is possible to view this surface layer as being similar to a flat polymer brush. However, the polymer density is still relatively low for such identification; at best it is a layer of (deformed) mushrooms. Alternatively, the teeth may be viewed as short adsorbing chains, which have their own adsorbed profile, arguably very

similar to what they would have had when they would have been detached from the backbone. However, in the free (detached) case the adsorbed amount of the teeth definitely would be less. Indeed, the teeth have some dual characteristics. For entropic reasons the free ends, and thus also the ends of the teeth, have the tendency to avoid the surface. This causes the weak local orientation of the teeth. We will return to this when we discuss the consequences of this for the free energy of interaction caused by the comb polymers. In the section on the ground state approximation we already point to the difference in scaling expected for the branch and teeth ends. However, it is not reasonable to try to go into these details here and we reserve this part of investigations to the case where the teeth dominate the profile.

In figure 4.5 a system where the teeth are somewhat longer, but where they do not yet dominate the adsorption profile, is presented.This system is selected because the central region appears to be lost in this case. Now the tooth length is $t = 20$ and the teeth are spaced $m = 5$ segments apart while $n = 200$. As in fig. 4.4 the proximal distance p is found by the point where the normalized teeth end profile merges with that of the branching points. As seen in fig. 4.5a we estimated $p \approx 10$, which is of the order of, but smaller than the full length of the teeth. From fig. 4.5b we notice that there is a significant distal regime as the $\log \varphi(z) \propto z$. In an attempt to position d, it appears that it coincides with p. That is why we have only one vertical line in fig. 4.5. The disappearance of the central region of the adsorption profile has several important consequences. One of these is that the classical train-loop-tail picture breaks down. The layer does not feature any long loops. As loops are important for the bridging attraction, one should once again anticipate important consequences for the colloidal stability. In fig. 4.5 we have within the proximal part of the profile drawn two vertical dashed lines and labeled these p' and d'. These distances will be discussed below.

It is possible to come up with comb polymers for which the structure of the adsorbed layer is fully dominated by the teeth. In figure 4.6 such case is presented where the teeth length $t = 100$ and $n = 500$ spaced $m = 10$ segments apart. In this system it is impossible to find both the classical central regime (as in fig 4.5) as well as a 'normal' distal regime. Instead the proximal part of the profile fully occupies the profile. Very characteristic for this layer is the strong dip in the volume fraction profile which is found at the position where the proximal part tries to merge to the bulk. Clearly the non-adsorbed molecules in the bulk have no tendency to interpenetrate the adsorbed layer. In such a case it is quite natural to expect a depletion zone to develop. As can be seen in fig. 4.6a the region over which the profiles of the ends of the teeth differ from the branching points extends completely to the end of the adsorption profile. This means that at the periphery the chains are significantly oriented. The isotropic bulk chains avoid such anisotropic layer. The relaxation of the density profile towards the bulk value occurs again with a decay length of order R_g. In other words the depletion layer thickness is of order R_g (of the full chain). In passing we note that overlap of depletion zones should give rise to attraction. This attraction is

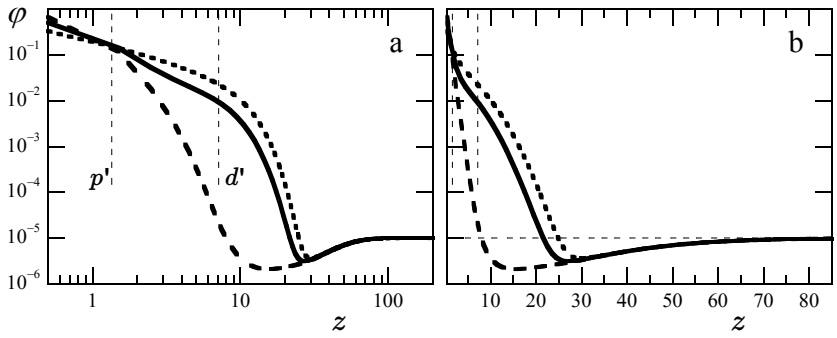

Figure 4.6: *Overall volume fraction profiles of comb polymers (solid lines), normalized volume fractions of free chain ends E (dotted line) and junction points C (dash-dotted line) on a) log-log coordinates and b) log-lin coordinates. Short vertical dotted lines are placed at estimations for p' and d', the new length scales within the proximal region of the system. Parameters: Total number of segment $N = 55000$, backbone length $N_{bb} = 5000$, spacer $m = 10$, teeth length $t = 100$ and $n = 500$. Other parameters as in fig. 4.3.*

.

proportional to the osmotic pressure in the solution times the overlap volume. As the osmotic pressure for dilute polymer solutions is low, we only expect a weak attraction from this.

In the next part the structure of the adsorbed layer is discussed in more detail. For this we focus on the properties of the teeth. As mentioned the proper way to look at this adsorbed layer is as being composed of chains with length equal to the teeth length. These side chains assume their train-loop and (one) tail conformation. It is therefore not unreasonable to adopt the scaling picture of de Gennes, but apply this on these shorter teeth. For a graphical illustration of this we point to fig. 4.7. Although for short chains it is difficult to identify the various regimes, it is nevertheless worthwhile to try to do so. The first observation is that the normalized distribution of the teeth ends has a clear power-law behavior and in line with the results presented in fig. 4.3 the profile $\varphi_e(z) \approx z^{-1}$ is recovered. Note that similar slopes are consistent with results shown in fig. 4.4a, 4.5a (dotted lines). Indeed in this range of distances the overall profile is consistent with $\varphi(z) \propto z^{-2}$. The branch points show a stronger dependence as expected, i.e. the profile shows a scaling close to $\varphi_b(z) \propto z^{-3}$. As a result one can try to identify the distances p' and d' that bracket the 'central' region of the teeth chains. We have shown these estimates in fig. 4.6a. Indeed the polymer density in the range $p' < z < d'$ is in the semidilute regime of side chains. In fig. 4.6b we may next attempt to see the distal regime of the profile of the teeth. Even though the teeth are very short we can identify a close-to-straight line between for $15 < z < 25$ indicating that indeed there is something like a distal zone in the proximal part of the overall profile. The slope of this line is consistent with R_g for the teeth

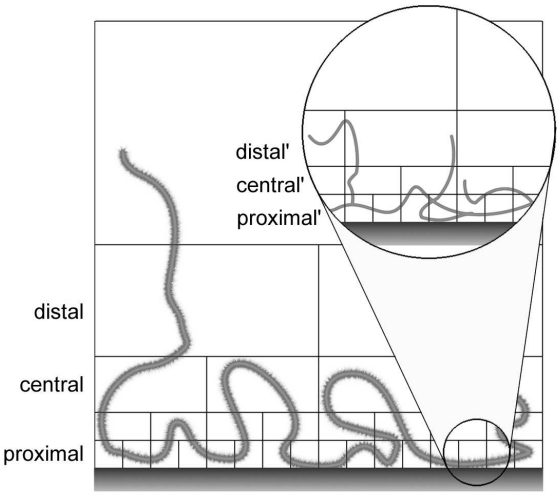

Figure 4.7: *Schematic illustration of how comb copolymer adsorb onto a solid substrate for the case that the backbone length is several orders of magnitude longer than the side chains. On the large scale the classical picture prevails, with two long tails and a self-similar region with many small and few larger loops (proximal, central and distal regions are indicated). At small length scales (zoomed in part) a similar self-similar structure exists where the side chains form the train-loop-tail distributions. For the inset we point to the proximal' central' and distal' regimes (note the primes).*

chains.

In trying to interpret d' values, it is noticed that it is much larger than R_g for the teeth chains. The reason for this is that the relatively short teeth are grafted to the backbone and due to this the adsorbed amount of the teeth is relatively high. The increased polymer density will decay as a power law until the volume fraction drops below the overlap. Note that we here refer to the overlap concentration of the teeth, not that of the overall chains. In any case, the central region is significantly stretched. Inspection of results in figs 4.4a, and 4.5b show similar trends albeit less outspoken.

The observation that the central region that is associated with the adsorption of the teeth is stretched over a relatively large distance, i.e. it exceeds the natural size of isolated teeth $R_g(t) \propto t^{1/2}$, is interesting. Above this was attributed to the fact that the teeth are irreversibly attached to the backbone and therefore can not choose the adsorbed amount independently. Indeed the cooperative effect causes the adsorption to be higher than their 'natural' value. Hence the teeth are somewhat more extended and this explains the fact that the central region is wider. It is also possible to argue that such phenomenon occurs only when the teeth along the backbone are sufficiently close to each other (sufficiently small value of m) so that neighboring teeth along the backbone feel each other and as a result stretch (as in a bottle brush), giving rise to an extended central region as well.

In summary, there exists a hierarchical structure inside the comb polymer adsorption layer. Again pointing to fig. 4.7 on a large scale there is a proximal central and distal regimes. The local effects of the side chains is fully contained in the proximal part. When the side chains are sufficiently long, we can further zoom into the proximal part and identify a proximal, central and distal regime that can be attributed to the side chains. We will next use similar systems to study the effects of adsorbed comb polymers on the colloidal stability.

Colloidal stability

The free energy of interaction $F^{int}(D)$ of two colloidal particles as a function of their separation D is well known for the linear homopolymer case. It is necessary to discuss this case for reasons of comparison. In figure 4.8 the free energy of interaction is given in two scales. In panel a relatively small values of D are selected and the free energy scale is of the order of 10^{-3} k_BT per unit area b^2. In panel b the results for $D > 6$ are shown on the 10^{-5} scale. As anticipated the interaction free energy is non-monotonic. At large distances there is a small repulsion which is attributed to the steric effect of overlapping tails and there is a huge attraction at short distances which is attributed to the bridging. Inspection shows that the maximum in F^{int} is very small indeed and in most cases too small to be of relevance to stabilize particular systems. One would need a contact area of approximately 10^6 b^2 before the free energy becomes of the order of the thermal energy k_BT. Thus the curve is essentially attractive (consistent with the ground

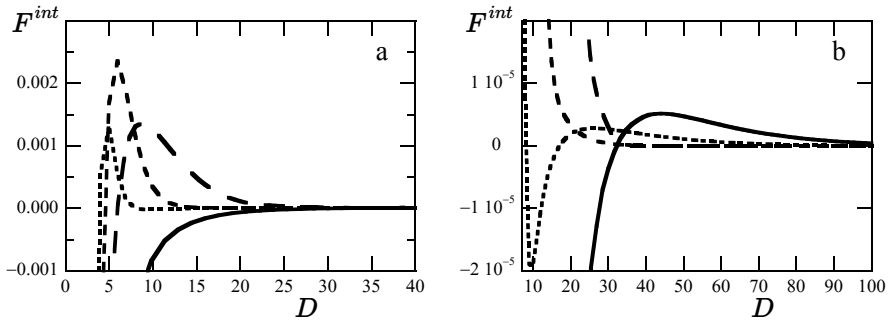

Figure 4.8: *Free energy of interaction F^{int} in units of k_BT per unit area (b^2) as a function of the distance D in units b between the surfaces. The four curves correspond to the four cases discussed above. The solid line is for the linear homopolymer case fig. 4.3, the dotted line corresponds to the case with relatively short side chains fig. 4.4, the short dashed line is for teeth with intermediate length of fig. 4.5 and the long dashed line represent the system with long teeth of fig. 4.6. In all cases the bulk volume fraction if fixed to $\varphi^b = 10^{-5}$ so that the system is close to, but below, overlap (for the whole chain) conditions. In panel a the free energy scale is 100 times larger than in panel b and in the latter one only the results for $D > 6$ are shown.*

state approximation). The bridging attraction is the universal feature that may be attributed to this system. Again, because the number of loops that can transform in bridges strongly increases with decreasing distance, the attraction is significant and strongly increases with decreasing distance.

In fig. 4.8 the curve with the dotted lines correspond to the system discussed above in figure 4.4. Here rather short teeth $t = 5$ are planted relatively close to each other (spacing $m = 2$). It was concluded that the classical picture was not yet destroyed even though the proximal region increased significantly. Inspection of the interaction curve shows that there are a few novel features. Upon compression first little free energy changes are recorded then for relatively short separations a significant repulsion is found which is followed by an even stronger attraction (near contact). Comparing length scales, we conclude that these two effects must be attributed to the teeth of the comb polymers. Above it was argued that the teeth are slightly oriented and due to this one should expect a repulsion. The 'contact' attraction is due to the formation of bridges made possible by the overlap of the loops of the teeth. In addition to these large free energy effect, inspections of fig. 4.8b shows that also for this case there exist a classical repulsion due to the overlap of large tails and some attraction due to the transformation of long loops into bridges. Both these effects may have been expected because of the observation that the central region of the adsorption profile was still present (cf. fig. 4.4).

From figure 4.5 it was concluded that when the teeth length was increased to $t = 20$ and the spacer length was increased somewhat that the central regime that

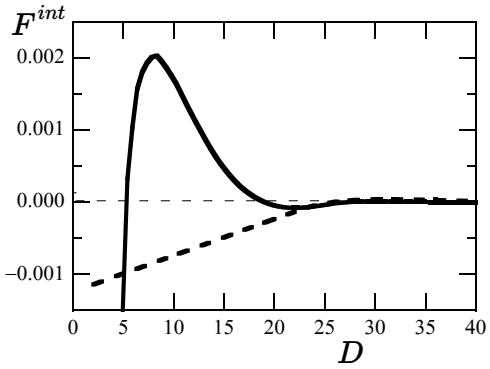

Figure 4.9: *Free energy of interaction in units k_BT per lattice site for polymers as in fig. 4.6 ($m = 10$, $t = 100$, $n = 500$) for $\varphi^b = 10^{-2}$. The solid line is the result for the default interaction with the surface, i.e., $\chi_s = 1$, the dashed line is the depletion case, $\chi_s = 0$.*

can be attributed to the structure of the backbone was lost. In line with this, the free energy of interaction simplified (see the short dashed line). Now only the features due to the teeth (overlap of the proximal part of the profile) give a noticeable contribution to the free energy of interaction. Indeed, the free energy is repulsive for all distances D except for the close-to-contact spacings. The onset of the repulsion $D \approx 20$ correlates with the lengths $p = d$ of the profile shown in fig. 4.5. The maximum of the free energy is several orders of magnitude higher than typical for the linear polymers. Indeed this can only be attributed to the fact that the comb polymer introduces a multitude of repulsive chain ends to the adsorption layer.

The long dashed lines in fig. 4.8 correspond to the case where the teeth length amounts to $t = 100$ (cf. fig. 4.6). Now the whole adsorption layer is dominated by the teeth structure. Compared to the previous case the maximum has shifted to somewhat larger distances and also the primary attraction sets in at somewhat larger D. With increasing length of the teeth we thus observe that the primary attraction becomes somewhat of longer range. This is consistent with the idea that the conformation of the adsorbed teeth can feature larger loops with increasing teeth length (appearance of a central' regime). These larger loops will enable bridge formation at larger values of D.

The dip in the profile observed in fig. 4.8, where the complete adsorption profile is characterized by weakly oriented teeth, was attributed to a depletion effect. When such depletion zones overlap one should expect to find a depletion attraction. The result of fig. 4.8 does not show such depletion attraction. The reason for this is that the osmotic pressure, which below overlap is estimated to be given by van 't Hoff's law, is extremely small in this case (overall degree of polymerisation is rather large $N = 5.5 \times 10^4$).For this reason we performed

calculations for the same polymers as in fig. 4.6 but with an increased polymer concentration in the bulk of $\varphi^b = 10^{-2}$. The volume fraction profile is relatively simple and not shown. Basically the profile as given in fig. 4.6a is followed up to $z = d'$, then a depletion dip is found before the profile relaxes to the bulk value 10^{-2}, qualitatively similar to the $\varphi^b = 10^{-5}$ case, albeit that it relaxes back to the bulk concentration more quickly for high concentrations (decay is given by the mesh-size in the semi-dilute which is smaller than the coil size in the dilute regime). In figure 4.9 the free energy of interaction is presented for this case (solid line). As anticipated we find a decrease of the free energy of interaction for distances $D \approx 20$ (which is close to two times d'). The depth of the minimum is close to 10^{-4} k_BT per site. In the same graph we present the free energy of interaction for the case that the polymer units have no interaction with the surface (dashed line). The density profiles show the depletion zone near the surface (not shown) and the free energy of interaction (depletion interaction) is of the same order of magnitude and range as in the case of adsorption. This confirms the idea that the minimum at $D \approx 20$ is due to depletion. Returning to the adsorption case, we see that at shorter separations $6 < D < 15$ there is a reasonably strong repulsion which is followed at short distances $D < 5$ by a strong attraction. This attraction is due to bridging and is much stronger than the depletion interactions (note the crossing of the solid and dashed lines). Hence, in the interaction curve there is a primary (near $D = 1$) as well as a secondary minimum ($D \approx 20$) separated by a primary maximum. To our knowledge such DLVO-like potential has never been reported in the polymer literature for polymer chains that have just one type of segment. Upon close inspection, there appears also a very small secondary maximum in the interaction curves and in fact the interaction curves are oscillatory with an exponentially decaying amplitude. Such effects have been reported and analyzed by Van der Gucht and coworkers[91] for linear polymers, and are largest when the polymer concentration is slightly above overlap. The fact that these oscillatory effects are stronger for comb than for linear chains is consistent with the idea that with increasing branching the polymer chains gradually become less soft and become more like hard colloids.

Figures 4.8 and 4.9 give all relevant types of interaction curves. Of course it is possible to present parameters that we can vary to go from one type of interaction curve towards another one. One of such exercises is discussed briefly. Let us consider systems for which the local parameters t and m are fixed and see how the curves change with increasing length of the backbone N_{bb} (and thus the overall molecular weight). The idea is that when the degree of polymerization is not too large, the length scale associated with the teeth dominates and the interaction curve is similar to, e.g. the short dashed line in fig. 4.8. Then, with increasing length of the backbone, the interaction curve will develop a secondary minimum as the dotted line in fig. 4.8. Eventually for very large values of the degree of polymerization the secondary minimum becomes so deep that effectively the system behaves as a linear homopolymer[92], the features at very small D values then become irrelevant. In a way, the system shown with the dotted line

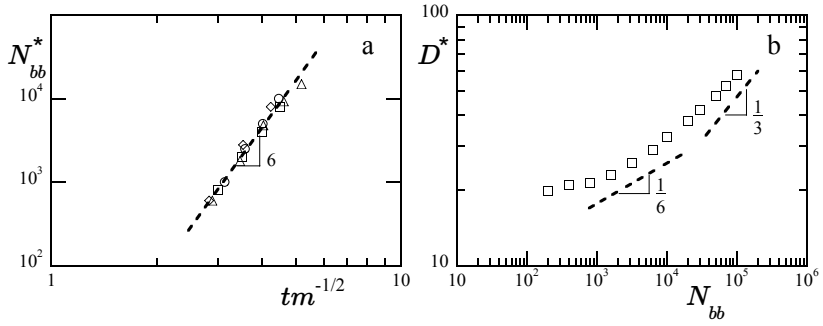

Figure 4.10: *a) The cross-over length of the backbone N^*_{bb} as a function of $t \times m^{-1/2}$ in log-log coordinates. The dashed line with slope 6 is plotted to guide the eye. Data points: $m = 2$ diamonds, $m = 3$ triangles, $m = 4$ squares, and $m = 5$ circles. b) The distance between two surfaces D^* (where the free energy of interaction switches from being negative to positive) as a function of the length of a linear homopolymer chain in log-log coordinates. For large N_{bb} the curve approaches the scaling regime with slope 1/3 (as indicated). In the relevant range $N_{bb} < 10^4$ the apparent scaling of 1/6 (slope indicated) appears appropriate.*

is in between two limiting cases. Indeed we can search for those cases for which the secondary minimum has a value of $F^{int} = 0$. The backbone length for which this occurs we denote by N^*_{bb}. Physically, for $N_{bb} < N^*_{bb}$, the teeth dominate and the interaction curves are mainly repulsive (except for the attraction for distances close to contact) and the polymers can be used to stabilize particular solutions. For $N_{bb} > N^*_{bb}$ the secondary minimum, which is attributed to the bridging effect, becomes important and these macromolecules can be used as flocculants.

We have collected estimates for N^*_{bb} values for systems with relatively short teeth $3 \leq t \leq 10$ and small values of the spacers ($2 \leq m \leq 5$). Results are shown in fig. 4.10a where the cross-over length of the backbone N^*_{bb} is plotted as a function of $t \times m^{-1/2}$ on a double logarithmic scale. In these coordinates the data, reasonably accurately, collapse onto a master curve. The dashed line presented in fig. 4.10a has a slope of 6, indicating that the critical number of teeth $N^*_{bb} \propto t^6 m^{-3}$ to a fair approximation.

To generate attraction in a system with long comb homopolymers, the backbone loops must protrude beyond the proximal zone $p(t)$ dominated by the side chains. As an estimate of the range accessible to the backbone loops we take D^*, which we here define as the point where the interaction curve for a linear chain crosses the axis and $F^{int}(D^*) = 0$. For distances larger than D^* the effect of the backbone ends is stronger than that of the loops, whereas for distances $D < D^*$, the bridging dominates. In fig. 4.10b we show for linear homopolymers that D^* scales with chain length with the expected power 1/3 for very long chains, i.e. $N_{bb} > 10^5$ and that for shorter chains the power is significantly smaller. More specifically, the apparent scaling exponent for chains with length $10^3 < N < 10^4$

(range of backbone lengths of fig. 4.10a) appears close to 1/6. We now may argue that when $D^*(N_{bb}) < p(t)$, the contribution of the backbone loops can not exceed that from the free ends and the interaction curve is repulsive. Only when $D^*(N_{bb}) \approx p(t)$ the local minimum in the interaction curve becomes important. For short teeth and small spacers m, $p \propto t$. The local minimum in the interaction curve appears when $D^*(N^*_{bb}) \approx t$, and we arrive at $N^*_{bb} \propto t^6$ which is consistent with the slope in fig. 4.10a). Again, with increasing N_{bb} the slope in 4.10b goes up. From this we may anticipate that the slope in figure 4.10a decreases with increasing N^*_{bb}. For combs with long teeth that are sparsely grafted, $m > t$, the scaling exponent may significantly decrease to $N^*_{bb} \propto t^{3/2}$.

As a practical consequence we mention that when m is not too large, i.e. when the teeth are planted frequently along the backbone, the length of the teeth may not need to be very long before N^*_{bb} becomes extremely large. To our mind this means that large families of homopolymers, in particular those with short molecular fragments as side chains, will have non-universal features up to rather high molecular weights.

4.4 Discussion

Results presented above are generated using the self-consistent field theory that features a (local) mean-field approximation. Indeed, inter and intra-molecular excluded-volume effects are accounted for in the polymer adsorption layers, but these effects are ignored for the chains in the bulk. For bulk chains it was assumed that these are Gaussian coils, irrespective their architecture. As the interfacial chains are equilibrated with the bulk chains, we find that the adsorbed amount is somewhat underestimated; in a SCF model polymers escape to the bulk at relatively low coverages (adsorbed amount approximately one equivalent monolayer).

Following de Gennes, we can argue that it is possible upgrade the mean-field results to account for the 'correlation' effects and replace the -2 exponents by the $-4/3$ (in the self-similar regions of the polymer volume fraction profiles). Due to the mentioned intramolecular excluded-volume effects, which are more important for the branched macromolecules than for the linear ones, the scaling theory will lead to higher adsorbed amounts in the plateau of the adsorption isotherms. Hence the crowding of the chains at the surfaces is higher for scaling than in mean field. Increasing the number of chains per unit area will obviously also affect the free energy of interaction for such systems. How large these effects are is not known, however, it is fair to expect that the repulsion will be larger for the scaling than for the mean-field cases.

Classical linear homopolymers are, as already explained in the introduction, not-so-good species to stabilize particular solutions. There is an extremely small repulsion found for distances between the surfaces close to the size of the coils, e.g. $D \sim R_g$ (and this is expected to remain very small for the scaling case). As the size of this repulsion is due to the overlap of tails, it reduces with increasing

length of the chains. In this sense there is a trend that homopolymers become better flocculants with increasing molecular mass. Comb macromolecules introduce many more chain ends (as the linear analogues) to the adsorbed layer and therefore are much much better to stabilize particular solutions than their linear analogous. Increasing (for fixed local architecture (t and m) the molecular weight, may eventually introduce a bridging mechanism into such systems. Hence, we may anticipate that there are macromolecules that operate as stabilizers for relatively low molecular weight, but are flocculants for very high molecular weights. Such anomalous effects will best be seen by comb polymers with a significant moiety as a side chain.

Comb polymers for which the backbones are a few orders of magnitude larger than their polymeric teeth, have adsorption characteristics with two length scales. Associated to these lengths there are regions of self-similar concentration profiles, i.e., there is a 'central' region. On the one hand there is the length scale associated with the backbone and one can find the self-similar structure of the adsorbed layer for distances to the surface less than the radius of gyration of the overall chain but larger than the size of the teeth ($R^{teeth} \propto t^{3/5}$). Then on the length scale of the side chains there is once again a self-similar adsorbed layer. In principle neutron scattering experiments may be able to pick up this behavior. We are not aware of reports on this issue.

Not only the adsorption, but also the bulk behavior of such comb polymer systems will be of interest. De Gennes showed that knowledge of the (semi-dilute) bulk behavior can be used to explain the adsorption characteristics. Here we can try to do the inverse and predict how comb polymers behave in the bulk from complementary knowledge of adsorption. Of special interest are comb polymers with two separated length scales, one associated to the dimensions of the teeth and one to the macromolecule as a whole. In the adsorption profile we could recognize two distinct self-similar regions in this case. (cf. fig. 4.4) The polymer concentrations where the power-law regions give way to the exponential parts, signals the overlap concentration. Apparently, for such systems there are two overlap concentrations. One overlap condition is at relatively low polymer concentrations, where the coils made by the comb polymers start to overlap, and there is a second much more concentrated polymer concentration above which the side chains start to overlap. As a result, physical quantities such as the osmotic pressure of such polymer solution should therefore be interesting functions of the polymer concentration as well.

Very often polymers may have short side groups on a monomeric level. Such polymers will behave as linear homopolymers in the limit of infinite chain length. However, in practice the polymers are of finite size and some of the complications discussed above may easily occur. Hence, to understand the behavior of polymers that have some complex structure on the monomeric level, it is reasonable to account for the monomeric properties in one way or another. The result of fig. 4.10 clearly shows that non-universal features can persist up to very high degrees of polymerization.

For typical non-trivial monomeric structures in complex macromolecules, it rarely is the case that the monomer structure is homogeneous in the sense that there is no amphiphilicity along the side chain. For example in many polyelectrolytes there is a charged group at the otherwise apolar side chains. Also the backbone has often a different chemical structure. Such amphiphilicity on the monomeric level will amplify the phenomena discussed in this paper. Indeed in this case we may expect that there is more orientation on the monomeric level and stronger repulsion when two of these oriented layers (on opposite surfaces) overlap. It is of interest to extend the present analysis to the case of some amphiphilicity inside the monomeric units.

4.5 Conclusions

The adsorption of comb polymers is studied by a lattice-based self-consistent field theory which effectively implements Edwards equation on a grid. We find that both the adsorbed layer as well as the effect of these polymers on the colloidal stability are strongly affected by the architectural parameters, such as, the tooth length t, as well as that of the spacer m and the number of teeth n. Unlike linear homopolymers, comb polymers can form adsorption layers that cause a significant repulsion when these are forced to overlap. Hence combs are relatively good species to induce colloidal stabilization. This extra repulsion is attributed to the presence of many chain ends. Indeed the side chains are found to be slightly oriented such that the overlap of these teeth is unfavorable from a free energy perspective. For very long backbone lengths, it was possible to recover the bridging attraction, but when the side chains are densely grafted and not too short, the expected universal behavior is found for macromolecules that fall outside the synthetic capabilities. An interesting situation occurs when the length scale of the backbone and that of the teeth are sufficiently separated. In this case we found two regions in the adsorption profile with self-similar structure. Such rather complex interfacial behavior is expected to be also reflected in a more complex semi-dilute behavior for comb polymers. Indeed in the bulk it should be possible to identify two overlap criteria, one for the chain as a whole and one for the side-chains. The overlap of the side chains will depend not only on the length of these side chains, but also on the spacing between them, because additional intra-molecular excluded-volume interactions will influence the dimensions of the teeth.

In experiments one rarely will find comb polymers that have homogeneous properties, i.e. having identical backbone- and side chain segments (as assumed in this paper). In many cases there will be disparities in solvent quality or surface affinity between backbone or side chain segments. Such local amphiphilicity/selectivity-of-interaction will make the effects reported in this paper even larger. We hope that the new ends to the tale of tails will trigger new experiments in this field.

Acknowledgment

Financial support from the EU POLYAMPHI/Marie Curie program (RT6-2002, Proposal 505027) and European Science Foundation EUROCORES program collaborative BIOSONS is also acknowledged.

CHAPTER 5

Fine Graining Strategy to Recover Structure and Thermodynamics for Coarse Grained Simulations of Inhomogeneous Polymer Systems [1]

[1] Submitted by Marat Charlaganov, Frans A.M. Leermakers to J. Phys. Chem.

A three-stage modeling approach for inhomogeneous polymer solutions is proposed. A molecularly-detailed 3d self-consistent field theory is used for fine-graining the results of a coarse-grained Monte-Carlo simulation where polymer chains are represented by soft particles. The method is illustrated by considering the depletion problem with polymer chains up to $N = 10^3$ segments in semi-dilute solutions and good solvent conditions. (i) Both the polymer-polymer pair - and polymer-wall effective interaction energies are computed by means of a 3d self-consistent field calculation in the dilute regime (ii) These energies serve as potentials in a coarse-grained Monte Carlo simulation on a set of soft particles. (iii) The positions of the particles obtained in step (ii) are used as constraints in complementary molecularly-detailed 3d self-consistent field calculations. As a result, both intra- and inter-molecular excluded-volume effects are accounted for, not only for chains near the surface, but in the bulk as well. Results are consistent with computer simulations and scaling considerations. More specifically, the depletion thickness, which is a measure for the bulk correlation length, scales as $\delta \propto \varphi^{-3/4}$ and converges to the mean field result in the concentrated regime.

5.1 Introduction

Covering appropriate length scales in an efficient computational method, without loosing the essential physics, is one of the prominent challenges of polymer physics. There are simulation methods that deal with all degrees of freedom rigorously. It is fair to say, however, that for systems composed of a large number of long polymers these methods are computationally challenging. A reasonable approach then is to solve coarse-grained models, wherein a chain is represented by, e.g. a single soft particle.[93] At the down side, however, one will loose information on the length scale smaller than the particle (coil) size. In this chapter we propose a fine-graining strategy to recover the information lost in the coarse graining. The idea is to use a coarse grained approach, for example, a Monte Carlo (MC) simulation that operates on just a few (translational) degrees of freedom of the chains and using the self-consistent field (SCF) model for the remaining (conformational) ones. Unlike the standard SCF method,[4] the MC-SCF hybrid scheme accounts (in the first order) for both inter- as well as intra-molecular excluded-volume effects. As a test case we consider the polymer depletion problem for which both simulation results and scaling type theory are available.[3,93,94] A hierarchy of models is envisioned which progressively improves on how the excluded volume effects are accounted for. The improvement is achieved by representing the polymer chain as a string of beads at the MC stage. The number of the beads corresponds to the number of constraints introduced in the subsequent SCF fine-graining step. In this chapter we demonstrate a proof of principle for the first-order MC-SCF method and outline possible characteristics of other hybrids.

5.2 Hybrid Monte Carlo - SCF method

There exists a strong analogy between a diffusing particle and an ideal chain. Of course the ideal chain is only a first-order model for the real chain because interactions are fully ignored. SCF methods advance this idea by considering the polymer as an ideal chain in an external field. This field is used to account for interactions of a polymer segment with its average surroundings.[60] For polymers at interfaces this approach is known to give good qualitative results.[4] In good solvent conditions, however, the method fails to account for the swelling of the chains and hence the mean field results fall short to give the correct scaling behavior.[3]

Calculating macroscopic properties of a system always involves averaging. There is a conceptual difference in averaging between conventional simulation techniques such as Monte Carlo and Molecular Dynamics methods and the SCF approach. Simulations rigorously consider microstates and calculate the interaction energies in a particular microscopical configuration. Macroscopic quantities are then obtained by averaging over relevant microscopical configurations. In SCF models the external field, that influences the statistical weights of chain conform-

ations, already is based on averaged characteristics. As this potential does not make a difference between inter- and intra-chain excluded volume contributions the chains do not swell in good solvents.

There are many different SCF approaches.[95–98] All of these have several aspects in common. Typically, there exists a) a rule that specifies how to obtain the potential field from the density distribution of components, b) a rule to find the density distributions of all components for given potential fields, and c) an algorithm that results in density and a potential distributions that are self-consistent with respect to rules (a) and (b). In particular, the potentials $u(\mathbf{r})$ are self-consistent when the densities derived by using rule (b) yields the same potentials $u(\mathbf{r})$ after applying rule (a). Below we will discuss these three aspects for a new SCF-like theory for which an additional step is introduced that allows us to better account for inter and intra-molecular excluded-volume effects.

This new approach modifies the standard Scheutjens-Fleer theory[87] on just a few points. We therefore start by presenting the basic steps of the classical theory first. Below we will use dimensionless units. This means that all energies and potentials are normalized by k_BT and all distances are measured in the units of a, where a is the statistical segment length of the polymer. The same value a is chosen as the cell size of a simple cubic lattice. The lattice sites are referred to by their coordinates $\mathbf{r} = x, y, z$ in a Cartesian coordinate system. In a lattice model the natural measure of the segment density or segment concentration is the volume fraction $\varphi(\mathbf{r})$, which may be interpreted as the probability to find a segment at the specified coordinate.

We consider a two component system consisting of a homopolymer and a monomeric good solvent near a non-adsorbing solid wall. As there are no interactions in the system (all Flory-Huggins interaction parameters are zero, $\chi = 0$) the solvent and the polymer monomers experience the same (external) potential $u(\mathbf{r})$. The solvent consists of just one segment and its concentration profile $\varphi_W(\mathbf{r})$ follows from the Boltzmann distribution $\varphi_W(\mathbf{r}) = C_W G(\mathbf{r}) = C_W e^{-u(\mathbf{r})}$, where C_W is a normalization constant. The single segment distribution function $G(\mathbf{r}) = e^{-u(\mathbf{r})}$ is introduced here for brevity. Using this result, we find that the potential field can be expressed as a function of the volume fraction of polymer segments $\varphi(\mathbf{r})$:

$$u(\mathbf{r}) = \ln C_W - \ln(1 - \varphi(\mathbf{r})) \tag{5.1}$$

where we have used the incompressibility condition $\varphi_W(\mathbf{r}) + \varphi(\mathbf{r}) = 1$.

One can exploit the analogy between random walks and polymer chains to obtain the concentration profile as a function of $u(\mathbf{r})$. Segment ranking numbers $s = 1, \cdots, N$ act as step numbers in a three-dimensional random walk problem. The probability to find segment s that belongs to a chain of N segments at coordinate $\mathbf{r}$, is related to the probability that two random walks with lengths s and $N-s+1$, respectively, meet at this position. Using the end point distribution function $G(\mathbf{r}, s)$, that represents the statistical weight of all random walks that

reach coordinate $\mathbf{r}$ after $s-1$ steps, one can express the polymer volume fraction as

$$\varphi(\mathbf{r}) = \frac{C}{G(\mathbf{r})} \sum_{s=1}^{N} G(\mathbf{r}, s) G(\mathbf{r}, N-s+1) \tag{5.2}$$

Here, the normalization constant C ensures that the system contains exactly n chains:

$$C = \frac{n}{\sum_{\mathbf{r}} G(\mathbf{r}, N)} \tag{5.3}$$

The single segment distribution function $G(\mathbf{r})$ used in Eq. 5.2 corrects for double counting of the statistical weight of segment s which contributes to both end point distributions. The end point distribution functions are generated recursively starting from the single segment distribution function, $G(\mathbf{r}, 1) = G(\mathbf{r})$, and propagates as:

$$G(\mathbf{r}, s) = \frac{G(\mathbf{r})}{6} \sum_{\mathbf{r}'} G(\mathbf{r}', s-1) \tag{5.4}$$

where the summation runs over the 6 coordinates $\mathbf{r}'$ that are nearest neighbors of lattice site $\mathbf{r}$.

Rule (a) to derive u from the concentration profile φ is specified by Eq. 5.1. Equations 5.2-5.4 define φ as a functional of u and thus implement rule (b). The iterative procedure that brings these two results to consistency involves making an initial guess for u, then calculating φ, calculating a new guess based on φ and so on until a stationary solution is found. We implemented a Hessian-free Newton-like minimization routine for this task which reaches 7 significant digits in order 10^2 iterations.

The boundary conditions are periodic in x and y directions. In the z direction the volume is bounded by two impermeable inert surfaces. For the classical SCF scheme described above these boundary conditions result in a self-consistent field that is uniform in x-y plane. Naturally, this yields a uniform along x and y polymer distribution and a loss of intra-chain correlations and a rather primitive account for inter-chain correlations. This is particularly bad in good solvent conditions and in low polymer concentrations. In semi-dilute solutions the results remain approximate. Only in the polymer melt, and at theta-conditions, the approach is expected to be accurate.

Earlier studies on single chains of different lengths have shown that the intra-chain correlations are recovered in SCF calculations with suppressed translational mobility of macromolecules.[24] In these calculations the central segment of the chain was restricted to a single site of the lattice. It was found that the radial volume fraction profile $\varphi(r)$ has various universal features that were long time ago envisioned by de Gennes.[3] There is a central region $0 < r < R_g$ where to a

good approximation $\varphi(r) = r^{-4/3}$. The volume fraction drops below the overlap value for $r > R_g$ and the profile becomes exponential (with a decay length given by the unperturbed coil size). From the N-dependence of the profiles we find, in line with Flory's arguments, that the gyration radius of the two-armed stars obeys the scaling $R_g \propto N^{\alpha}$, with $\alpha \sim 0.6$ and the overlap concentration is found to be consistent with $\varphi^{\mathrm{ov}} \propto N^{-0.8}$.

We extend this approach to the problem of n macromolecules. The chains consist of an odd number of segments N. For each chain i $(i = 1, \cdots, n)$ we define a unique lattice site $\mathbf{r}_i$ to which we fix the central segment of the chain.

The restriction to the central segments of the chains is introduced by a modification of the propagation procedure. The restriction sites and constrained segments need special attention while computing the end point distribution functions Eq. 5.4. More specifically,

$$G(\mathrm{r}) = \begin{cases} \sum\limits_{\mathrm{r}_i} \delta^{\mathrm{r}}_{\mathrm{r}_i} & s = \frac{1}{2}(N+1) \\ \left(1 - \sum\limits_{\mathrm{r}_i} \delta^{\mathrm{r}}_{\mathrm{r}_i}\right) \exp\left(-u(\mathrm{r})\right) & s \neq \frac{1}{2}(N+1) \end{cases} \tag{5.5}$$

is used instead of the free segment distribution function $G(\mathbf{r})$. With these modifications only chains with central segments in one of the grafting points have non-zero statistical weight and contribute to the polymer density distribution Eq. 5.2. In passing we note that with these positional constraints, the normalization constant for the solvent in Eq. 5.1 becomes unity, that is, $C_W = 1$.

The free energy F for the n molecules with constrained positions $\{\mathbf{r}_i\}$ is

$$F(\{\mathbf{r}_i\}) = n \ln C + \sum_{\mathbf{r} \notin \{\mathbf{r}_i\}} \ln \varphi_W(\mathbf{r}) \tag{5.6}$$

where the coordinates $\mathbf{r}_i$ where the central segments are places are omitted in the sum. Physically, F thus collects the logarithm of the number of conformations lost for the n chains compared to the Gaussian chains. The conformational loss not only comes from the positional constraints on their central segments, but also from the interactions between chains which occurs when a chain is near a surface or when two or more neighboring chains partial overlap (interact). Note that the translational entropy of the monomeric solvent is included in eq 5.6, but the corresponding entropy of the polymer chains is not. The next task is thus to introduce translational degrees of freedom for the polymer chains into the problem. Here we suggest to use a Monte Carlo simulation for this, but note that there are various possible alternatives.

At the Monte Carlo stage, polymer chains are modeled as soft particles interacting with each other and the wall in an effective solvent. The potentials for the simulations are measured in complimentary SCF calculations as is explained next.

Let us consider the problem of bringing (in SCF mode) one isolated chain towards a solid boundary and compute corresponding change in the free energy

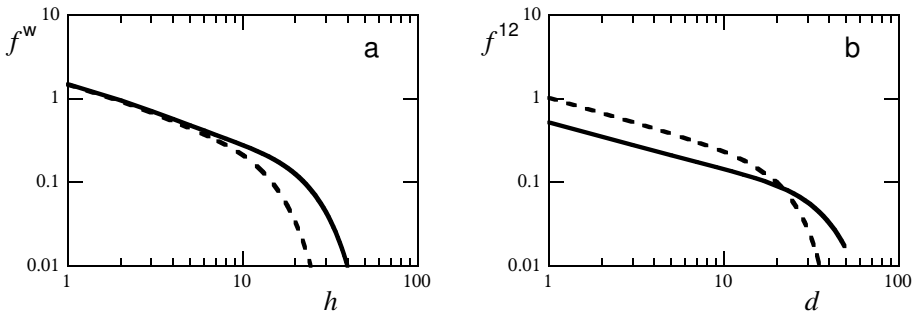

Figure 5.1: *a) The gradient of the interaction potential $f^{\rm w} = \partial F^{\rm w}/\partial h$ with the surface as a function of the distance h of the central segment to the surface. b) The gradient of the pair interaction $f^{12} = \partial F^{12}(d)/\partial d$ as a function of the distance d between the two central segments. $N = 1001$ - solid lines, $N = 401$ - dashed lines.*

$F^{\rm w}(h)$ where h is the distance between the constrained segment of the chain and the surface. The wall restricts the conformations of the chain and this gives rise to an entropic repulsion. In Figure 5.1a we present the derivative $f^w = -\partial F^{\rm w}/\partial h$ on log-log coordinates which gives the depletion force acting on a single polymer chain. In passing we mention that averaging the polymer concentration profiles for each value of h, $\varphi_h(\mathbf{r})$, collected in this measurement, can be used to obtain the polymer concentration profile in the dilute regime:

$$\varphi(z) = C_d \sum_h \sum_{x,y} \varphi_h(x,y,z) e^{-F^w(h)} \tag{5.7}$$

where the constant C_d is used to match the desired (low) bulk concentration.

Another essential ingredient that is needed in the MC simulations is the free energy of bringing two chains towards each other. Again, we perform the calculations in a three dimensional system far away from the boundaries. The central segments of two chains are fixed at positions $\mathbf{r}_1$ and $\mathbf{r}_2$ respectively. In SCF mode we obtain the energy of interaction $F^{12}(d)$ where $d = |\mathbf{r}_1 - \mathbf{r}_2|$ is the distance between the two grafting points. The corresponding force, f^{12} is presented in 5.1b.

The forces $f^{12}(d)$ and $f^{\rm w}(h)$ presented in Fig. 5.1 and hence the corresponding potentials have very similar features. For small values of their arguments the forces are inversely proportional to the separation. Therefore a logarithmic dependence is found for the corresponding potentials. This is consistent with simulations and renormalization group theory.[99] At longer distances an exponential decay is found for both F and f, as expected.

The volume in the MC simulations is identical to that in the SCF calculations. There are two surfaces bracketing the z-coordinate and periodic boundary conditions in the x and y directions. Here the focus is on n particles that interact with

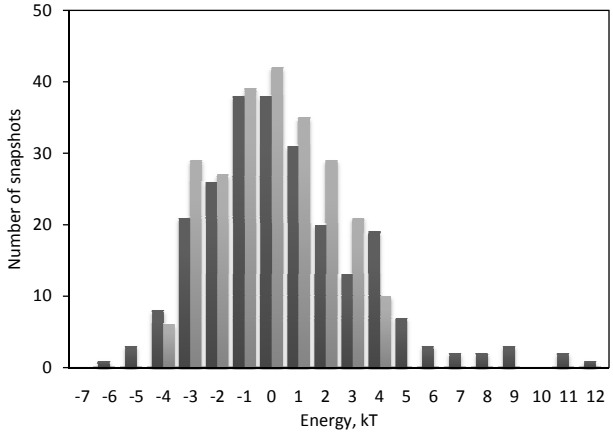

Figure 5.2: *Distributions of energies of 239 snapshots around median values as estimated on the Monte-Carlo stage (light bars) and calculated on the SCF stage (dark bars).* $N = 1001$, $n = 26$, $\varphi^b = 0.069$

a surface by the $F^{\mathrm{w}}(h)$ potential and suffer a pair potential with the characteristics $F^{12}(d)$. Typically, there are just order 10^2 particles in the volume and thus the simulations are straightforward. Using the standard Metropolis algorithm, an initial equilibration is followed by a production run wherein for a finite number, $j = 1, \cdots, J$, with typically $J \approx 10^2$ so-called snapshots, the coordinates $\{\mathbf{r}_i\}_j$ as well as the corresponding prediction of the interaction free energy F_j^{MC} are recorded.[101]

The energies F^{MC} that are found in the MC-train are Boltzmann distributed. For each snapshot j the SCF equations are solved with the method explained above. Numerically exact volume fraction profiles $\varphi_j(\mathbf{r})$ as well as the free energy F_j^{SCF} were obtained. In figure 5.2 the distributions of free energies for $J = 239$ snapshots are shown. Both distributions indicate that the snapshots are nicely spread around the median values. The free energy differences $\Delta F_j = F_j^{\mathrm{MC}} - F_j^{\mathrm{SCF}}$ are of order unity, which means that the estimates of the MC train are predictive for the free energy in the SCF calculation.

When the $\{F^{\mathrm{MC}}\}$ would have coincided with those of SCF, we could have performed a flat-averaging of the J density profiles $\varphi_j(\mathbf{r})$ to obtain $\varphi(\mathbf{r})$. The subsequent averaging over the x-y plane then results straightforwardly in the normal density profile $\varphi(z)$. However, the energy differences ΔF are not zero and hence we have to correct for the bias:

$$\varphi(\mathbf{r}) = \frac{\sum_j \varphi_j(\mathbf{r}) e^{-\Delta F_j}}{\sum_j e^{-\Delta F_j}} \tag{5.8}$$

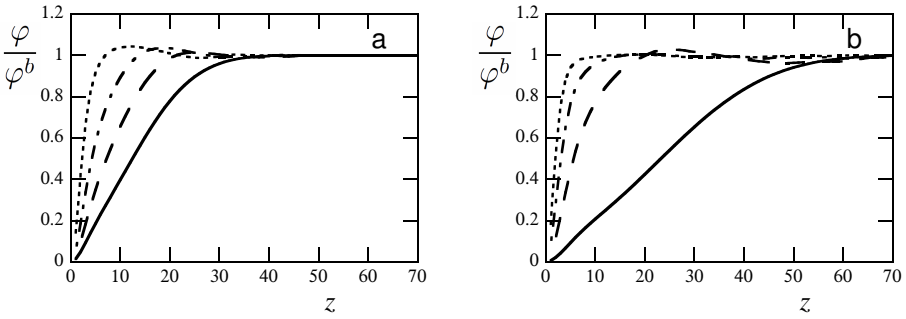

Figure 5.3: *Polymer concentration profiles normalized by bulk polymer volume fraction. a) Chain length $N = 401$, bulk concentrations 0.05 (dotted line), 0.022 (dot-dash), 0.011 (dashed line), and dilute solution (solid line). b) Chain length $N = 1001$, bulk concentrations 0.069 (dotted line), 0.033 (dot-dash), 0.013 (dashed line), and dilute solution (solid line).*

5.3 Results and discussion

The primary results from the MC-SCF calculations is the polymer volume fraction (averaged over the x-y plane) profile normal to the surface. Figure 5.3 presents, for various bulk volume fractions, such profiles for chains with length a) $N = 401$ and b) $N = 1001$. For ease of comparison we have normalized the profiles to the polymer volume fraction in the bulk. Completely in line with expectations we find that the profiles become wider with decreasing polymer concentrations. Also, for dilute polymer concentrations the profiles become wider with increasing chain length. Qualitatively, these trends are well known and completely understood.[4]

It is of interest to compare the new results to the classical SCF results. Here we focus on the results in the semi-dilute regime. It is known that the classical results compare extremely well to analytical results that are obtained by using the ground state approximation (GSA).[75] More specifically, to a very good approximation GSA gives $\varphi(z) = \varphi^b \tanh^2(z/\xi)$. Here $\xi = 1/\sqrt{3\varphi^b}$ is the mean-field correlation length in a semi-dilute solution, which is a very good measure for the depletion layer thickness. As can be seen in fig 5.4 the differences between the classical SCF and the MC-SCF results are significant. First of all this is because the correlation length and thus the depletion thickness in the MC-SCF method differs noticeably from that in the classical SCF theory (cf Fig. 5.4a). Moreover, the MC-SCF result does not fit to the squared hyperbolic tangent profile. In part this is because of a significant oscillatory dependence of the profile, which is discussed below in more detail. Intra-molecular excluded-volume effects accounted for by MC-SCF and essentially ignored by the classical SCF theory must be the reason for the mentioned differences.

The depletion thickness is an important quantity that can be used to quantify the range over which the polymers feel the surface. A measure of the depletion

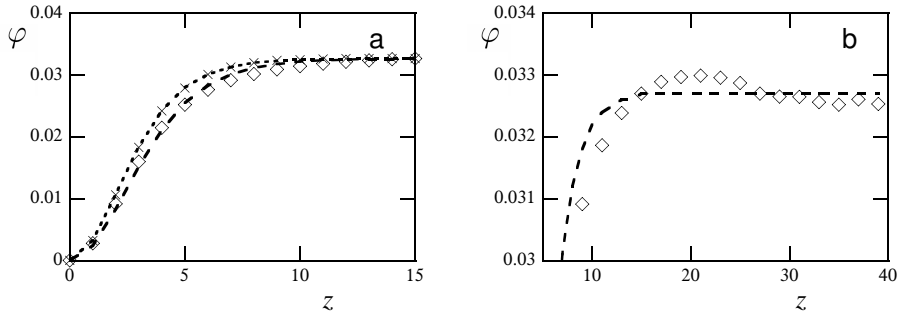

Figure 5.4: *Polymer concentration profiles obtained by the classical SCF (crosses), and the hybrid MC-SCF (diamonds) methods. Bulk concentration* $\varphi^b = 0.0327$, $N = 1001$. *The lines are the best fit of the form* $\varphi(z) = \varphi^b \tanh^2(z/\xi)$ *with* $\xi = 3.08$ *(dot) and* $\xi = 3.61$ *(dash). In panel a the profiles near the surface (small z values) are shown, whereas in panel b it is shown how the profile goes to the bulk value for the MC-SCF profile.*

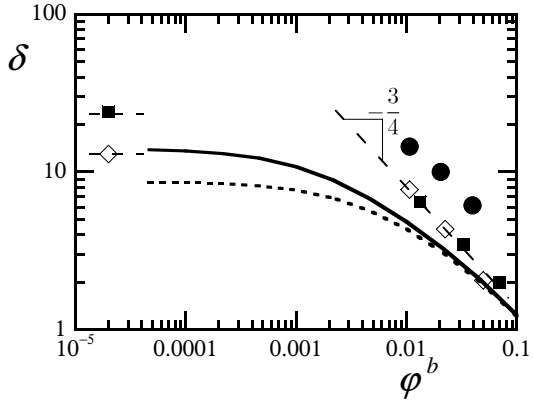

Figure 5.5: *Logarithm of depletion layer thickness versus logarithm of bulk polymer concentration. MC-SCF results for chain lengths* $N = 1000$ *(squares),* $N = 400$ *(diamonds) Dashed lines are added to guide the eye. Classical SCF results for chain lengths* $N = 1000$ *(solid line),* $N = 400$ *(dashed line), results from Ref.*[100] *rescaled for* $N = 1000$ *(circles). The theoretical slope* $-\frac{3}{4}$ *is indicated.*

layer thickness is obtained by taking the first moment over the excess profile

$$\delta = \frac{\sum_z z(\varphi(z) - \varphi^b)}{\sum_z (\varphi(z) - \varphi^b)} \tag{5.9}$$

As can be seen in figure 5.5, where we present our results for the depletion thickness as a function of the bulk volume fraction in log-log coordinates, we basically recover the expected behavior. At low polymer concentrations the results depend strongly on the chain length and the depletion layer is given by the radius of gyration of the chains: $\delta \approx R_g$. Above the overlap concentration the depletion thickness is no longer a function of the molecular weight, but becomes a function of the polymer concentration only. Completely in line with expectations, in semi-dilute solutions a power-law dependence is found. A fit of the depletion layer thickness as a function of the polymer volume fraction in the bulk gives $\delta^{\mathrm{MC-SCF}} \propto (\varphi^b)^\alpha$. Inspection of fig. 5.5 proves that the MC-SCF results are consistent with $\alpha = -3/4$. As the depletion layer thickness is an accurate measure for the bulk correlation length, we note that $\alpha = -3/4$ is consistent with the scaling prediction of de Gennes [3]. This proves that the excluded-volume interactions are reasonably accurately accounted for in the MC-SCF calculations.

This should be contrasted to the classical results of the mean field theory for which the value of $-1/2$ is found if the chains are long enough. For comparison with the classical SCF result we also present the classical result for the depletion thickness as a function of the poymer concentration in figure 5.5. Indeed relatively large differences between the classical SCF and the new MC-SCF results are observed, especially for low polymer concentrations. With increasing concentration, however, the differences diminish. Indeed, when the depletion thickness becomes of order of the segment size, that is in the concentrated regime, the MC-SCF results converge to the classical mean field results. This is expected because in the melt the mean field theory is known to be accurate. The two results are expected to merge because both approaches are based on the same freely-jointed chain model.

We feel that it is necessary to compare the MC-SCF results to computer simulations. To begin with, there are very limited accurate results available in the literature. The reason for this is clear. Basically, in order to arrive in the regime where the de Gennes scaling is expected one has to have long chains in the system. Moreover, one needs many chains in such a system and thus the necessary simulations are huge. In figure 5.5 we compare results to computer simulations by Bolhuis et al[2]. [100] It must be noted that these authors did not present atomistic simulation results, but rather turned to a coarse graining strategy. They measured the pair potentials between polymers and evaluated the depletion problem using the soft-particle approach. As can be seen in figure 5.5 there are remarkable differences in absolute values between predictions by Bolhuis et al, and our results.

[2]Bolhuis et al have presented their results in reduced units. They normalised the depletion thickness by the radius of gyration and the concentration by the overlap concentration. We used Eq 9 in Ref. [100] to transform their results to the units used in Fig. 5.5

Most likely these differences may be attributed to differences in chain models used. More specifically, in the Bolhuis simulations, while measuring their pair potentials the chains were fully self-avoiding, whereas in our SCF analysis the freely-jointed chain model was used. The scaling of the depletion thickness with polymer concentration found by Bolhuis et al. is the same as in our calculations and both are in agreement with the de Gennes scaling prediction.

We now shortly elaborate on the characteristics of the depletion profile as one would extract from the coarse grained MC simulations, that is, in the absence of the fine-graining step. In the MC simulations the polymer chain is essentially replaced by a single particle. The particle interact with the solid wall other particles via effective potentials calculated in the dilute regime. In semi-dilute regime these potentials are only approximately correct as they do not account for screening effects. Moreover, by using an isotropic radial volume fraction profile of such particle to calculate overall polymer concentration profile one strongly overestimates the width of the depletion layer and underestimates the depth of it. This is no surprise as to obtain accurate information on the depletion zone requires information on length scales smaller than the particle size. The error exemplifies the necessity for our fine-graining procedure.

The density profile for the depletion problem is not monotonically increasing, but a depletion layer is followed by a small overshoot followed by an even smaller undershoot, etc. (cf. Fig. 5.4b) In principle these oscillatory features have been reported before and also exist to a lesser extend in the classical SCF results[91], that is, in calculations that go beyond the GSA. Oscillatory density profile are perhaps best known for densely packed hard spheres near a flat interface. The softer the particles are the more the oscillations are damped. Polymer chains are very soft particles as may also be deduced from $F^{\mathrm{w}}(h)$ and $F^{12}(d)$. Full overlap of coils however costs significant amount of entropy. Hence the particles have a finite softness and therefore there are small over and undershoots visible in the profile. From a polymer point of view one can argue that the overshoot is the result of chain ends. Polymer ends can be inserted into the depletion zone more efficiently than middle segments, and therefore there is some 'adsorption' affinity of the polymer chain to accumulate at the boundary of the depletion zone. We note that in dilute solution, when all chains interact with the surface individually, there is no possibility to develop an overshoot in the profile and also in the limit of an incompressible melt the overshoot must vanish. Hence the amplitude of the overshoot is, in line with the results, a non-monotonic function of the polymer concentration, and the chain length.

From the above we conclude that the MC-SCF method gives an improved description of inhomogeneous polymer solution over the classical SCF method. This improvement comes with a price. The computation time for the MC-SCF is estimated to be about J hours CPU on a desktop PC per problem, as the CPU time per snapshot is approximately one hour. Still the method is extremely efficient as the CPU time is linearly proportional to the volume of the system and the length of the polymer chains. The method is independent of the number

of molecules n, if we ignore the fact that the value of J needed to average out fluctuations will be a weak function of n. In full scale simulations, on the other hand, the calculation time heavily depends on the length of the chains and further depends super linearly on the number of polymer chains in the solution. Also the number of snapshots needed to obtain an accurate estimate of some observable is much larger than in the MC-SCF method. Hence we claim that the CPU time gain of the present MC-SCF compared to MC may easily be significantly more than a factor 10^2 and this number grows quickly with system size.

One realistic target for future modeling is to study the adsorption of homopolymers and polyelectrolytes adsorbing from (semi) dilute solutions onto (charged) interfaces. The classical SCF method fails badly for many regimes, basically because it assumes that the chains in the bulk remain Gaussian (intra-molecular excluded volume is basically ignored). In the limit of strong adsorption, however, we foresee that it may be more beneficial to use a hybrid Brownian Dynamics (BD) - Self-consistent field approach. In this approach we need for each time step the forces that act on the centers of mass of the particles. These forces can be found by solving the SCF equations, while keeping these central positions as constraints similarly as done in the MC-SCF method used above. The (time) averaging of results along a BD trajectory will allow us to outperform mean field theories, while keeping CPU time within bounds of modern computers.

At this stage it is worthwhile to pay attention to still relatively weak points of the MC-SCF method. To our mind the Ansatz that just one positional constraint is used per chain is still a significant simplification of the real excluded-volume problem. The next step to improve the situation is to specify two constraints per macromolecule, e.g. by assigning constraining positions to both end points of the chain. Without going into all computational details, it is evident that an implementation of this idea requires a measurement (in SCF-mode) of the end-to-end 'potential', $F^{\mathrm{e-e}}(R)$ where R is the distance between the two ends of a probe chain. The MC step will be somewhat more complicated, because there will be two times more degrees of freedom and one extra potential and the SCF part must be modified in order to prevent the exchange of end-points between molecules. It is expected that the computation time per snapshot will not grow much for systems that feature molecules with two constraints, but we can foresee a significant increase in number of snapshots needed to measure properties of the system accurately. This idea can be extended. One may arrive at a model were one consideres a string of blobs and then the method has several aspects in common with a recently suggested theoretically informed MC simulations by de Pablo and coworkers.[102,103] In short these authors combine a particle-based MC method with interactions derived from a local density functional theory. Instead of solving the Edwards equation as in our case these authors implemented a still primitive smearing of the density to allow an easy evaluation of the interactions. Possibly, merging our MC-SCF method with theoretically informed simulations may be a feasible route to improve both methods.

Compared to classical MC simulation, the MC-SCF method has the intrinsic

advantage that thermodynamic quantities can be calculated rather accurately. The idea is that for semi-dilute solutions of long enough chains the translational entropy is not important and one can simply average the free energy of the snapshots, i.e. $F^{\mathrm{SCF}} = \sum_j F_j^{\mathrm{SCF}}/J$. When for some system the translational entropy is important one may get a reasonable estimate form the MC simulation using standard techniques.

5.4 Conclusions

We have presented a hybrid Monte Carlo, Self-Consistent Field approach for polymers in good solvent near a non-adsorbing surface. This method accounts for inter as well as intra-molecular excluded volume effects and the results are consistent with scaling predictions. Compared to full scale simulations the method has modest computation times albeit that the computation costs are several orders of magnitude larger than the classical SCF method. The method introduces a MC step where a coarse grained simulation is performed, and an SCF step to recover the structural details on a shorter length scale (fine graining). In other words, conformational degrees of freedom are accounted for by the classical propagator method (analogous to the Edwards diffusion equation) for which the centers of mass are fixed to coordinates specified by the MC snapshot. The MC-SCF approach can be extended to further improve on the excluded-volume problem in inhomogeneous systems. Alternative hybrid approaches are foreseen which may be used in the cases where the polymers are strongly perturbed with respect to the Gaussian size.

Acknowledgements

Financial support from the EU POLYAMPHI/Marie Curie program (RT6-2002, Proposal 505027) and European Science Foundation EUROCORES program collaborative BIOSONS is also acknowledged.

CHAPTER 6

Summary and General Discussion

In this thesis we have visited a number of problems where polymers demonstrate various forms of self-organization. We employed a numerical self-consistent field analysis to study polymeric effects that are hardly accessible to other modeling techniques. Where possible we compared our findings to the results of analytical theories. In this chapter we briefly summarize the results of our work and discuss the possible directions for the future research.

In *Chapter 2* we presented an analytical theory and results of self-consistent field modeling for the mechanical unfolding of a globule formed by a single flexible polymer chain in a poor solvent. We identified three regimes in the force-distance dependence. The response to an initial stretching, that is by increasing the end-to-end distance of the chain, is a linear function of the distance. The spherical globule deforms as a whole to an ellipsoidal one. Upon further stretching, the chain exhibits a transition into a two-phase tadpole conformation, with a globular head and a stretched tail. Finally, at large extensions, the chain adopts an uniformly stretched conformation. The conformational transition from the tadpole to the stretched chain is accompanied by an abrupt unfolding of the depleted globular head and a corresponding jump-wise drop in the intra-chain tension. The unfolding-refolding cycle demonstrates a hysteresis loop in the vicinity of the transition point. It is found that the system exhibits a negative extensional modulus in the intermediate range of deformations.

Thanks to recent advances in the single chain spectroscopy, pulling a single macromolecule by its ends has become experimentally feasible. The existence of a regime with an anomalous extension modulus was observed in experiments on synthetic and biological macromolecules.[13,104] The presented theory appears to be a minimal model for such force-distance dependence, as the only interaction considered is that between the solvent and the monomers. Such minimal model may not be completely irrelevant because often rather specific interactions can often be approximated by effective monomer-solvent interactions. Therefore we argue that our result have in fact a broad applicability, ranging from single molecule experiments with forced unfolding of globular proteins. Our results may also prove relevant for the collapse of a polyelectrolyte chain. Here the so-called pearl-necklace formation is found, which in fact also results as a compromise between stretching of the ends (due to electrostatic forces) and the collapse of the chain due to poor solvent conditions.

In *Chapter 3* we reported on numerical self-consistent field predictions for the formation of spherical micelles by $A_N B_M C_N$ triblock terpolymers in a selective solvent, i.e., a good solvent for the A_N and C_N blocks and a poor solvent for the middle B_M block. Above some threshold value for the repulsion between the A and C monomers, we predicted micelles with a laterally segregated corona, i.e., Janus micelles. We consider the thermodynamic stability, the size, and the size fluctuations of these micelles. The transition between the homogeneous and the segregated states occured smoothly upon increasing the repulsion between A and C. There were a number of reasons for the fact that the transition was smooth. First of all we argued that this is because of the finite size of the system.

Secondly, this was attributed to the compositional symmetry within the triblock terpolymer. It was found that the aggregation number decreases with increasing repulsion between A and C below-, and increases above the transition point. The formation of the interface is triggered by the high polymer density near the core, and we found that the threshold density could be predicted by the bulk phase behavior A_N and B_N polymers in a common solvent.

The richness of this problem lays in the interplay between two microphase transitions. We showed that the segregation of the micellar corona may be considered as a perturbation on top of a stronger segregation that leads to the core-corona structure. However, the transition in the corona affects the aggregation number and the shape of the micelle. The later was experimentally observed in complex-coacervate micelles where the interfacial tension lays in the sub millinewtons per meter range.[105–107] In experimental systems the corona blocks are likely to have different interactions with the solvent. Worsening the solvent quality for one of the corona blocks will promote the segregation of the chains in the corona. This segregation, however, may switch from the Janus type (two sides) to the onion type (radial segregation). When the solvent quality for one of the corona blocks becomes poor, we may anticipate the formation of a complex structured core. Depending on parameters, one may find a single domain ("janus" type), a shell around the core ("onion" type) or multiple domains ("raspberry" micelles). The study of these exotic morphologies and transitions between them is a natural continuation of this project. Another open question concerns the possibility of higher levels of self-assembly of Janus micelles. There are experiments proving that cross-linked aggregates of terpolymers can form "super micelles" where individual micelles act as amphiphilic compounds..[44,45] Whether it is possible to make "super micelles" without chemical linking is still unknown. Most likely this will require different association mechanisms and/or stopping forces for the assembly. Similar problems are expected when one becomes interested in the behavior of Janus micelles at interfaces. Despite the natural interest in these problems from the experimental point of view, the theory for these systems is non-existing.

In *Chapter 4* we revisited the classical problem of homopolymer adsorption at the solid-liquid interface and discuss its implications for colloidal stability. More specifically, our focus was on comb-like homopolymers in the strong adsorption limit being in good solvent conditions. A self-consistent field analysis shows that for relatively long side chains, but still much longer backbones, the adsorbed layer is dominated by the side chains near the surface, whereas at larger distances the layer has features that belong to the backbone. As a rule, homopolymer adsorption promotes flocculation of colloids. This is attributed to the long polymer chains that can form attractive bridges between the colloidal particles. However, the free ends of the chains do not participate in the formation of bridges. Tails therefore contribute with a small repulsive term to the pair interaction. For comb polymers, the free ends of the side chains amplify the repulsion dramatically. As a result, in contrast to linear adsorbed homopolymers, comb polymers typically

prevent flocculation. The concentration profile of homopolymers adsorbing at a solid liquid interface is known to have several generic features. For example, according to de Gennes there exist a proximal, a central and a distal regime. In the distal regime the concentration profile is thought to decay exponentially to the bulk value. In the central regime the profile is self-similar and the power-law exponent is linked to the way the mesh size scales with the polymer concentration in a semi-dilute polymer solution. Finally in the proximal region the profile is thought to depend on the way the polymer interacts with the surface. For comb polymers, with sufficiently long teeth, we have shown that the proximal region can in itself develop the proximal, central and distal characteristics.

The stabilizing effect of polymers on the colloidal solution is traditionally attributed to the kinetic effects. One typically argues that when two particles, covered by adsorbing polymers approach each other, the adsorbed layers are trapped. In this scenario one is forced to reconsider the polymer adsorption problem. Scheutjens and Fleer suggested to use the semi-open ensemble for this case and predicted a non-monotonic interaction curve, where attraction at large separation is followed by repulsion at shorter distances. In this argument there is no function for the chain ends. In our paper we prove that one can have non-monotonic interaction curves in full equilibrium: a deep attractive minimum at short separation is followed by a maximum at somewhat larger distances. The barrier is significantly high when there are many chain ends. The higher the barrier the more likely the barrier can prevent the bridging flocculation. Hence, our stabilization mechanism is also based on a kinetic argument.

In the final *Chapter 5* we presented the most recent work, which has still many features of a partially finished project. In this chapter we forward a computationally efficient multi-stage modeling approach for inhomogeneous polymer solutions. A coarse-grained Monte Carlo simulation on a set of soft particles (representing chains) is used to give relevant snapshots of center-of-chain positions, which are subsequently imposed in complementary molecularly realistic 3d self-consistent field (SCF) calculations. The method is illustrated by polymer depletion near a flat wall for semi-dilute solutions in good solvent. The depletion profile and layer thickness is consistent with full scale computer simulations and scaling considerations. We therefore claim that these calculations show that it is possible to account for intermolecular as well as intramolecular excluded volume effects for polymers near interfaces. As such the theory corrects the classical self-consistent field theory of Scheutjens and Fleer who failed to account for these rigorously.

The main approach used in this thesis is the self-consistent field (SCF) theory and more specifically we have used the Scheutjens Fleer variant (SF-SCF). In the hierarchy of models SF-SCF occupies a niche between atomistically exact models and coarse grained models that neglect the molecular details. The smallest unit in the classical SF-SCF model is the statistical segment length, which typically represents several atoms. Hence we may refer to the models treated by the SF-SCF theory as being molecularly detailed. This is important because polymers possess several unique physical properties that are universal in the sense that they

do not depend on the chemical nature of the comprising monomers. The size of these macromolecules makes statistical methods, such as SCF, ideal to study them. Because of the connectivity, polymer systems are always partially ordered, that is, they are never completely ordered and never completely disordered. This makes questions such as the range of correlations and interactions central topics of polymer physics. One of the problems that we encountered is that the SF-SCF approach, even though very powerful for treating some problems, is not able to accurately account for intramolecular excluded volume effect in cases where the polymers are freely floating in solution. The problem may be traced to the particular implementation of the mean-field approximation in these system. In the case of the polymer globule, or in the problem of polymer micelles, polymer brushes, etcetera, there are positional constraints on the molecules and results compare extremely well with simulations and experiments, but in the absence of these constraints, e.g. for polymers adsorbing at interfaces, or the polymer depletion problem, the results are known to be approximate.

The main idea of the SF-SCF model is to consider random walks in an external field. Using the freely-jointed chain, it is possible to set up a very efficient formalism that uses the external fields and produces the distribution of the molecules in space. As already mentioned this external field is typically smeared over a region much larger than the coil size, and hence only poorly represents the intramolecular forces. As a result the chains do not swell. Fixing some coordinate of the chain to a specified coordinate changes the picture in a very dramatic way. Now the potential field, in the region of the positional constraint, is mainly due to intra-molecular interactions rather than inter-molecular ones. As a result the chains swell. Flory already explained the result of the swelling, namely that the coil size scales as $R_g \propto N^{0.6}$. The implementation of this idea to an ensemble of n chains in a volume V rests on two major developments. First, modest memory requirements of the limited memory BFGS algorithm used in *Chapter 5* to solve the self-consistent field equations allowed us to perform calculations on a sufficiently large three-dimensional lattice.[108] And second, partial parallelization of the code significantly reduced the execution times on modern desktop computers.

The proof of principle is given in *Chapter 5* for the depletion problem. For this problem we were lucky that the polymer-wall and polymer-polymer interactions could be computed for the dilute situation. These interactions were used in a simple MC simulation to generate snapshots that specified the locations of all polymer chains in a system. These positions were then used as constraints in 3d SF-SCF calculations. The averaging over a few hundred SF-SCF profiles for different snapshots gave accurate results for the depletion problem. We have tried to use the same idea for a system with adsorbing chains. In the case of very weak adsorption reasonable results were found, but in the limit of strong adsorption the method failed dramatically. The reason for this failure is that the isolated chain near an adsorbing interface is strongly deformed. More specifically it was found that the chain conformations assumed the flower conformation: a strongly adsorbed crown is connected to a stem with length proportional to the chain

length. These flower conformations do not occur in a saturated adsorption layer.

We can only speculate at this stage what the solution is for this problem. One attractive idea is to set up a hybrid Brownian-dynamics SCF method. In this case the time-evolution of the system is computed and the pair interactions are 'measure' on the flight. We must anticipate that relatively long trajectories are needed to equilibrate a system. In this case it is obviously that before this method can become effective, one must be able to solve the SF-SCF equations for the set of n macromolecules much more efficiently than currently possible.

Given the relatively low computational costs of SF-SCF calculations, it may prove beneficial to upgrade the theory to account properly for the excluded-volume effects. Then many regimes for polymers at interfaces should be revisited, including the polymer adsorption problem presented in *Chapter 4*. Such theory may be helpful to understand how polymers with non-trivial interactions, such as polyelectrolytes, organise at interfaces. Such theory may further be used to study more complex examples of self-assembly, e.g., when complex micelles occur that organize on different length scales under the influence of orthogonal driving forces and complementary stopping mechanisms.

Most of the topics that were studied are very classical indeed. We have shown that even for these classical problems new results can be obtained. This proves that polymer self-organization is a topic that is extremely rich and much progress is still to be expected in the near future. With the current advances in polymer synthesis, the importance of the ongoing research in polymer theory continues to grow. Ultimately, the pieces added by the polymer theory to the understanding of the mosaic of self-organization will bring new technological applications.

Bibliography

[1] A.J. Peacock. *Handbook of polyethylene: structures, properties, and applications* CRC Press, 2000.

[2] P.J. Flory, *"Principles of Polymer Chemistry"*, Cornell Univesity Press, Ithaca NY (1953).

[3] P.G. De Gennes. *Scaling Concepts in Polymer Physics* Cornell Univ. press, Ithaca NY, 1979.

[4] G.J. Fleer, M.A. Cohen Stuart, J.M.H.M. Scheutjens, T. Cosgrove, B. Vincent", *"Polymers at Interfaces"*, Chapman and Hall, London, **1993**.

[5] Finkelstein, A. V.; Ptitsyn, O. B. *Protein Physics : A Course of Lectures*; Academic press, 2002

[6] Schrödinger, E. *What is Life?*; Cambridge University Press: Cambridge, 1944

[7] Rief, M.; Gautel, M.; Oesterhelt, F.; Fernandez, J. M.; Gaub, H. E. *Science* **1997**, *276*, 1109–1112

[8] Hugel, T.; Seitz, M. *Macromol. Rapid. Commun.* **2001**, *22*, 989–1016

[9] Haupt, B. J.; Senden, T. J.; Sevick, E. M. *Langmuir* **2002**, *18*, 2174–2182

[10] Smith, S. B.; Cui, Y.; Bustamante, C. *Science* **1996**, *271*, 795–799

[11] Kellermayer, M. S. Z.; Smith, S. B.; Granzier, H. L.; Bustamante, C. *Science* **1997**, *276*, 1112-1116

[12] Skvortsov, A. M.; Klushin, L. I.; Birshtein, T. M. *Polym. Sci. (Russia)* **2009**, *51 (A)*, 469-491

[13] Forman, J. R.; Clarke, J. *Curr. Opin. Struct. Biol.* **2007**, *17*, 58–66

[14] Halperin, A.; Zhulina, E. B. *Europhys. Lett.* **1991**, *15*, 417

[15] Cooke, R.; Williams, D. R. M. *Europhys. Lett.* **2003**, *64*, 267–273

[16] Craig, A.; Terentjev, E. M. *J. Chem. Phys.* **2005**, *122*, 194901

[17] L.D. Landau, E.M. Lifshitz, L.P. Pitaevskii; *Statistical Physics. part I*, Pergamon press: Oxford, **1980**.

[18] Rayleigh, L. *Phylos. Mag.* **1882**, *14*, 184–186

[19] Dobrynin, A. V.; Rubinstein, M.; Obukhov, S. P. *Macromolecules* **1996**, *29*, 2974–2979

[20] Borisov, O. V.; Halperin, A. *Eur. Phys. J. B* **1999**, *9*, 251–259

[21] Halperin, A.; Zhulina, E. B. *Macromolecules* **1991**, *24*, 5393–5397

[22] Klushin, L. I.; Birshtein, T. M.; Mercurieva, A. A. *Macromol. Theory Simul.* **1998**, *7*, 483–495

[23] Feuz, L.; Leermakers, F. A. M.; M, T.; Borisov, O. V. *Macromolecules* **2005**, *38*, 8891–8901

[24] J. van Male, *Self-consistent-field theory for chainmolecules: extensions, computational aspects, and applications*, PhD thesis **2003**, Wageningen Univesity, the Netherlands

[25] Pincus, P. *Macromolecules* **1976**, *9*, 386–388

[26] Birshtein, T. M.; Amoskov, V. M. *Polym. Sci. (Russia)* **2000**, *42 (C)*, 172–207

[27] Klushin, L. I.; Birshtein, T. M.; Amoskov, V. M. *Macromolecules* **2001**, *34*, 9156–9167

[28] Birshtein, T. M.; Amoskov, V. M.; Klushin, L. I.; Mercurieva, A. A.; Polotsky, A. A.; Iakovlev, P. A. *Macromol. Symp* **2003**, *191*, 51–58

[29] Amoskov, V. M.; Birshtein, T. M. *Polym. Sci. (Russia)* **2003**, *45 (B)*, 237–263

[30] Klushin, L. I.; Skvortsov, A. M.; Leermakers, F. A. M. *Phys. Rev. E* **2004**, *69*, 061101

[31] Skvortsov, A. M.; Klushin, L. I.; Leermakers, F. A. M. *J. Chem. Phys.* **2007**, *126*, 024905

[32] Frisch, T.; Verga, A. *Phys. Rev. E* **2003**, *65*, 041801

[33] Grassberger, P.; Hsu, H.-P. *Phys. Rev. E* **2002**, *65*, 031807

[34] Marenduzzo, D.; Maritan, A.; Rosa, A.; Seno, F. *Phys. Rev. Lett.* **2003**, *90*, 088301

[35] Marenduzzo, D.; Maritan, A.; Rosa, A.; Seno, F. *Eur. Phys. J. E* **2004**, *15*, 89–93

[36] D.F. Evans, H. Wennerström, *"The colloidal domain where physics, chemistry, biology, and technology meet"*, VCH Publishers, Inc, **1994**.

[37] F. Nagarajan, E. Ruckenstein, *Langmuir* **1991**, *7*, 2934-2969.

[38] R.G. Laughlin, *"The aqueous phase behavior of surfactants"*, Academic Press **1994**.

[39] G. Riess, *Prog. Polym. Sci.* **1999**, *28*, 1107-1170.

[40] F.S. Bates, G.H. Fredrickson, *Physycs today* **52**, 32-38.

[41] C.A. Fustin, V. Abetz, J.F. Gohy, *Eur. Phys. J. E* **2005**, *16*, 291-302.

[42] A. Halperin, *J. Phys. France* **1988**, *49*, 131-137.

[43] A. Halperin, *Macromolecules* **1990**, *23*, 2724-2731.

[44] R. Erhardt, M.F. Zhang, A. Boker, H. Zettl, C. Abetz, P. Frederik, G. Krausch, V. Abetz, A.H.E. Muller, *Journal of the American Chemical Society* **2003**, *125*, 3260-3267.

[45] R. Saito, A. Fujita, A. Ichimura, K. Ishizu, *J. Polym. Sci. A Polymer chemistry* **2000**, *38*, 2091-2097.

[46] I.K. Voets, A. de Keizer, P. de Waard, P.M. Frederik, P.H.H. Bomans, H. Schmalz, A. Walther, S.M. King, F.A.M. Leermakers, M.A. Cohen Stuart, *Angew. Chem. Int*, **2006**, *45*, 6673-6676.

[47] J.F. Gohy, E. Khousakoun, N. Willet, S.K. Varshney, R. Jerome, *Macromolecular Rapid Communications* **2004**, *25*, 1536-1539.

[48] E.B. Zhulina, M. Adam, I. LaRue, S.S. Sheiko, M. Rubinstein, *Macromolecules* **2005**, *38*, 5330-5351.

[49] C.W. Wijmans, E.B. Zhulina, *Macromolecules* **1993**, *26*, 7214-7224.

[50] H. Li, T.A. Witten, *Macromolecules* **1994**, *27*, 449-457.

[51] K.M. Hong, J. Noolandi, *Macromolecules* **1981**, *14*, 736-742.

[52] D.G. Hall, B.A. Pethica, *"Non-ionic surfactants"* Chapter 16, Marcel Dekker **1976**.

[53] J.N. Israelachvili, D.J. Mitchell, B.W. Ninham, *J. Chemical Society, Faraday Transactions II* **1976**, *72*, 1525-1568.

[54] G. Porte, *J. Phys. Chem.* **1983**, *87*, 3541-3550.

[55] J.C. Eriksson, S. Ljunggren, *Langmuir* **1990**, *6*, 895-904.

[56] T.L. Hill, *"Thermodynamics of Small Systems", Parts 1 and 2*; Dover Pub. Inc.: New York, **1994**.

[57] A.B. Jódar-Reyes, J.L. Ortega-Vinuesa, A. Martín-Rodríguez, F.A.M. Leermakers, *Langmuir* **2003**, *19*, 878-887.

[58] M.R. Böhmer, L.K. Koopal, R. Janssen, E.M. Lee, R.K. Thomas, A.R. Rennie, *Langmuir* **1992**, *8*, 2228-2239.

[59] A.B. Jódar-Reyes, J.L. Ortega-Vinuesa, A. Martín-Rodríguez, F.A.M. Leermakers, *Langmuir* **2002**, *18*, 8706-8713.

[60] S.F. Edwards, *Proc. Phys. Soc* **1965**, *95*, 613-624.

[61] O.A. Evers, J.M.H.M. Scheutjens, G.J. Fleer, *Macromolecules* **1990**, *23*, 5221-5233.

[62] M. Daoud, C.P. Cotton, *J. Phys.* **1982**, *43*, 531-538.

[63] F.A.M. Leermakers, J. Sprakel, N.A.M. Besseling, P.A. Barneveld, *Phys. Chem. Chem. Phys.*, **2007**, *9* 167-179.

[64] D. Broseta, G.H. Fredrickson, E. Helfand, L. Leibler, *Macromolecules* **1990**, *23*, 132-139.

[65] T. Futterer, G.A. Vliegenthart, P.R. Lang, *Macromolecules* **2004**, *37*, 8407-8413.

[66] E. Eisenriegler; *Polymers near Interfaces*, World Scientific Publishing: Singapore **1993**.

[67] R.A.L. Jones, R.W. Richards; *Polymers at Surfaces and Interfaces*, University Press, Cambridge, **1999**.

[68] G.J. Fleer, J.M.H.M. Scheutjens; *J. Colloid Interface Sci.*, *111*, **1986**, 504-515.

[69] C.M. Wijmans, F.A.M. Leermakers, G.J. Fleer; *J. Colloid Interface Sci.*, *167*, **1994**, 124-134.

[70] D.H. Napper; Polymer Stabilization of Colloidal Dispersions Academic Press: London, **1983**.

[71] S. Alexander; *J. de physique, Paris*, *38*, **1977**, 983.

[72] S. Marcelja, N. Radic; *Chem. Phys. Lett.*, *42*, **1976**, 129.

[73] H.J. Butt, J.J. Wang, R. Stark, M. Kappl, B.A. Wolf, J. Eckelt, A. Knopf; *Soft Materials*, *5*, **2007**, 47-60.

[74] A. Vrij, *Pure and Applied Chemistry*, *48*, **1976**, 471-483

[75] G.J. Fleer, F.A.M. Leermakers, *Fundamentals of homopolymers at interfaces and their effect on colloidal stability* in: H. Stechemesser and B. Dobias, eds., *Coagulation and Flocculation* 2nd ed. (*Surfactant Science Series* **2005**, *126*, 349.

[76] J. Klein, P.F. Luckham; *Macromolecules*, *17*, **1984**, 1041; *19*, **1986**, 2007.

[77] A.N. Semenov, J. Bonet-Avalos, A. Johner, and J.-F. Joanny; *Macromolecules*, *29*, **1996**, 2179.

[78] J.B. Avalos, J.F. Joanny, A. Johner, A.N. Semenov *Europhys. Lett.*, *35*, **1996**, 97-102

[79] J.M.H.M. Scheutjens, G.J. Fleer, M.A. Cohen Stuart; *Colloids Surfaces*, *21*, **1986**, 285-306.

[80] A. Johner; J.B. Avalos; C.C. vanderLinden, A.N. Semenov, J.F. Joanny *Macromolecules*, *29*, **1996**, 3629-3638

[81] J. des Cloizeaux, G. Jannink; *Les Polymeres en Solution*, Les Ulis: France, **1987** Editons de Physique.

[82] R. Zajac, A. Chakrabarti, *Phys. Rev. E*, *52*, **1995**, 6536 - 6549.

[83] H.M. Schneider, P. Frantz, S. Granick, *Langmuir 12*, **1996**, 994.

[84] M. Giesbers, J.M. Kleijn, G.J. Fleer, M.A. Cohen Stuart; *Colloids Surf., A*, *142*, **1998**, 343-353.

[85] L. Feuz, F.A.M. Leermakers, M. Textor, O. Borisov, *Macromolecules*, *38*, **2005**, 8891-8901.

[86] C.C. van der Linden, F.A.M. Leermakers, G.J. Fleer; *Macromolecules*, *29*, **1996**, 1000-1005.

[87] J.M.H.M. Scheutjens, G.J. Fleer; *J. Phys. Chem.*, *83*, **1979**, 1619.

[88] J.M.H.M. Scheutjens, G.J. Fleer; *J. Phys. Chem.*, *84*, **1980**, 178-190.

[89] A. Silberberg; *J. Phys. Chem.*, **1962**, *66*, 1972; **1962**, *66*, 1884.

[90] C.C. van der Linden, F.A.M. Leermakers; *Macromolecules* , *25*, **1992**, 3449-3453.

[91] J. van der Gucht, N.A.M. Besseling, J. van Male, M.A. Cohen Stuart *J. Chem. Phys.*, *113*, **2000**, 2886-2893.

[92] J.F. Joanny, A. Johner, *J. de Physique II*, *6*, **1996**, 511-527

[93] A.A. Louis, P.G. Bolhuis, J.P. Hansen, E.J. Meijer. *Phys. Rev. Lett.* **85**, 2522 (2000).

[94] G.J. Fleer, A.M. Skvortsov, R. Tuinier. *Macromol. Theory Simul.* **16**, 531 (2007).

[95] G.H. Fredrickson, F. Drolet *Macromolecules*, *35*, **2002**, 16-39.

[96] M. Muller, G.D. Smith *J. Pol. Sci., Part B 43*, 934-358 **2005**.

[97] R. Elliott, K. Katsov, M. Schick *J. Chem. Phys. 122*, 044904 **2005**.

[98] G.J.A. Sevink, J.G.E.M. Fraaije, H.P. Huinink *Macromolecules* , *35*, **2002**, 1848-1859.

[99] C. von Ferber, Yu. Holovatch, A. Jusufi, C.N. Likos, H. Löwen, M. Watzlawek. *J. Mol. Liquids* **92**, 151 (2001).

[100] P.G. Bolhuis, A.A. Louis, J.P. Hansen, E.J. Meijer. *J. Chem. Phys.* **114**, 4296 (2001).

[101] N. Metropolis, A.W. Rosenbluth, M.N. Rosenbluth, A.H. Teller, E. Teller. *J. Chem. Phys.* **21**, 1087 (1953).

[102] F.A. Detcheverry, D.Q. Pike, P.F. Nealey, M. Mueller, J.J. de Pablo. *Phys. Rev. Lett.* 102, **2009**, 19781.

[103] D.Q. Pike, F.A. Detcheverry, M. Mueller, J.J. de Pablo. *J. Chem. Phys.* 131, **2009**, 084903.

[104] N Gunari, A.C. Balazs, G.C. Walker *J. Am. Chem. Soc.*, *129*, **2007**, 10046-10047

[105] I.K. Voets, R. Fokkink, T. Hellweg, S.M. King, P. Waard, A. de Keizer, M.A. Cohen Stuart *Soft Matter*, *5*, **2009**, 999-1005.

[106] L. de Ruiter, H.B. de Jong *Proceedings of the Section of Sciences, Koninklijke Nederlandse Akademie van Wetenschappen*, *50*, **1947**, 836-848.

[107] E. Spruijt, J. Sprakel, M.A. Cohen Stuart, J. van der Gucht *Soft Matter* **2009**, DOI: 10.1039/b911541b.

[108] L. Kaufman *SIAM J. Optim. 10*, **1999** 56-69.

Samenvatting

In dit proefschrift hebben we een aantal problemen onderzocht, waarin polymeren verschillende vormen van zelfassemblage ten toon spreiden. We hebben ons toegelegd op een zelfconsistent veld methode waarmee het mogelijk is om polymeereigenschappen te analyseren die heel moeilijk met andere modelleertechnieken toegankelijk zijn. Waar mogelijk zijn de voorspellingen met resultaten van analytische theorien vergeleken. In deze samenvatting bespreken we kort welke resultaten we bereikt hebben en geven we aan in welke richting ons inziens toekomstig onderzoek vruchtbaar lijkt.

In *hoofdstuk 2* presenteren we een analytische theorie en de resultaten van een zelfconsistent veld model voor het mechanisch ontvouwen van een polymeerglobule, gevormd door een flexibele polymeerketen in een slecht oplosmiddel. In dit proces hebben we drie regimes gedentificeerd in de kracht-afstand relatie. Bij een geringe strekking, die door middel van een verhoging van de eindpuntsafstand tot stand komt, is de initile reactiekracht lineair met de opgelegde afstand. De globule verandert van een bolvormige naar een ellipsoïdale vorm. Bij een toenemende strekkingsgraad ondergaat de globule een overgang naar een inhomogene, zogenaamde dikkoptoestand, waarin een dichtgepakte kop en een sterk gestrekte staart met elkaar in evenwicht zijn. Tenslotte, bij een zeer hoge strekkingsgraad, verdwijnt de steeds kleiner wordende kop abrupt en is de keten weer homogeen gestrekt. Deze conformatiefaseovergang gaat gepaard met een sprongsgewijze verandering in de strekkingskracht, welke waargenomen wordt in het gestrekte deel van de keten. De kracht-afstand relaties, verkregen bij een verhoging van de opgelegde kracht en bij een verlaging van de opgelegde kracht, verschillen iets rond de faseovergang. In dit gebied hebben we waargenomen dat de uitrekmodulus een negatieve waarde kan aannemen.

In *hoofdstuk 3* bespreken we voorspellingen voor de vorming van bolvormige micellen die gevormd worden door tri-blok copolymeren met een samenstelling $A_N B_M C_N$, welke we gevonden hebben uit een numerieke analyse van een zelfconsistent veld theorie. In een selectief oplosmiddel, dat slecht is voor het centrale B_M blok en goed voor de twee buitenblokken, wordt boven een gegeven repulsieve wis-

selwerkingsenergie tussen de A en C segmenten een lateraal ontmengde corona voorspeld. Deze micellen noemen we, naar de griekse god met twee gezichten, Janus micellen. We bespreken de thermodynamische stabiliteit, de grootte, en de fluctuaties in micelgrootte. De overgang van een homogene naar een lateraal ontmengde corona ontstaat geleidelijk als de repulsie tussen A en C toeneemt. Een aantal oorzaken hiervoor hebben we besproken. Allereerst merken we op dat het micelsysteem klein (dus niet macroscopisch) is en daarom geen sprongsgewijze overgang mag hebben. Daarnaast hebben we beargumenteerd dat de symmetrie in het copolymeer een sprongsgewijze overgang in de weg staat. Het aantal polymeren per micel, het zogenaamde aggregatiegetal, bleek een afnemende functie te zijn van de repulsiesterkte tussen A en C als de corona homogeen is, maar een toenemende functie van deze repulsie in het Janus-regime. De vorming van het grensvlak tussen de A-rijke en C-rijke gebieden vindt het eerst plaats dicht bij de kern van het micel, alwaar de polymeerconcentratie van A en C het hoogst is. Er is een kritische waarde van de polymeerconcentratie gevonden waarboven de ontmenging begint. Deze waarde is gecorreleerd aan het bulk fasegedrag van elkaar afstotende A_N and B_N homopolymeren in een gemeenschappelijk goed oplosmiddel.

In *hoofdstuk 4* hebben we een klassiek onderwerp uit de kast gehaald en opnieuw bestudeerd, namelijk de adsorptie van homopolymeren aan een vast-vloeistof oppervlak. In dit hoofdstuk bespreken we ook de gevolgen voor de collodale stabiliteit. Met name hebben we kamvormige homopolymeren in een goed oplosmiddel onderzocht in het regime van sterke adsorptie-energie. Een zelfconsistent veld analyse laat zien dat voor relatief lange zijketens, maar voor een nog veel langere hoofdketen, de adsorptielaag dicht bij het oppervlak door de zijketens wordt bepaald, en dat op grotere afstand van het oppervlak de laag eigenschappen vertoont die terug te voeren zijn naar hoofdketeneigenschappen. Eerder onderzoek heeft aangetoond dat normaliter adsorberende homopolymeren aanleiding geven tot flocculatie van een collodale oplossing. Dit wordt toegeschreven aan het feit dat lange polymeerkentens attractieve bruggen kunnen slaan tussen de deeltjes. Echter, de ketenuiteinden dragen niet bij aan de brugvorming. Staarten geven derhalve een kleine repulsieve bijdrage aan de interactie tussen twee deeltjes. De zijstaarten van de kampolymeren hebben allemaal een eindsegment en deze einden versterken de repulsie enorm. Het gevolg is dat, in tegenstelling tot de lineaire polymeren, kampolymeren het vlokken van colloïden tegengaan. Het concentratieprofiel van adsorberende homopolymeren heeft diverse universele eigenschappen. Zo heeft de Gennes, een proximaal, een centraal en een distaal gebied in deze laag aangewezen. In het distale regime vervalt de concentratie via een exponentiële functie tot deze de bulkwaarde heeft aangenomen. In het centrale regime wordt het profiel beschreven door een machtswet en is de locale polymeerdichtheid gekoppeld aan hoe de correlatielengte in een half-verdunde polymeeroplossing gerelateerd is aan de polymeerconcentratie. In het proximale gebied tenslotte wordt het profiel beïnvloed door de manier waarop polymeersegmenten aan het oppervlak binden. Voor kampolymeren met voldoende lange

zijkentens hebben we laten zien dat het proximale gebied opnieuw opgedeeld kan worden in een proximaal, een centraal en een distaal gebied met overeenkomstige karakteristieken.

In het laatste *hoofdstuk 5* bespreken we het meest recente werk, dat nog diverse tekenen vertoont van een gedeeltelijk afgerond project. In dit hoofdstuk presenteren we een meerstappen, maar nog steeds efficiënte, rekenmethode om inhomogene polymeeroplossingen te analyseren. Een grofkorrelige Monte Carlo simulatie voor een verzameling van zachte deeltjes (die polymeerketens representeren) is gebruikt om relevante verdelingen van de zwaartepunten van de ketens te generen. Deze zwaartepunten worden opgelegd als een randvoorwaarde voor een moleculair gedetailleerde 3d zelfconsistent veld berekening. De methode is, ter illustratie, toegepast op polymeerdepletie dichtbij een harde wand voor een halfverdunde polymeeroplossing in een goed oplosmiddel. Het depletieprofiel en de depletielaagdikte is consistent met computersimulaties en de schalingstheorie. We beweren daarom dat de berekeningen aantonen dat het mogelijk is om zowel intermoleculaire als intramoleculaire uitgesloten-volume interacties in rekening te brengen voor polymeren nabij grensvlakken. Deze nieuwe aanpak corrigeert derhalve de klassieke zelfconsistent veld theorie van Scheutjens en Fleer, die maar gedeeltelijk deze interacties in rekening brengt.

De meeste onderwerpen die in dit proefschrift zijn beschreven hebben een klassieke uitstraling. We hebben aangetoond dat ook voor klassieke themas nieuwe resultaten kunnen worden bereikt. Dit laat zien dat zelfassemblage van polymeren een buitengewoon rijk onderwerp is, waarvoor veel vooruitgang geboekt kan worden in de nabije toekomst. Met een voortschrijdende controle over de polymeersynthese, en de beschikbaarheid van goedgedefinieerde polymeren, groeit ook het belang van verdergaande theorievorming. Uiteindelijk zullen de voortschrijdende inzichten, die voor allerlei aspecten van zelfassemblage door de polymeertheorie worden aangereikt, nieuwe technologische toepassingen mogelijk maken.

List of Publications

This dissertation:

- Charlaganov, M.; Borisov, O. V.; Leermakers, F. A. M., Modeling of triblock terpolymer micelles with a segregated corona. *Macromolecules* **2008**, 41 (10), 3668-3677.
- Charlaganov, M.; Kosovan, P.; Leermakers, F. A. M., New ends to the tale of tails: adsorption of comb polymers and the effect on colloidal stability. *Soft Matter* **2009**, 5 (7), 1448-1459.
- Polotsky, A. A.; Charlaganov, M. I.; Leermakers, F. A. M.; Daoud, M.; Borisov, O. V.; Birshtein, T. M., Mechanical Unfolding of a Homopolymer Globule Studied by Self-Consistent Field Modeling. *Macromolecules* **2009**, 42 (14), 5360-5371.
- Charlaganov, M.; Leermakers, F.A.M., Molecular modeling of intermolecular and intramolecular excluded volume interactions for polymers at interfaces, *Submitted to J. Chem. Phys.*

Other work:

- Polotsky, A.; Charlaganov, M.; Xu, Y. Y.; Leermakers, F. A. M.; Daoud, M.; Muller, A. H. E.; Dotera, T.; Borisov, O., Pearl-necklace structures in core-shell molecular brushes: Experiments, Monte Carlo simulations, and self-consistent field modeling. *Macromolecules* **2008**, 41 (11), 4020-4028.
- Polotsky, A.; Daoud, M.; Borisov, O.; Charlaganov, M.; Leermakers, F. A. M., Analysis of the longitudinal structure of a collapsed molecular bottle brush using a self-consistent field approach. *International Journal of Polymer Analysis and Characterization* **2007**, 12 (1), 47-55.

Acknowledgements

This thesis would not have been possible without the help and support from many amazing people. Only while working on a thesis one has a chance to encounter so many talented people who give their time and knowledge so generously. I am thankful to all the people who created and maintained the atmosphere of cooperation and friendship which surrounded me during the last four years.

My foremost thanks go to Frans Leermakers, for his infinite energy which served as a constant source of inspiration throughout the whole project, to Martien Cohen Stuart for his advice which was always result-oriented and arrived just on time, and Oleg Borisov for many fruitful discussions we had in different locations all over Europe.

I gratefully acknowledge the informal community of scientists who work or used to work in the Lab 25 of The Institute of Macromolecular Compound in St.Petersburg. I would like to thank specifically T.M. Birshtein for her wise guidance during my master's studies, E.B. Zhulina for suggestion of the topic for the first chapter of this dissertation, A.M. Skvortsov for our conversations in the FYSKO coffee room, and Alexei Polotsky for collaborations.

People of FYSKO, you were always helpful at work and fun during breaks. Ilja Voets, Bas Hofs, Joris Sprakel, thanks for helping with my experiments. My officemates, Wout Knoben, Monika Butrimaite, Cecilia Bernardini, Junyou Wang, thanks for sharing the evenings in the lab. Peter Košovan, your frequent visits have made you a FYSKO'er in your own right, thanks for collaborations, climbs and descends we did together. Josie Zeevat and Roelfina Mihalj-IJken, thanks for covereing me on the bureaucratic front. To all who gave so many things to me and my family: thanks!

The financial support from the EU Marie Curie Research and Training Network Polyamphi is gratefully acknowledged. I would also like to thank people who formed this network. Many meetings and productive discussions with you significantly contributed to the contents of this thesis.

Друзья, спасибо за то, что вы есть. Мама, эта книжка посвящается

тебе. Хотя бы потому, что ты больше всех волновалась. Ренат, береги маму.

Саня и Лия, без вас все было бы совсем по-другому. Не было бы этой книжки, не было бы Голландии, и еще много чего просто не было бы. Спасибо за то, что все это есть.

Leiden, *Marat*
November 2009

Overview of completed training activities

Self-Assembling Block Copolymers Summer School, Chodová Planá (Czech Republic), 2005.

Screening, Charge Inversion and Condensation of Macroions Workshop, Leiden, 2005.

Modeling Techniques Training, Saclay (France), 2005-2006.

Physical Chemistry Winterschool, Han-sur-Lesse (Belgium), 2006.

Neutron Scattering Training, Budapest (Hungary), 2006.

Caput College, Wageningen, 2006-2007.

Polyelectrolytes in Solutions and at Interfaces Summer School, Biezenmortel, 2007.

European Student Conference, Ven (Sweden), 2007.

STIPOMAT Conference, Les Diablerets (Switzerland), 2007.

Amsterdam - New Amsterdam meeting, 2007.

PhD Trip, Sweden & Denmark, 2007.

Molecular Order and Mobility in Polymer Systems Conference, St.Petersburg (Russia), 2008.

SAXS Training, Grenoble (France), 2008.

EU RTN Polyamphi Meetings, 2005-2009.

Group Meetings & Colloquia, Wageningen, 2005-2009.

Cover graphics by Alexandra Arshanskaya
Printed by Wöhrmann Print Service, Zutphen (www.wps.nl)